THE UNIVERSITY OF CHICAGO

MANIPULATING THE VEGF-C/VEGFR-3 AXIS TO MODULATE VACCINE OUTCOMES AND ANTITUMOR IMMUNITY

A DISSERTATION SUBMITTED TO
THE FACULTY OF THE PRITZKER SCHOOL OF MOLECULAR ENGINEERING
IN CANDIDACY FOR THE DEGREE OF
DOCTOR OF PHILOSOPHY

BY
TREVIN ROBERT KURTANICH

CHICAGO, ILLINOIS
DECEMBER 2023

Dedicated to my father.

I could have not done this without you. You may not have had any idea what I was doing, but you were always so supportive in working to keep me sane and happy these last 5 years. Thank you for always supporting me.

I love you so much.

"*Somewhere, something incredible is waiting to be known.*"

- Carl Sagan

TABLE OF CONTENTS

LIST OF FIGURES

LIST OF TABLES

ACKNOWLEDGMENTS

It is really hard to figure out how to thank everyone who has contributing to helping me get through this PhD. They say "it takes a village", but in this case I feel like "it takes a city" is more adequate to describe how many people were involved in keeping getting me through the past 5 years. So first, to those who are unnamed in the following acknowledgements, I'm sorry, but if I singled out everyone who I wanted to thank individually this section would never end. That does not mean your companionship was not appreciated.

I would like to thank my advisor, Melody Swartz, for giving me the liberty to explore scientifically, even sometimes at odds with her opinion. Your willingness to promote my scientific growth and independence was extremely valuable to me, and I am thankful for having the opportunity to have worked with you. I would also like to thank my committee members Jeffrey Hubbell and Aaron Esser-Kahn for their comments and criticism as well as previous committee members Justin Kline and Anne Sperling for their insightful experimental recommendations.

Next I would like to thank my two mentors, Lambert Potin and Emiliano Gomez Medellin. First, thank you to Lambert for taking me under your wing when I was a lab baby and introducing me to the world of lymphangiogenic potentiation. While my project changed a lot, the skills I learned on how to conduct in vivo experiments were critical for my ability to grow and develop as a scientist once you had left. To Emiliano, thank you so much for your patience in helping me develop as an immunologist and a hypothesis driven researcher. I would not be the scientist I am today without your insight and willingness to always talk science.

To all the Swartz lab members, past and present, I feel privileged to have met and engaged with everyone scientifically and socially, and to be able to call many of you friends. I will not be able to name everyone individually, but know that your time, friendship, and knowledge have been appreciated.

To those graduate students in the lab who I have mentored or advised (Thomas, Colleen, Camryn, and Trevor): thank you for giving me the courtesy of listening to what this old man has to say. I know it is hard to figure out who to listen to when you are starting out, but I am glad that you have trusted me enough to listen to what I had to say and to seek my advice. Please don't hesitate to seek me out in the future.

For those former lab members who I have worked directly with in the past: Lea, Peyman, and Nick, thank you for trusting me enough to collaborate and for both teaching me and learning from me. I learned a lot from the short time we worked together, and while this work did not make it into this thesis, that work was critical for my scientific growth.

Thank you to Kelly, who has been the most amazing lab manager for the past 2 years, and has done so much to make the lab a much more well run and happy place for all. To Kristen, thank you for being such an awesome and fun person. It has been amazing to see you work as as scientist and to get to know you as a friend. I look forward to seeing great things from you.

While I may be part of the Swartz lab, I would be remiss without acknowledging the companionship of so many of those in the Hubbell lab. We may be technically separate groups, but we share a lab space (and a group chat) and at times feel like one massive group. Thank you to Kevin Chang, Angie (Hye Rin) Chun, and others for being great friends, and for always being down to grab food. I would also like to single out Seounghun Kang for his collaboration. You let me into your project, and I feel like together our skills and abilities synergized nicely and came together to produce a cohesive story. And more than just as a collaborator, thank you for being a friend.

Finally I would like to thank my family (my mom, dad, and sister) for always offering their steadfast support and unconditional love. Most importantly, I would like to thank my sister's cat, Luna, for being my inspiration and for not hiding from me when I visit.

ABSTRACT

The lymphatic system is the main transport route for fluid, antigens, exosomes, and immune cells from peripheral tissues to the lymph nodes (LNs). Lymphatics pervade all tissues and surround the LN capsule as well as penetrating into the T cell zone. Lymphangiogenesis, or lymphatic vessel proliferation, is a process dependent on the VEGF-C/VEGFR-3 axis. The first part of this thesis elucidates the role of the VEGF-C/VEGFR-3 axis in modulating vaccine outcomes and immunotherapy efficacy in cancer. In the second part of this thesis, I will assess the mechanisms of action of collagen-binding cytokines for cancer immunotherapy.

Chapter 1 introduces to the main concepts contained within this thesis, including a description of the lymphatic system as well as known functions of lymphatic endothelial cells (LECs). I furthermore explore other key concepts such as cancer immunotherapy and characteristics of a vaccine response, including antibody subclasses and their distinct functions. In Chapter 2, I explore how the VEGF-C/VEGFR-3 axis modulates the vaccine response. I observe that the VEGFR-3 axis modulates type 2 immunity, specifically through regulation of cytokine secretion by T cells and downstream IgG1 class switch, and this affect was dependent on LEC MHC II. Chapter 3 elucidates mechanisms by which intratumoral lymphatics in VEGF-C overexpressing melanomas potentiate immunotherapy efficacy. Here I determine that LEC derived CXCL9 and the CXCR3 axis are critical for driving therapeutic efficacy in an adoptive cell transfer immunotherapy model. Chapter 4 explores the mechanisms of action of two distinct collagen-binding domain (CBD) cytokine therapies that were combined with CBD-IL-12 to form distinct combinations with the toxic, but highly effective, IL-12. By combining IL-12 with other less toxic cytokines, GM-CSF and IL-7, the effective dose of IL-12 could be lowered dramatically without affected toxicity. I demonstrate that while both cytokines synergize excellently with CBD-IL-12, they have completely distinct mechanisms of action. Lastly, in Chapter 5 I discuss future directions for interesting and relevant avenues of exploration based on the novel work presented herein.

CHAPTER 1

INTRODUCTION

1.1 The Lymphatic System

The lymphatic system is a network of vessels whose canonical function is drainage [1]. Lymphatics vessels pervade throughout the body in most tissues such as the skin, meninges, and intestine and connect these tissues to the lymph nodes [2] The cellular component of the lymphatic system is the lymphatic endothelial cell (LEC), which are the endothelial cell component that lines the interior of the lymphatic vessel. LECs are characterized by expression of the master transcription factor, Prox1, and its main mitogenic growth factor receptor—vascular endothelial growth factor receptor 3 (VEGFR-3) [2–4].

Since, lymphatics serve as key connections between peripheral tissues and lymph nodes, they are essential for proper coordination of adaptive immune responses. Immune responses in mice without dermal lymphatics are severely impaired, and current literature suggests that migratory DC traffic to the lymph node is mediated by the lymphatic endothelium [5–7]. While certainly not the only important cell type in initiating an adaptive immune response, DCs are particularly effective activators of both CD4 and CD8 T cells, and as such are critical. DC migration is CCR7 dependent, and the CCR7 ligand, CCL21 is constitutively expressed by LECs [6]. Furthermore, DC migration is dependent on integrin binding to vascular cellular adhesion molecular 1 (VCAM-1) and intercellular adhesion molecular 1 (ICAM-1), both of which are expressed by LECs [8]. Lymphatics can secrete many other chemokines such as CCL2, CXCL10, and CXCL13 and as such contribute to immune cell trafficking of additional cell types such as monocytes, effector T cells, and B cells respectively [9, 10]. Thus, lymphatics are critical as conduits and coordinators of cell trafficking, which are essential for the initiation and maintenance of adaptive immunity.

In the lymph node, LECs line the capsule and are in a unique position with the many immune cells that traffic through them as well [2]. LECs in the LN are now thought to be distinct from peripheral tissue LECs. LN LECs consist of substantial heterogeneity in human and mouse where 6 or more distinct subsets have been identified by single cell RNA-

seq [11, 12]. Because of these recent findings, it important to keep in mind that previous findings utilizing more easily accessible peripheral tissues LECs may not hold with LN LECs and vice versa [13–15].

1.1.1 Lymphangiogenesis and the VEGFR-3 Axis

Lymphatic vessel expansion, or lymphangiogenesis, occurs during many pathological conditions such as cancer, graft versus host disease, and many other inflammatory conditions [16, 17]. At the steady state, lymphatics are relatively quiescent and active vascular endothelial growth factor C (VEGF-C), the main lymphangiogenic growth factor, signalling is only required for lacteal maintenance, but did not substantially alter other lymphatics [18]. When it occurs, lymphangiogenesis can occur in both peripheral tissues and in the draining lymph nodes [19]. VEGFR-3 stimulation through VEGF-C (or to a lesser extent VEGF-D) is required for lymphangiogenesis [20]; however, it is not sufficient on it's own. Many inflammatory cytokines including IFN-γ, IL-4, and IL-13 antagonize lymphangiogenesis [21, 22]. Beyond VEGFR-3, neuropilin-2 (NRP2) is expressed by LECs and interacts with VEGFR3 to bind VEGF-C and VEGF-D and enhance lymphangiogenesis [23]. Furthermore, other factors which may have lymphangiogenic activity include VEGF, fibroblast growth factor (FGF), and insulin-like growth factor-1 (IGF1) [16]. Thus, there are a multitude of different ways lymphangiogenesis can be regulated, and while the VEGFR-3 axis is critical, it is not sufficient to simply have abundant VEGF-C to induce lymphangiogenesis, and the full process involving all critical cofactors, agonists, and antagonists is not well understood.

1.1.2 LECs as Immunomodulators

In the lymph node, LECs are a major source of IL-7 [24]. IL-7 is a key survival cytokine for T cells that express the IL-7R, including naïve and central memory T cells. Furthermore, upon inflammatory stimuli such as LPS, LECs upregulate IL-15 [25], which is involved in naïve and

memory T cell homeostasis [26]. However, it is unknown to what extend LECs in peripheral tissues express these molecules. LECs also produce colony stimulated factor 1 (CSF1) which is a growth factor involved in the survival and maintenance of macrophages, and LEC-derived CSF1 is an essential component of the medulary and subcapsular sinus macrophages in the LN [27]. LECs are also critical regulators of lymph node organogenesis. Thus, LECs are critical for formation, survival, and homeostasis of critical immune components in the lymph node [28].

LECs can also directly interact with T cells in contact dependent ways via both MHC I and MHC II [29, 30]. LECs in the steady state are able to directly prime naïve CD8 T cells to a memory-like phenotype in an MHC I dependent manner [31]. However, the role of LEC education to CD4 T cells is controversial. It is thought that MHC II on LECs is unable to activate naïve CD4 T cells as LECs don't have proper antigen presentation machinery [32]; however, the absence of MHC II on lymph node stromal cells—which include LECs—results in autoimmunity [33]. Furthermore, in the tumor MHC II on LECs promotes regulatory T cell function and expansion [34]. Thus while MHC II on LECs does have an immunomodulatory function, it is unclear under which contexts its function is relevant. LECs also express PD-L1, which is antagonistic to T cell activation, and do not express appreciable levels of costimulatory molecules such as CD80 and CD86 [35]. Thus, T cells that are exposed to MHC I or MHC II on LECs are exposed to a non-activating milieu.

1.2 Cancer Immunotherapy and The Role of Lymphatics

Cancer immunotherapy, in particular checkpoint blockade, has revolutionized the treatment of certain cancers. "Immune checkpoint blockade" (ICB) involves blocking specific pathways involved in T cell exhaustion, mainly the PD-1:PD-L1 axis or CTLA-4:CD80/86 axis [36]. However, not every patient is responsive to immunotherapy and the side effects can be severe [37].

1.2.1 T Cells and Immunotherapy

A critical criteria for responding to immunotherapy is T-cell infiltration, as tumors that are not well infiltrated do not respond to immunotherapy [38]. While the presence of T cell infiltrates is critical for immunotherapy efficacy, the quality of the T cell is also essential [39]. High levels of PD-1 signal T cell exhaustion, but beyond PD-1 expression there are levels of T cell function that make the T cell more likely to respond to ICB or not [40]. Besides PD-1, Tim3 and Lag3 are other surface marker of exhaustion, with Tim3 generally associated with a more terminal exhausted phenotype [40]. True exhaustion is epigenetically encoded and while phenotypically cells may look similar due to high levels of PD-1 and lack of effector function, they can be epigenetically distinct and have different abilities to respond to ICB or other immunotherapies [41]. Tox, a transcription factor, has been identified as a key mediator of CD8 T cell dysfunction that is sufficient to induce features of terminal T cell exhaustion [42].

In terms of what constitutes a productive and responsive T cell, the main factor identified has been TCF-1. TCF-1 is a transcription factor originally known for its key involvement in T cell development in the thymus [43]. However, TCF-1 expressing, antigen experienced cells have demonstrated capacity for self-renewal, and have the capacity to continuously generate an effector CD8 T cell response, thus driving immunotherapy responsiveness [43, 44]. Loss of TCF-1 is conversely associated with progression towards exhaustion [42]. Beyond TCF-1, KLRG1 has also been identified as a marker of effector function in CD8 TILs, and KLRG1+ TILs produce more IFN-γ, a classical anti-cancer pro-inflammatory cytokine [45]. However, these few markers are not an exhaustive list of potentially relevant markers of distinct function due to the heterogeneity of CD8 T cells in the tumor. In short, CD8 T cells in the tumor have many distinct functional states defined by a variety of various molecules, both on the cell surface and nuclear transcription factors, and these states can demonstrate distinct ability to respond to immunotherapy.

1.2.2 Types of Immunotherapy

There are many types of immunotherapies that are both clinically used and in preclinical development. The first class is antibody-based therapeutics such as α-PD-1 or α-CTLA-4 that are clinically in use [46]. But due to their limited therapeutic benefit in the majority of patients, novel antibodies are being developed to target other components of the exhaustion pathway such as Tim3 or Lag3 [47]. None of these have received clinical approval, but the goal is to find an target that would synergize well with the already approved ICB therapeutics.

The other main immunotherapy that has received clinical approval is adoptive cell transfer (ACT). ACT comes in two main forms: chimeric antigen receptor (CAR) T cells or TIL therapy. CAR T involves taking a patients autologous cells and engineering them with a CAR that is specific to a tumor antigen. This has shown great success with B cell lymphomas using a CD19 CAR, but has limited success with solid tumors [48]. On the other side, TIL therapy involves taking a sample of a patients tumor, isolating the T cells, and then expanding them ex vivo to high quantities before re-infusing [48]. The idea is to expand tumor specific T cells away from the immunosuppressive tumor microenvironment, and then reinfuse them with the hope they will be functional and able to kill the tumor. In this case the quality of the TILs may be immensely important in determining the therapeutic effect [49].

One very promising class of therapies are cytokine based therapeutics. There has been a recent explosion of interest in cytokine based cancer therapies, and many varieties have emerged [50]. The first cytokine immunotherapy used to treat cancer was IL-2 [50]. IL-2 is a cytokine involved in activated T cell survival, but also can expand Tregs [51]. IL-2 has been approved as a therapy for decades, but does not see wide use due to its toxicity and it's low efficacy [51]. On the preclinical side, IL-12 serves a promising candidate for cytokine based immunotherapy. IL-12 promotes Th1 polarization and IFN-γ secretion by CD4 T cells, as well as activating cytotoxic CD8 T cells [52, 53]. Furthermore, IL-12 can also

stimulate antigen presentation which could further enhance CD4 and CD8 T cell activation and function [54, 55]. One of the main limitations of cytokine therapies is their toxicity. While they can be very potent, they are highly toxic, partially due to their off-target systemic effects on healthy tissue. IL-12 in particularly is notorious for its toxicity, due to it's potent ability to stimulate IFN-γ [52]. One way to attempt to get around this issue is through engineering approaches using various modifications of these cytokines to better target the tumor and thus increase their efficacy with reduced toxicity.

The last class of immunotherapy is the tumor vaccine. Tumor vaccines have had a long history of research, but have not had a true breakthrough that has led to a clinically potent therapeutic. One of the most studied tumor vaccine types is the whole cell vaccine [56]. Whole cell vaccines involve taking a tumor sample, irradiating it so it can no longer replicate, and then injecting into the patient with the idea that it will be able to generate a tumor-specific immune response [57]. One of the most common whole cell vaccines is called GVAX, which is where the tumor cells are transduced to express GM-CSF, a growth factor involved in DC and macrophage activation, with the idea that the edition of GM-CSF will aid in the mounting of an effective vaccine response [58]. Unfortunately, whole cell vaccines have not been very successful in clinical trials, despite the many different attempts. Another vaccine strategy that has been attempted is DC vaccines either using tumor lysate or defined antigens from the tumor. However, these as well still have not demonstrated robust antitumor efficacy [59].

1.2.3 Lymphatics in Cancer

Historically, lymphatics have correlated poorly with survival in cancer. Tumors with higher lymphatic vessel density are more metastatic and VEGFR-3 dependent lymphangiogenesis has been reported to be required to initiate the early events of lymphangiogenesis in a VEGF-D overexpressing tumor model [60]. Lymphatic vessels serve as excellent routes of escape for

the tumor cells, towards the sentinel lymph node and then peripheral tissues. Furthermore, LECs themselves have many immunosuppressive functions [61]. Through upregulation of CCL21, melanomas are able to recruit more regulatory immune populations and induce the formation of a lymphoid-like stroma [62, 63]. CCL21 (and CCL19) is the ligand to CCR7, and CCR7+ cells include B cells, naïve and central memory T cells, certain regulatory T cells, and dendritic cells. In tumors with locally ablated lymphatics, there was enhanced recruitment of inflammatory cells and increased levels of pro-inflammatory cytokines such as TNF and IL-1β [64], demonstrating that intratumoral lymphatics are actively suppressing inflammation. Specifically, LECs are able to negatively impact immune responses through multiple inhibitory enzymes, including nitric oxide (NO) and indoleamine-2,3-dioxygenase (IDO) [65–67]. Additionally, LECs can dampen the ability of DCs to activate T cells by reducing DC CD86 expression [68]. In short, lymphatic-rich tumors are both more metastatic and more immune-suppressed.

However, in spite of these negative associations, lymphangiogenesis in tumors does have positive aspects. Lymphangiogenic melanomas have increased T cell infiltration, which synergizes with immunotherapy including adoptive T cell transfer (ACT) and tumor vaccines, to lead to enhanced therapeutic efficacy compared to when the VEGFR-3 pathway is blocked and thus lymphangiogenesis cannot occur. Furthermore, in a clinical trial of the Melan-A/Mart1 peptide vaccine, patients with high serum VEGF-C levels correlated to enhanced progression-free survival [69]. This "lymphangiogenic potentiation" is not exclusive to melanoma, as ectopic expression of VEGF-C via adeno-associated virus serotype 9 (AAV9) synergized with ICB to eradicate glioblastoma, which is normally non-responsive to ICB [70, 71]. Thus despite the increased metastasis, there is also increased responsiveness to immunotherapy, thus making it not so straightforward a pathway to target. For example, blockade of VEGFR-3 to antagonize lymphangiogenesis, could actually worsen outcome if it dampens responsiveness to immunotherapy, at least for those subsets of cancer well treated

by immunotherapies.

1.3 Vaccine Responses

Vaccines are a biological preparation with the intent of conferring immunity towards various pathogens including viruses and bacteria. Vaccines have been around for 100s of years, and have been a highly invaluable tool in fighting spread of dangerous pathogens such as smallpox. Over the years, some vaccines have proven to be incredibly effective. For example, the smallpox vaccine was so effective that smallpox has been eradicated from the world [72]. However, not all vaccines are this effective, for various reasons. For example, the flu vaccine is notoriously not highly effective because of the diversity of the virus due to it's ability to alter itself [73]. In a given year the flu vaccine can be less than 50% effective [74]. Many labs are working for better vaccine design for enhanced efficacy, and recently mRNA has begun to be used as a platform for vaccines, and has proven immensely successful with the launch of the highly effective SARS-CoV-2 vaccines from Moderna and Pfizer/BioNTech [75]. It is still not well understood what makes a good vaccine and what type of cell populations would be involved in generated a superior vaccine, but it is known that one type of molecule is critical: antibodies [76].

1.3.1 Antibodies

One of the canonical goals of a vaccine is to generate antibodies [77]. Antibodies exist in many isotypes, the most prominent in blood being IgG, which is generally considered to be the most relevant for the generation of protective immunity [78]. Antibodies are useful because they can bind to the infectious agent (i.e. bacteria or virus) before it has entered into a cell. Some antibodies are considered "neutralizing antibodies", which prevent the ability of the infectious agent to infect cells and are considered the gold standard for what an ideal vaccine would develop. If people have a high enough quantify of neutralizing

antibodies, then in theory they would be immune from even getting infection [79]. Even non-neutralizing antibodies can be useful though. They can alert inflammatory cells, such as macrophages or activate inflammatory pathways in complement or cytotoxic cells [79]. Complement dependent cytotoxicity (CDC) involves the binding of antibody to the surface of target cells and the recruitment of complement, which is a distinct set of proteins in plasma that can induce various inflammatory processes, to fight infection [80]. Complement then binds to the antibody and initiates a cascade of events that lead to lysis of the target cell. Similarly, there is antibody dependent cellular cytotoxicity (ADCC) upon which NK cells recognize the antibody bound to a cell expressing the target antigen. The NK cells will degranulate and the target cell will apoptose [80]. Thus antibodies are critical in mediating immunity as they can both prevent the pathogen from entering cells and can activate various methods to kill the infected cell.

Antibody Subclass and Distinct Functions

IgG is not one simple class, it is comprised of different "flavors" or subclasses. The subclasses, in mice, are IgG1, IgG2b, IgG2a/c, and IgG3. The subclasses have distinct abilities to activate inflammatory responses: IgG1 has weak ability to activate CDC but no ability to activate ADCC. IgG2 subclasses have much greater effector function than IgG1 and both IgG2b and IgG2a/c strongly promote both CDC and ADCC. IgG3 strongly activates ADCC, but only weekly activates CDC [81].

While antibody class-switch is a complex and highly regulated process, it is known that the cytokines that the B cell are exposed to are critical for the subclass of antibody that will generate. For IgG1 class-switch the cytokine IL-4 is canonically known to be essential for IgG1 class-switch [82]. For IgG2a/c and IgG3, IFN-γ promotes class-switch, and conversely actually antagonizes IgG1 class-switch [82]. Lastly, IgG2b class switch is promoted by TGF-β [83]. While various cell types can secrete the cytokines of interest, it is often CD4 T

cells that are considered the most critical due to their established role in B cell help and the existence of T folicular helper (Tfh) cells which are necessary for the germinal center reaction. CD4 T cells can produce both IL-4 that promotes IgG1 as well as IFN-γ that promotes IgG2 [84].

IgG1 is more often associated with the type 2 immune response due to it's association with IL-4 and allergic sensitization while the more effector-like IgG2 is more associated with the Type 1 immune response and thus the clearance of intracellular pathogens [85, 86]. In short, while the generation of antibodies is critical for effective vaccines, the subclass generated also may be relevant due to their distinct functions and various associations.

1.3.2 LN Lymphatics in Vaccination

In the lymph node (LN), LECs line the subcapsular sinus, but also penetrate into the medullary sinus and the T cell rich paracortex [13, 87]. The absence of lymphatics in the skin results in impaired humoral immunity [5]. LECs have many potentially interesting functions as described earlier including their ability to present antigen through both MHC I and MHC II, their role in coordinating cell trafficking, and their role in producing key survival cytokines. Also due to their location, they are in prime location to interact with immune populations. Despite all the key functions of lymphatics, the role of LN LECs in coordinating a vaccine response has not been explored.

CHAPTER 2

THE VEGF-C/VEGFR-3 AXIS MODULATES VACCINE OUTCOMES IN AN MHC II DEPENDENT MANNER

2.1 Abstract

Lymphatic vessels are the main transport routes for fluid, antigens, exosomes, and immune cells from peripheral tissues to the lymph nodes (LNs). In addition to being pervasive through tissue, lymphatic vessels are also abundant within the LN, where they route lymph and cells around the B cell follicles and throughout the paracortical zone; thus, lymphatic endothelial cells (LECs) have unique access to lymph-borne molecules and interactions with immune cells. Upon acute inflammation or vaccination, LN LECs undergo expansion along with lymphocyte proliferation, in a VEGFR-3 dependent manner; however, it is not well understood how LN lymphatics and their expansion contribute to vaccine responses. Here, we assessed how altering VEGFR-3 signaling in LN LECs affects the vaccine response, using OVA + CpG (a TLR9 agonist) as a model. We found that deleting VEGFR-3 specifically in LECs led to decreased plasma levels of α-OVA IgG1, while LN stimulation with exogenous VEGF-C_{C156S}, a VEGFR-3-specific agonist, prior to and during vaccination led to increased α-OVA IgG1 and IgG1+ germinal center B cells as well as increased production of Th2 cytokines (IL-4, IL-5, and IL-13) upon restimulation. Lastly, we observed that deleting MHC II specifically in LECs abrogates this VEGFR-3 dependent increase in Th2 cytokine production and restricts secretion of the Th1 cytokine IFN-γ. Together, these findings suggest that in response to vaccination, VEGFR-3 signaling in LN LECs promotes type 2 immunity.

2.2 Introduction

Lymphatic vessels are the critical connections that drain fluid from peripheral tissues to the lymph node, and as such are key for the initiation of adaptive immune responses [88, 89]. In the lymph node (LN), LECs line the subcapsular sinus, but also penetrate into the medullary sinus and the T cell rich paracortex [13, 87]. While previously, differences

between tissue and LN LECs were not considered, it is now becoming more apparent that LN LECs are distinct from peripheral tissue LECs, and that previous studies performed using tissue LECs may not hold in LN LECs [13–15]. Under many inflammatory contexts, such as infection or immunization, LECs undergo proliferation, a process termed lymphangiogenesis [17, 90]. Canonically, the VEGF-C:VEGFR-3 axis is essential for lymphangiogenesis [17, 91, 92], though VEGFR-2 is also involved in lymphangiogenesis in many contexts it is also involved in angiogenesis and is thus less specific [93, 94]. Furthermore, VEGFR-3 expression is largely restricted to LECs, and thus serves as an attractive target for selective modulation of lymphangiogenesis, either through stimulation or blockade [95–97].

Beyond their canonical role in draining to the lymph node, LECs can directly serve as immunomodulators. LECs produce many chemokines such as CCL21, CCL2, and CXCL13 involving T cell, DC and B cell trafficking [10, 98, 99], as well as essential cytokines such as IL-7 and CSF1, key T cell and macrophage survival factors respectively [24, 27]. LECs also express many immunomodulatory molecules such as PD-L1 and TGF-β, but lack many costimulatory molecules such as CD80 and CD86 and thus generally are considered suppressive and tolerogenic at the steady state [29]. LECs can also directly serve as antigen presenting cells (APCs), as they can cross-present antigen via MHC I and also express MHC II, in an IFN-γ inducible manner, and therefore have the potential to interact with both CD4 and CD8 T cells [29, 100]. LEC cross-presentation through MHC I promotes CD8 T cell apoptosis, but the surviving fraction of CD8 T cells have central memory phenotype [30, 101]. The role of LEC MHC II is less established, as it remains equivocal what types of antigen LECs can present via MHC II [29, 32]. Recently it has been established that LEC MHC II in the tumor microenvironment promotes intratumoral regulatory T cell (T_{Reg}) suppressive functions, demonstrating that LECs can modulate CD4 T cells in an MHC II dependent manner [102]. Another study showed that mice developed autoimmunity when lymph node stromal cells, which include LECs, lacked MHC II [33]. In summary, while it remains clear

that LECs serve critical roles in the adaptive immune response, it is understudied how LECs can specifically modulate complex immune responses such as infection or immunization.

Due to this lack of knowledge, we investigated the hypothesis that the VEGFR-3 axis and LECs could modulate the immunization response. We found that the VEGFR-3 axis regulates antigen-specific IgG1 class switch, without altering class switch to other IgG subclasses. Upon VEGFR-3 stimulation, we observe an increased number of lymph node LECs, and a corresponding increase in Th2 cytokine production that coincides with an increase in IgG1. With ablation of VEGFR-3 specifically on LECs, there is a reduction in IgG1 class-switch, thus demonstrating the role of LECs as the key cell type modulating class-switch in this model. Stimulation of VEGFR-3 during immunization further leads to increased accumulation of CD4 T cells that express IL-4, but not in total IL-4 expressing immune infiltrates, suggesting a selective interaction with CD4 T cells. We observe that MHC II on LECs drives this VEGFR-3 dependent increase in Th2 cytokines that are likely to drive class switch, and it further restricts IFN-γ secretion in restimulated T cells in a non-VEGFR-3 dependent manner. Together, these data indicates the LECs are critical for directly modulating CD4 T cell polarization in an MHC II dependent manner, and that this polarization has the downstream functional implication of increasing IgG1 class-switch, without substantial alterations to total IgG class-switch.

2.3 Results

2.3.1 VEGFR-3 blockade selectively antagonizes IgG1 in an immunization model

Previous work has shown that the presence of lymphatics in the skin promotes humoral immunity, as mice that lacked dermal lymphatics have reduced antibody titers after immunization with either LPS or alum [5]. Thus we first assessed whether VEGFR-3 blockade

modulates antibody levels. We used CpG (ODN 1826, Trilink) and chicken ovalbumin (OVA) as our model immunization. We blocked VEGFR-3 through intraperitoneal (i.p.)

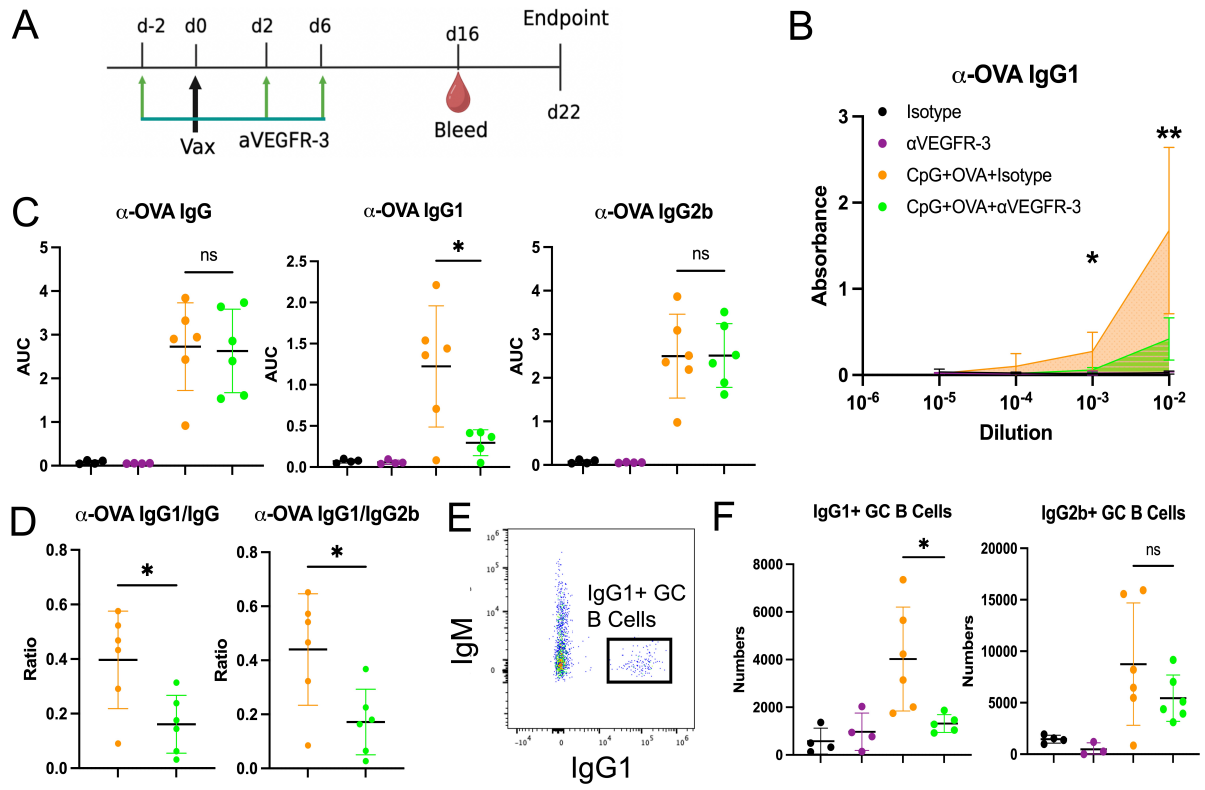

Figure 2.1: **VEGFR-3 blockade selectively antagonizes IgG1 in an immunization model** | (A) Schematic of experimental timeline. Mice were vaccinated with 10 μg CpG-B (ODN 1826) and 10 μg OVA. Mice were treated with either α-VEGFR-3 blocking antibody (clone mF4-31C1) or isotype control as shown. (B) Dilution curve showing α-OVA antibody levels by ELISA (C) Quantification of area under the dilution curve (AUC) of α-OVA IgG, IgG1, and IgG2b (D) Ratio of α-OVA IgG1 AUC to total α-OVA IgG AUC and α-OVA IgG2b AUC (E) Sample flow plot showing IgG1+ Germinal Center (GC) B cells by flow cytometry (B220+CD19+IgD-GL-7+CD95+) (F) Total counts of IgG1+ and IgG2b+ GC B cells by flow cytometry

injections of a monoclonal α-VEGFR-3 blocking antibody (mF4-31C1, Eli Lilly) as shown (**Fig 2.1A**). After waiting about two weeks for B cell class switch to occur and for antibodies to be secreted, we bled mice to assess antigen specific antibody plasma levels via ELISA. We observed that blocking VEGFR-3 did not alter total α-OVA IgG levels, nor did it alter α-OVA IgG2b levels, but blocking did reduce α-OVA IgG1 levels (**Fig 2.1B-C**). To assess if

this reduction in α-OVA IgG1 was indeed selective, the ratio of α-OVA IgG1 was normalized to the total α-OVA IgG amount, and indeed we observed a selective decrease in this ratio upon VEGFR-3 blockade (**Fig 2.1D**). We subsequently normalized α-OVA IgG1 to α-OVA IgG2b levels to assess whether this decrease in IgG1 did not correspond with a decrease in IgG2, and we still observed this selective decrease (**Fig 2.1D**). Next, to ascertain if this decrease of antigen specific IgG1 levels by blockade of the VEGFR-3 axis also corresponded to decrease of IgG1+ B cells in the immunization draining lymph node (idLN), flow cytometry was performed on the idLN and GC B cell subclass was assessed. Consistent with the α-OVA plasma antibody levels, we also observed a decrease in IgG1+ germinal center B cell numbers, but not IgG2b+ germinal center B cells (**Fig 2.1E-F**). Thus VEGFR-3 blockade antagonizes IgG1 formation as evidenced by selective decreases in antigen specific IgG1 and a decrease in IgG1+ GC B cells in the immunization draining LN.

2.3.2 VEGFR-3 blockade reduces LN LECs and promotes secretion of interferon gamma independent of CCL21

We next verified that VEGFR-3 blockade actually reduced idLN LEC expansion. We immunized mice and blocked VEGFR-3 as shown (**Fig 2.2A**). Near the peak of the inflammatory phase, idLN were harvested, digested and analyzed by flow cytometry for LECs. Validating the efficacy of our VEGFR-3 blockade, we did observe a decrease in LECs as a fraction of all CD45- cells (**Fig 2.2B**). With the efficacy of the VEGFR-3 blockade verified, we next probed for what may explain this difference in antibody subclass.

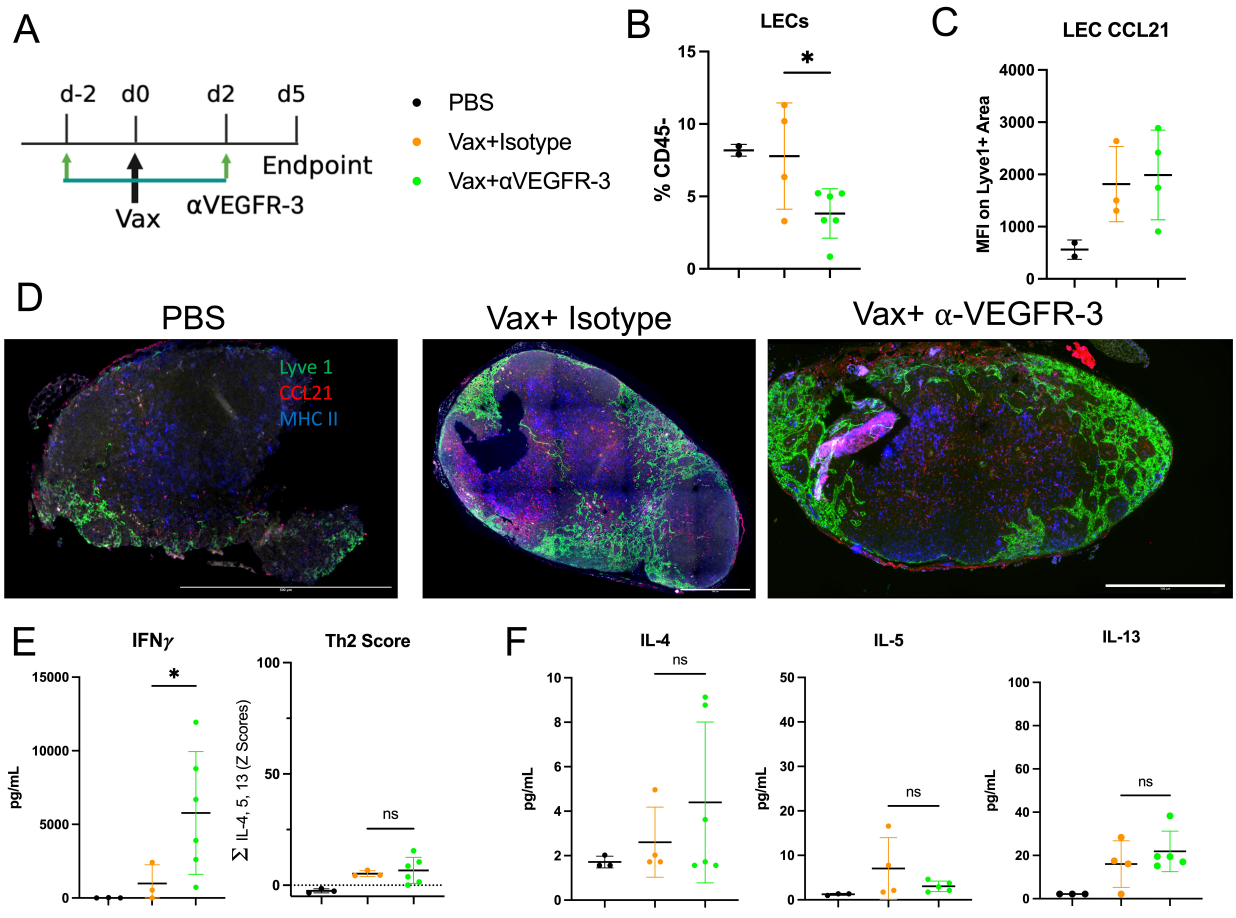

Figure 2.2: **VEGFR-3 blockade reduces LN LECs and promotes secretion of IFN-γ independent of CCL21**| (A) Schematic of experimental timeline. Mice were vaccinated with 10 μg CpG-B (ODN 1826) and 10 μg OVA. Mice were treated with either α-VEGFR-3 blocking antibody (clone mF4-31C1) or isotype control as shown (A). (B) LECs (CD45-CD31+gp38+) quantified via flow cytometry. (C) LEC CCL21 quantified as the CCL21 MFI on the Lyve1+ area as determined by immunofluorescence. (D) Representative immunofluorescence of Lyve1 (green), CCL21 (red), and MHC II (blue) of lymph node sections. Scale bar= 500 μm. (E-F) LNs were restimulated with OVA protein for 4 days and supernatant was assessed by Legendplex for cytokine production. (E) Interferon gamma (IFN-γ) and Th2 cytokine production by OVA-restimulated lymph node cells as quantified by ELISA. (F) Individual Th2 cytokines from LN restimulations shown.

We hypothesized the cytokines derived from T cells in the lymph node during the inflammatory peak could be involved in antagonizing this class-switch to IgG1: specifically IFN-γ and the Th2 cytokines: IL-4, IL-5, and IL-13. Canonically, IFN-γ antagonizes IgG1 class-

switch and IL-4 promotes IgG1 class-switch [103]. Furthermore, IL-13 has certain homology to IL-4 promotes subclass switch IgG1 and IL-4-/- mice can even produce modest amounts of IgG1 in an IL-4-independent methods [82]. Lastly, IL-5 can both induce some IgG1 class-switch by itself and augment IL-4 induced IgG1 class-switch [104, 105]. We immunized mice and blocked VEGFR-3 as shown (**Fig 2.2A**). We harvested, digested, and restimulated idLNs ex vivo with the immunization antigen, OVA. We observed in these restimulated LNs that IFN-γ secretion was increased upon VEGFR-3 blockade, with no corresponding alteration in the type 2 cytokines, as shown by a "Th2 score" or the normalized summation of IL-4, IL-5, and IL-13 (**Fig 2.2E**). Furthermore, if we focus on the Th2 cytokines individually, we saw no individual differences in any of these cytokines. Thus, an increase in IFN-γ, with no corresponding change in the type 2 cytokines could be sufficient to antagonize IgG1 formation (**Fig 2.2F**).

We lastly assessed LEC CCL21 as we hypothesized whether VEGFR-3 blockade altered CCL21 expression by LECs and whether this could have downstream effects that could alter the recruitment of IFN-γ producing cells. LECs are a major source of CCL21, and CCL21 is essentially for the migration of CCR7+ cells which include dendritic cells and naive and memory T cells [98, 106]. We performed immunofluorescence on parrafin sections to assess CCL21 levels, and specifically to assess CCL21 expression by Lyve1+ cells (LECs). Interestingly, though we did observe an increase in expression by LECs CCL21 due to immunization, we did not observe an alteration in LEC CCL21 levels upon VEGFR-3 blockade (**Fig 2.2C**). Of note, it is clear that other cells are producing CCL21 since there is substantial CCL21 staining distal to LECs near MHC II+ cells (**Fig 2.2D**). Thus, VEGFR-3 blockade reduces LN LECs as a fraction of CD45- cells, promotes IFN-γ secretion in restimulated LNs, but does not alter LEC expression of CCL21.

2.3.3 VEGFR-3 stimulation via a VEGFR-3 selective agonist has dose dependent effects on LN LECs

We next queried whether VEGFR-3 stimulation would lead to the reciprocal phenomenon, and thus lead to an increase in IgG1. However, we first needed to ascertain what dose of VEGF-C_{C156S} would induce LEC expansion via local delivery as we had no preliminary data to indicate the ideal dose. We injected VEGF-C_{C156S} locally in all 4 hocks, just as we would vaccinate the mice, either 50 ng or 250 ng of VEGF-C_{C156S} per hock, or PBS as a negative control (**Fig 2.3A**). We injected 5 total times to maintain VEGF-C levels and maximize potential LEC proliferation. Interestingly we found that only the 50 ng dose of VEGF-C_{C156S} induced LN LEC expansion, without substantial alterations to other stromal cells (fibroblastic reticular cells (FRCs) and blood endothelial cells (BECs)) (**Fig 2.3B**). When normalizing LEC numbers to other stromal subsets, we observe that this expansion of LECs is specific (**Fig 2.3C**). It is an interesting to note that while VEGFR-3 stimulation specifically expands LECs in the stromal compartment, the 50 ng dose also led to increased total immune infiltrates (**Fig 2.3D**); however, due to the essential role of LECs in immune cell trafficking, we hypothesize this enhanced immune trafficking is an unavoidable effect of expanding LECs. Thus, this is likely not some direct effect of VEGFR-3 stimulation on immune cells. We do not see alteration in immune cells with the high dose of VEGF-C_{C156S} and LECs were not expanded compared to control mice. It has been reported that high doses of VEGF-C can condition LECs to downregulate VEGFR-3 and thus lose responsiveness to VEGFR-3 stimulation and downstream proliferation [107]. Thus it may be critical note for future work that there may be a "Goldilocks zone" of VEGFR-3 stimulation appropriate to induce lymphangiogenesis: too little, and there is not sufficient VEGFR-3 stimulation and downstream phosphorylation and signalling, while too much would lead to the downregulation of responsiveness towards VEGFR-3 stimulation. In both cases, the result would be a lack of lymphangiogenesis. Fortunately, we found that 50 ng of VEGF-

C_{C156S} is sufficient to induce LN lymphangiogenesis in a non-inflammatory environment, and we will proceed using this dose for all future experiments.

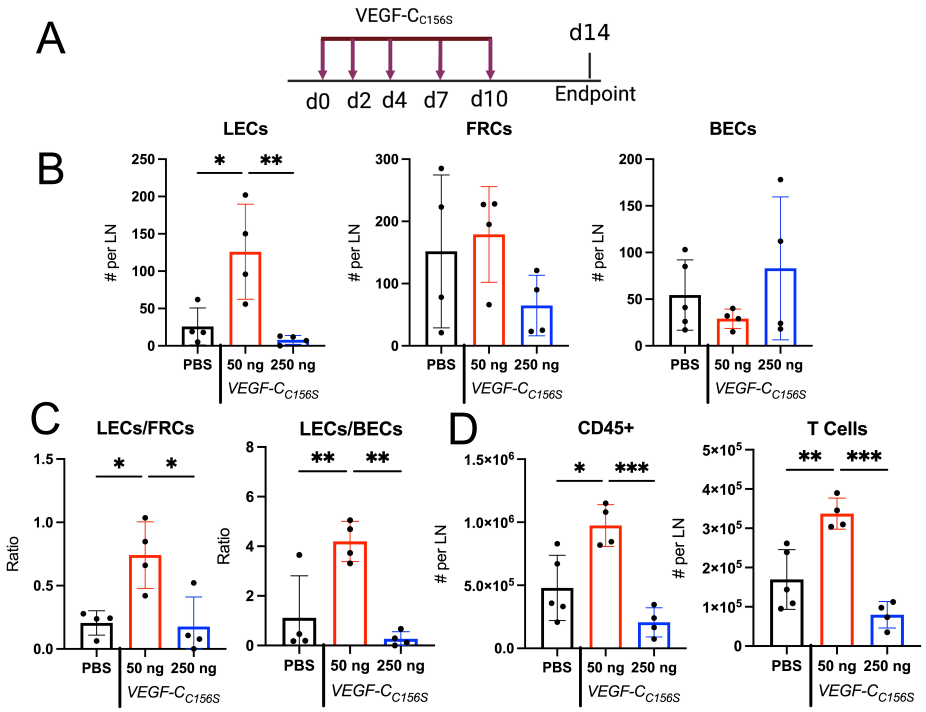

Figure 2.3: **50 ng of VEGF-C_{C156S} is sufficient to induce LN LEC Proliferation while 250 ng is not** | C57BL/6 mice were injected in all 4 hocks with either 50 ng VEGF-C_{C156S}, 250 ng VEGF-C_{C156S}, or 25 μL of PBS as shown. (A) Experimental schedule (B) Stromal subset counts as quantified via flow cytometry: LECs (CD31+gp38+), BECs (CD31+gp38-), and FRCs (CD31-gp38+) (C) Ratio of LECs to the LN stromal FRCs and BECs. (D) Counts of CD45+ cells and T Cells (CD45+CD3+) cells as quantified by flow cytometry

2.3.4 VEGFR-3 stimulation selectively enhances IgG1 formation due to immunization

Using this dose of VEGF-C_{C156S}, we queried whether VEGFR-3 stimulation would lead to the reciprocal phenomenon, and thus lead to an increase in IgG1. We stimulated VEGFR-3 with VEGF-C_{C156S} and immunized mice as shown (**Fig 2.4A**). We observed increases in α-OVA IgG1 levels in the plasma but did not observe significant increases in total α-OVA

IgG (**Fig 2.4B-C**). When normalizing α-OVA IgG1 to total α-OVA IgG, we observed an increase in this ratio upon VEGFR-3 stimulation, thus confirming the selectivity of this increase (**Fig 2.4D**). Consistently, we further saw an increase in IgG1+ germinal center B cell numbers (**Fig 2.4E**). Together, this demonstrates that VEGFR-3 stimulation promotes IgG1 class-switch and that the VEGFR-3 axis selectively modulates antigen specific IgG1 plasma levels, but not total antigen specific antibodies.

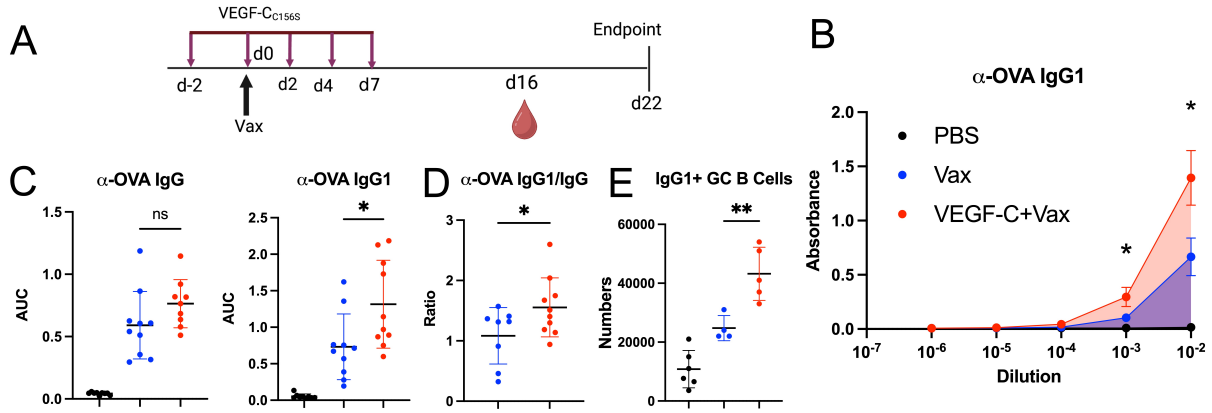

Figure 2.4: **VEGFR-3 stimulation during immunization promotes increased IgG1 class switch**| Schematic of experimental timeline. Mice were vaccinated with 10 μg CpG-B (ODN 1826) and 10 μg OVA. Mice were treated with either VEGFR-3 agonist (VEGF-C_{C156S}) or PBS in vaccine site as shown.(B) Dilution curve showing α-OVA antibody levels by ELISA (C) Quantification of area under the dilution curve (AUC) (D) Ratio of α-OVA IgG1 AUC to total α-OVA IgG AUC (E) Total counts of IgG1+ Germinal Center (GC) B cells by flow cytometry (B220+CD19+IgD-GL-7+CD95+)

2.3.5 VEGFR-3 stimulation selectively upregulates Th2 cytokine secretion in restimulated lymph nodes but does not alter LEC CCL21 expression

We next analyzed the cytokine secretion during the peak of the inflammatory response using the experimental schedule shown (**Fig 2.5A**), but first wanted to assess whether VEGFR-3 stimulation was actually expanding idLN LECs. We already established this dose of VEGF-C_{C156S} is sufficient to increase LEC numbers in the draining LN, but wanted to verify that this dose still increased LEC numbers in the context of the immunization. We

performed immunofluorescence to stain for LECs and performed microscopy of whole LN sections. Using this imaging, we quantified Lyve1 to ascertain the LEC area relative to the LN area, and observed a significant increase in LECs by area using this quantification (**Fig 2.5B,D**). Thus this 50 ng of VEGF-C_{C156S} still expands LECs in the immunization context. Next, we restimulated lymph nodes with OVA to assess the cytokine secretion as done previously. Since VEGFR-3 blockade increases IFN-γ, we hypothesized that VEGFR-3 stimulation would reduce it and that this reduction of an IgG1 antagonist would be sufficient to increase IgG1 levels. Surprisingly, we actually observed an increase in IFN-γ secretion, but critically also observed an increase in the Th2 cytokine score (**Fig 2.5E**). Individually, we see a significant increase in IL-13, though IL-4 and IL-5 may follow this trend as well (**Fig 2.5F**). This increase in type 2 cytokines collectively may be sufficient to drive the increased IgG1 class-switch we observe due to VEGFR-3 stimulation, even in the context of more IFN-γ. Thus our initial hypothesis was incorrect, but the observed increase in Th2 cytokines may be sufficient to explain the phenomenon.

While we posit that this increase in Th2 cytokines would promote IgG1 class switch, we wanted to assess in the context of VEGFR-3 stimulation if CCL21 was altered. Even though VEGFR-3 blockade did not alter CCL21 expression, it has been published that VEGF-C increases LEC secretion of CCL21 [108]. Thus, despite our previous data, we still decided to assess if this phenomenon was occurring in our model. Using the same immunofluorescence microscopy as described previously, we assessed the expression of CCL21 on the Lyve1+ area as quantified by MFI, and did not observe any change in LEC CCL21 due to VEGFR-3 blockade (**Fig 2.5C**. Thus we observed that while VEGFR-3 stimulation expands LN LECs and increases Th2 cytokines, this effect appears to be independent on any regulation of CCL21.

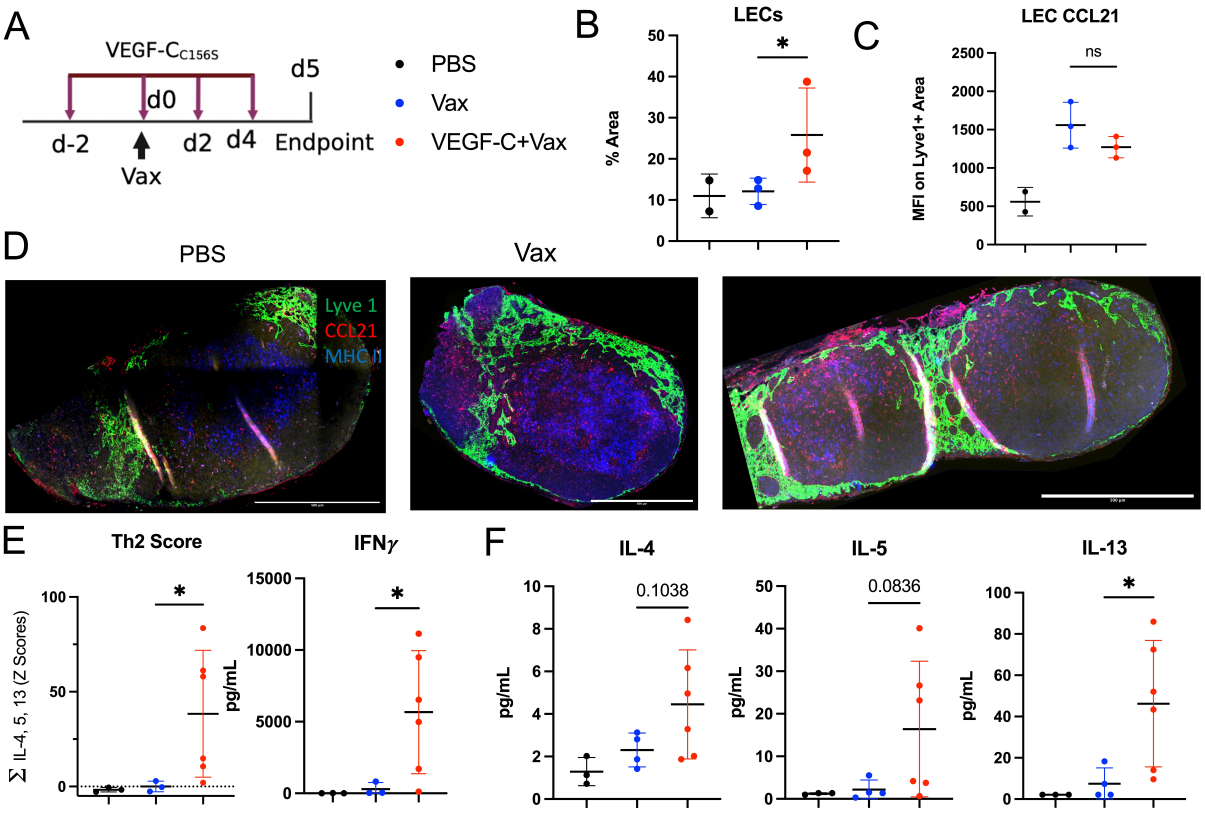

Figure 2.5: **VEGFR-3 stimulation selectively upregulates Th2 cytokine secretion in restimulated lymph nodes but does not alter LEC CCL21 expression**| (A) Schematic of experimental timeline. Mice were vaccinated with 10 μg CpG-B (ODN 1826) and 10 μg OVA. Mice were treated with either VEGFR-3 agonist (VEGF-C_{C156S}) or PBS in vaccine site as shown. (B) LECs quantified from immunofluorescence (Lyve1+ % area) (C) LEC CCL21 quantified as the CCL21 MFI on the Lyve1+ area as determined by immunofluorescence. (D) Representative immunofluorescence of Lyve1 (green), CCL21 (red), and MHC II (blue) of lymph node sections. Scale bar= 500 μm. (E) Interferon gamma (IFN-γ) and Th2 cytokine production by OVA-restimulated lymph node cells as quantified by ELISA. (F) Individual Th2 cytokines from LN restimulations shown.

2.3.6 VEGFR-3 stimulation during immunization increases Th2 cytokine secretion by CD4 T cells, but the addition of OT-IIs has unclear effects

To look more specifically at CD4 T cells, which would be the key cell type involving in "helping" B cells and can make all the Th2 cytokines, we utilized the OT-II transgenic CD4 T cells. OT-II CD4 T cells are specific to the peptide $OVA_{323-339}$, which is the immun-

odominant CD4 T cell epitope to OVA. Furthermore, these transgenic T cells are labelled with the CD45.1 congenic marker, which allows for easy identification by flow cytometry. This gives us the ability to analyze antigen specific CD4 T cell responses by flow cytometry. We performed the experiment as shown (**Fig 2.4A**), except that one day before immunization, we adoptively transferred in 100,000 isolated OT-II CD4 T cells by i.v. injection. At endpoint, we evaluated the cytokine secretion by restimulating using the $OVA_{323-339}$ peptide, we observed an increase in the Th2 cytokines, both collectively and individually (**Fig 2.6A-B**). Interestingly, we did not observe any increase in IFN-γ (**Fig 2.6A**) Thus, VEGFR-3 stimulation enhances Th2 cytokine secretion of CD4 T cells, but does not alter IFN-γ secretion.

While we observed an increased in CD4 T cell secretion of Th2 cytokines, we next wanted to assess the phenotype of these antigen specific CD4 T cells. We observe that VEGFR-3 stimulation induces a trending increase in OT-II infiltration in the lymph node but that it does not alter T_{Reg}s and Th1 polarization (**Fig 2.6C**). Interestingly, VEGFR-3 stimulation may lead to a trending increase in both the Th2 and Tfh compartments (**Fig 2.6C**). Furthermore, we do not detect any difference in central memory or effector/memory phenotypes of these OT-IIs (**Fig 2.6D**). Thus VEGFR-3 does not have a dramatic effect on the polarization or phenotype of OT-IIs, but it may enrich for Th2s.

For a more unbiased analysis, we next performed supervised clustering using FlowSom. We observe 3 distinct T_{Reg} clusters out of 8 total clusters as shown by the expression of Foxp3 and CD25. We observe two distinct clusters that express Rorγt (Cluster 2 and Cluster 5), as well as an undifferentiated naive like cluster (Cluster 1) and a Tfh-like cluster (Cluster 0) (**Fig 2.7A**). While we observe a distinct Th1 cluster (Cluster 4), we do not observe a distinct Th2 cluster (**Fig 2.7A**). When quantifying the clusters as a fraction of total OT-IIs, we do not observe any notable differences in the clusters (**Fig 2.7B**). Thus while clustering does produce distinct clusters, further insights into the phenotype of the OT-IIs are not

unveiled.

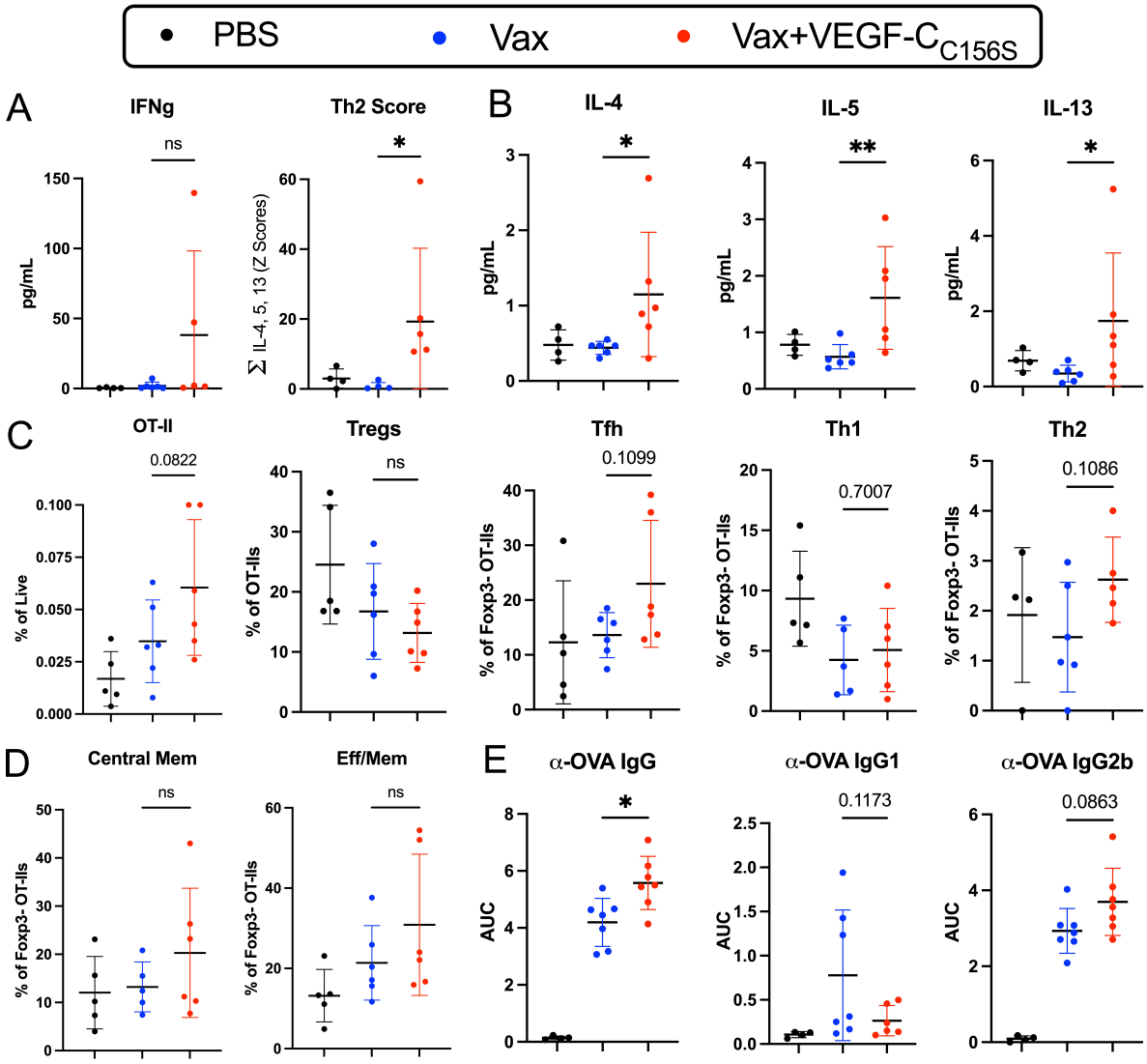

Figure 2.6: **VEGFR-3 stimulation during immunization increases Th2 cytokine secretion by CD4 T cells, but does not substantially alter the phenotype of adoptive transferred antigen specific CD4 T cells and disrupts IgG1 class switch** | C57BL/6 mice were injected in all 4 hocks with either 50 ng VEGF-C_{C156S} or 25 μL of PBS as shown in Fig 2.4A. One day before immunization, 100,000 isolated OT-II CD4 T cells were i.v. injected into all mice. (A) Cytokine secretion of IFN-γ and total Th2 cytokines of $OVA_{323-339}$ restimulated LNs by ELISA (B) Individual Th2 cytokines of restimulated LNs (C-D) OT-IIs (CD45.1+CD3+CD4+) analyzed via flow cytometry see Figure 2.16 for complete gating strategy (E) Day 18 plasma levels of antigen-specific antibodies analyzed by ELISA

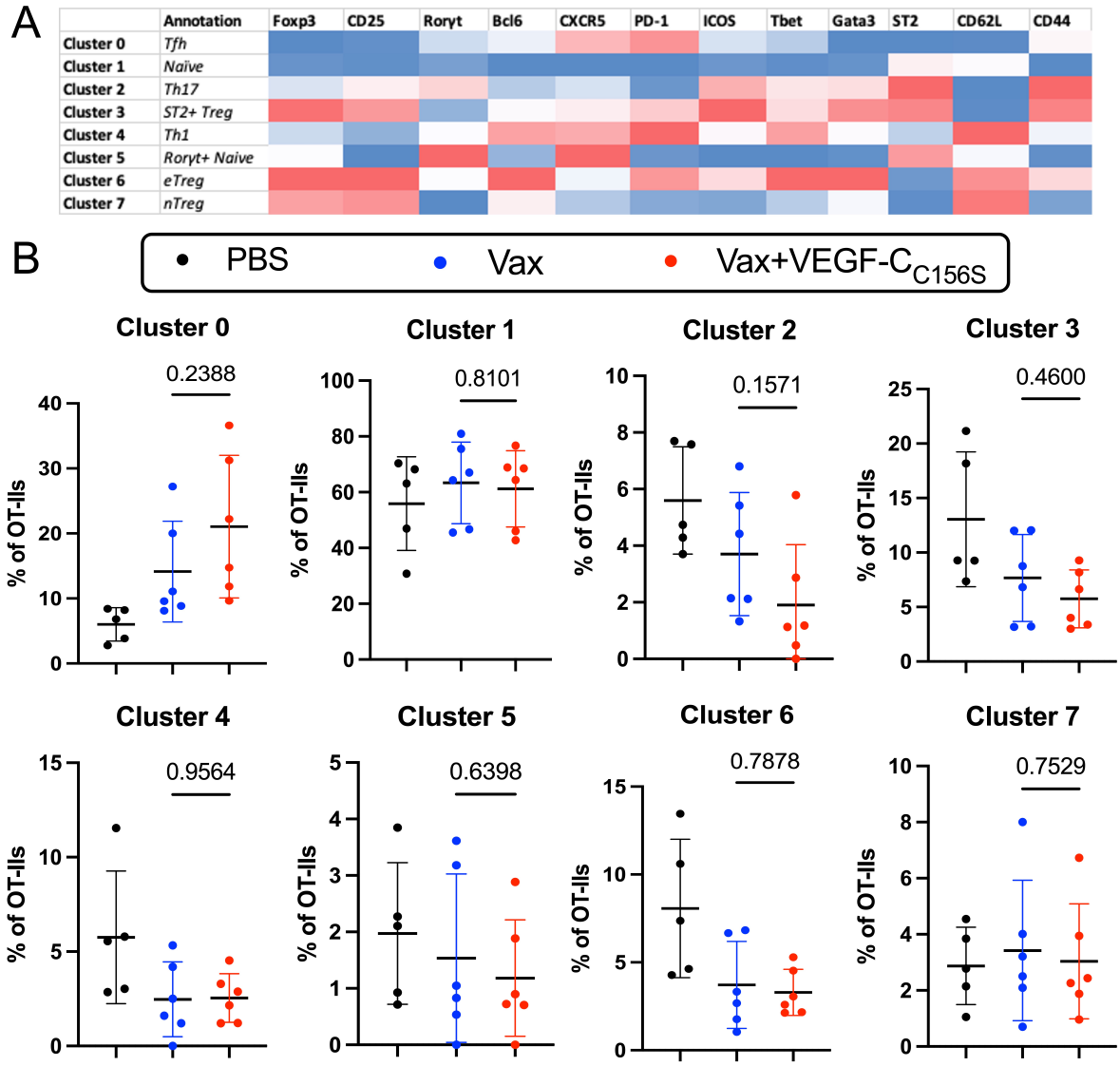

Figure 2.7: **Unsupervised clustering of exogenous antigen specific CD4 T cells does not reveal differences in T cell polarization** | Mice were treated as described in Fig 2.6A. LNs were digested, filtered, and resuspended in a single cell suspension (A) Heatmap of expression of FlowSom clusters of concatenated OT-IIs (B) Proportions of each cluster as a fraction of total OT-IIs

What makes this data more difficult to interpret, is that the transfer of OT-IIs disrupted the VEGFR-3 dependent increase in IgG1 (**Fig 2.6E**). Thus we hesitate to perform subsequent experiments to attempt to elucidate further insights about VEGFR-3 stimulation's effect on antigen specific CD4 T cells. In the future, it may be useful to titrate down the

transferred dose of OT-IIs until we still observe the increase in IgG1, and then perform the phenotyping analysis by flow cytometry. However, for now we decided to move on using $OVA_{323-339}$ peptide restimulations as our main readout for antigen specific CD4 T cell responses.

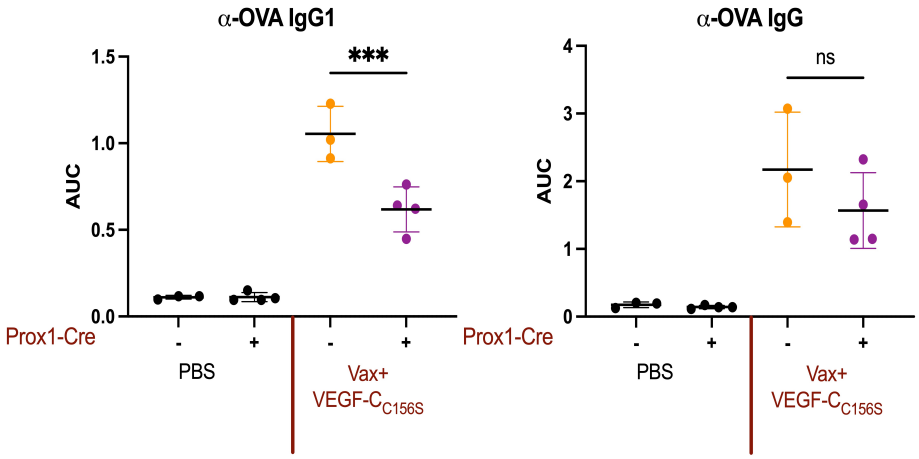

Figure 2.8: **VEGFR-3 on LECs is Necessary to Promote Elevated IgG1 Levels after VEGFR-3 Stimulation** | LEC-specific (Prox1) inducible VEGFR-3 KO (Prox1CreER^{T2}-VEGFR-3$^{lox/lox}$) or VEGFR-3$^{lox/lox}$ littermate control mice were subjected to CpG-driven inflammation and modulated with VEGF-C$_{C156S}$ as shown in Fig 2.4A. 2 weeks before vaccination mice were given tamoxifen daily for 7 days to activate Cre recombinase activity. α-OVA IgG and IgG1 shown as quantified by ELISA.

2.3.7 VEGFR-3 on LECs is necessary to promote elevated IgG1 levels after VEGFR-3 stimulation

While VEGFR-3 is generally considered selective towards LECs, it can be expressed by other cell types in inflammatory contexts [109]. To ensure that this IgG1 class-switch induced by VEGFR-3 stimulation was LEC VEGFR-3 dependent, we used an inducible, conditional knockout of VEGFR-3 in Prox1 expressing cells (LECs). After tamoxifen application for 7 consecutive days and subsequent resting for 7 days, mice were injected with VEGF-C$_{C156S}$ and vaccinated as shown (**Fig 2.4A**). Mice were bled at endpoint and plasma antibodies were analyzed by ELISA. We observed that upon loss of VEGFR-3 in Prox1-expressing cells,

that α-OVA IgG1 levels were decreased while total α-OVA IgG levels were unaltered (**Fig 2.8**). Thus LEC VEGFR-3 is necessary to promote maximal α-OVA IgG1, but not total α-OVA IgG levels, in this model.

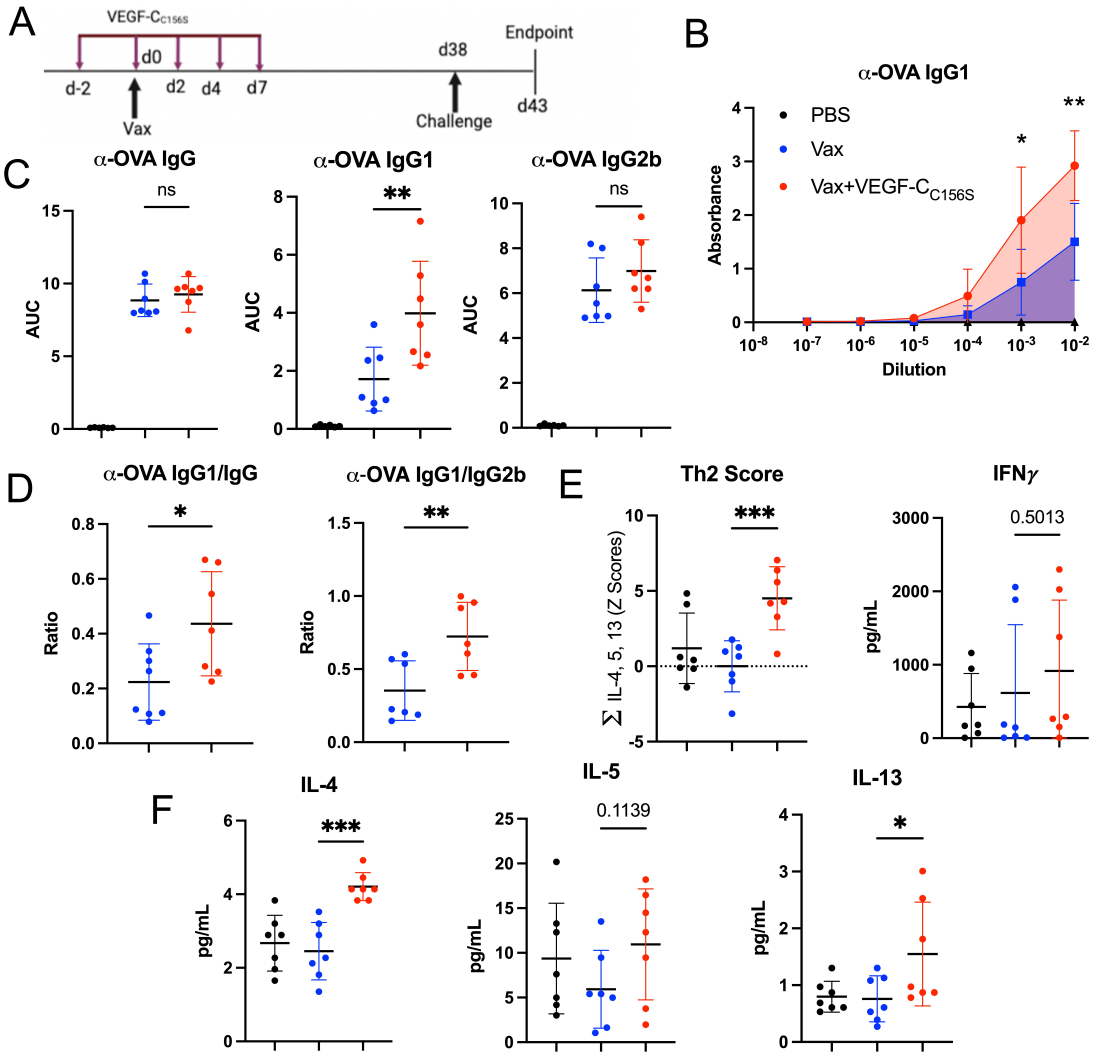

Figure 2.9: **VEGFR-3 dependent type 2 biasing persists after recall**| (A) Schematic of experimental timeline. Mice were vaccinated with CpG/OVA or PBS and were injected with either VEGF-C_{C156S} or PBS. All mice were challenged 5 days before endpoint with CpG/OVA. (B) Dilution curve showing α-OVA antibody levels by ELISA (C) AUC of α-OVA antibodies from plasma as quantified by ELISA at endpoint (D) Ratios of α-OVA IgG1 to total of α-OVA IgG and α-OVA IgG2b. (E-F) Quantification of cytokine secretion by $OVA_{323-339}$ restimulated lymph node cells as measured by ELISA

2.3.8 VEGFR-3 dependent type 2 biasing persists after recall

We next assessed if this polarization would still be maintained with a secondary inflammatory stimulus. We treated the mice as shown and all mice were recalled in vivo with CpG/OVA (**Fig 2.9A**). Mice were euthanized in the inflammatory phase and plasma antibodies and cytokine secretion of T cells were assessed. We first analyzed the plasma antibody levels and observed the same increase in α-OVA IgG1, but no change in total α-OVA IgG (**Fig 2.9B-C**). When normalizing to total α-OVA IgG and α-OVA IgG2b, we observe that this increase is still selective, as we have observed previously without recall (**Fig 2.9D**). Next, we assessed the cytokine secretion of the CD4 T cells via restimulation with $OVA_{323-339}$. We observed an increase in the Th2 cytokine score and of IL-4 and IL-13 individually, but no alterations in the antagonistic IFN-γ (**Fig 2.9E-F**). Thus, after recall in vivo this type 2 polarization due to VEGFR-3 stimulation persists.

2.3.9 VEGFR-3 stimulation increases IL-4 expressing CD4 T cells after immunization

Though we have established that VEGFR-3 stimulation during immunization promotes type 2 immunity, we wanted to explore what could cause this elevated Th2 cytokine secretion that drives this increased class-switch. This led us to first look more in depth at IL-4. One of the old paradoxes of immunology is that you need IL-4 to make more IL-4 [110] and IL-4 is one of the most potent factors involved in differentiation CD4 T cells into Th2 effectors that would produce the canonical Th2 cytokines: IL-4, IL-5 and IL-13 [111]. We queried whether VEGFR-3 stimulation could alter early IL-4 producing populations in the acute inflammatory phase, which could seed the idLN with IL-4 to promote Th2 polarization and further increases in Th2 cytokines.

To assess the cell populations that express IL-4 in vivo, we utilized an IL-4 reporter mouse (4get) upon which enhanced green fluorescence protein (EGFP) is expressed under the IL-4

promoter [112], allowing reliable in vivo tracking of IL-4 producing cells. We treated mice as previously shown (**Fig 2.5A**), digested lymph nodes, and analyzed by flow cytometry (**Fig 2.10A**). First, we assessed the proportion of all immune cells that expressed IL-4, and showed that the dominant fraction was CD4 T cells (**Fig 2.10B**). Upon immunization, the fraction of IL-4 expressing cells that are CD4 T cells does not substantially change, but upon VEGFR-3 stimulation the fraction of IL-4 expressing cells that are CD4 T cells increases while VEGFR-3 stimulation doesn't appear to substantially alter other IL-4 expressing populations (**Fig 2.10B**). Next we analyzed the number of IL-4 expressing cells to quantify this difference, and we observed a trending increase in IL-4 expressing CD4 T cells; however, when we phenotype these cells using CD44 and CD62L, we see a significant increase in IL-4 expressing effector-memory (CD44+CD62L-) CD4 T cells (**Fig 2.10C**). We next assessed if the expression level of IL-4 was altered as well, and did not observe any difference in the MFI of EGFP on the IL-4 expressing (EGFP+) cells (**Fig 2.10E**). Lastly, we did not detect differences in many other IL-4 expressing populations including macrophages and CD8 T cells (**Fig 2.10C-D**). Interestingly, we did observe an increase in IL-4 expression by LECs due to VEGFR-3 stimulation, but as LECs are a very small fraction of not a large population of cells, this results in less than 1% of total IL-4 expressing cells (**Fig 2.10D**). We also do not observe alterations to total CD45+ infiltrates that express IL-4 (**Fig 2.10C**). Thus, VEGFR-3 stimulation specifically increases the numbers of IL-4 expressing CD4 T cells, but not the expression level of IL-4, during the acute inflammatory phase of the immunization.

We next performed immunofluorescence microscopy to assess if LECs were in contact with IL-4 expressing cells as well as attempting to assess through a secondary method whether LECs were actually expressing IL-4. While we see clear colocalization of Lyve1+ LECs and

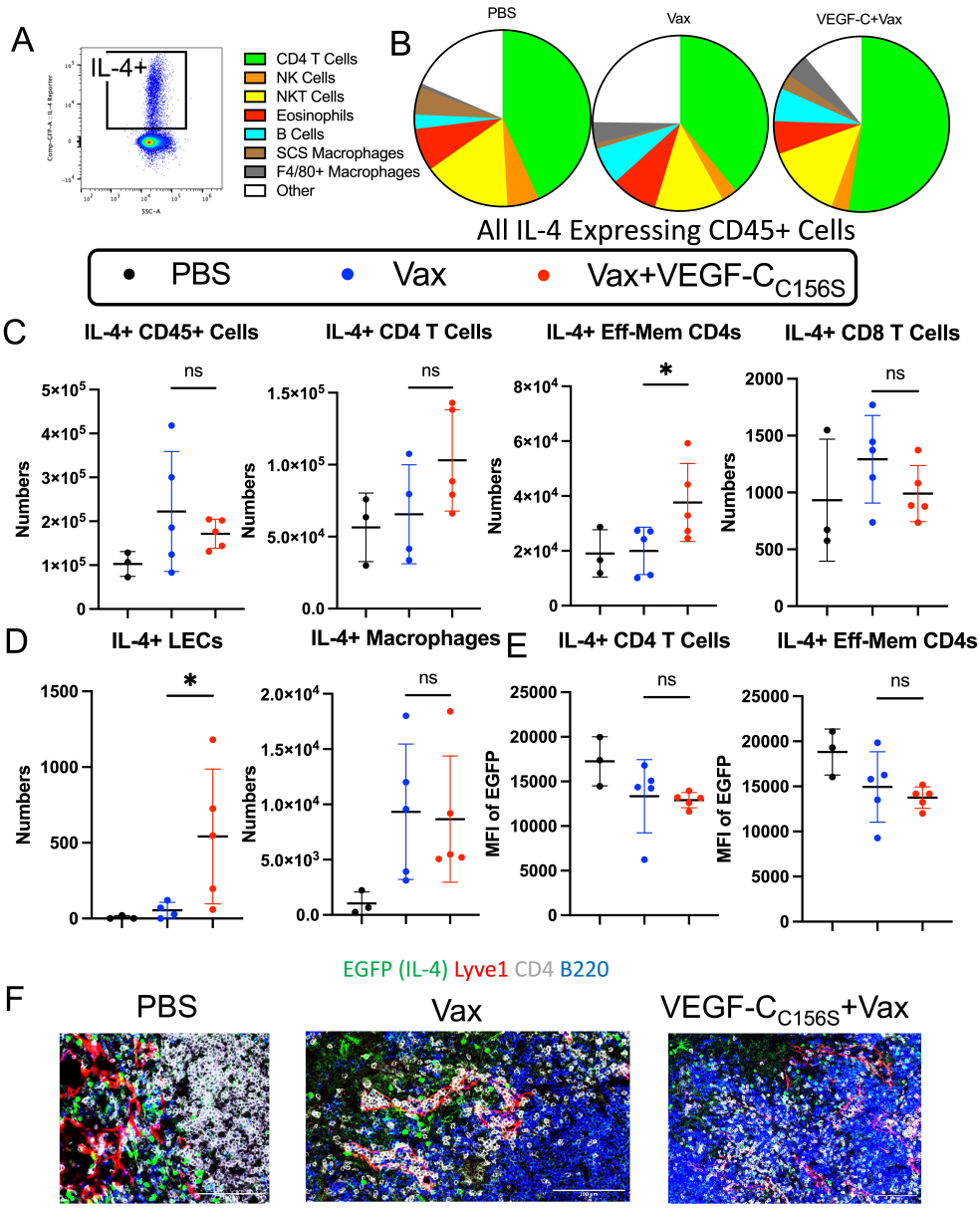

Figure 2.10: **VEGFR-3 stimulation increases accumulation of IL-4 expressing CD4 T cells in the lymph node, but does not alter expression level of IL-4** | (A) IL-4 reporter (4get) mice were immunized and dosed with VEGF-C_{C156S} as shown in Fig 2.5A. (A) Sample flow plot showing IL-4 expressing (EGFP+) cells (B) Pie chart showing IL-4 expressing populations (C) Numbers of IL-4 expressing cell populations as quantified by flow cytometry (D) MFI on EGFP on IL-4 expressing CD4 T cells as quantified by flow cytometry (E) Representative immunofluorescence images of IL-4 expression in lymphatic rich areas of idLN. EGFP (green), Lyve1 (red), CD4 (white), B220 (blue). Scale bar= 100 μm

IL-4 expressing CD4 T cells, we did not observe IL-4 expression directly by the LECs in any of

the images (**Fig 2.10F**). This colocalization was independent of VEGFR-3 stimulation as it occurred in all three conditions (**Fig 2.10F**), but due to the fact that VEGFR-3 stimulation promoted increased effector-memory IL-4 expressing CD4 T cells as well as expanding LECs, it is likely that this interaction would occur more frequently. Thus, VEGFR-3 stimulation promotes increased numbers of IL-4 expressing effector-memory CD4 T cells and these IL-4 expressing cells can be in contact with LECs.

2.3.10 MHC II on LECs is required for the VEGFR-3 dependent upregulation of Th2 cytokine secretion by CD4 T cells

Due to the observed colocalization of LECs and IL-4-expressing CD4+ cells, we next assessed whether there was a direct interaction with the LEC and CD4 T cell that could cause this skewing towards IL-4 expression and downstream type 2 cytokine production. LECs express MHC II, and thus potentially LECs could interact with with CD4 T cells as APCs and cause this increased Th2 polarization of CD4 T cells [102]. To address this question, we crossed Prox-1-CreER^{T2} mice with MHC II$^{fl/fl}$ mice (MHC II$^{\Delta Prox1}$ mice) to allow selective deletion of MHC II in LECs upon tamoxifen treatment. MHC II$^{fl/fl}$ mice were used as controls (MHC II^{WT}). MHC II$^{\Delta Prox1}$ mice and MHC II^{WT} mice were all treated with tamoxifen for 5 consecutive days and then rested for a week before experimental onset. Mice were treated as shown (**Fig 2.11A**). Lymph nodes were restimulated with OVA and cytokine secretion was analyzed. We observed that littermate control mice had increased Th2 cytokine secretion upon VEGFR-3 stimulation, but no alteration of IFN-γ secretion. However, in mice that lacked MHC II on LECs, there was no corresponding increase in Th2 cytokine secretion due to VEGFR-3 stimulation (**Fig 2.11C-D**). Most critically, when looking at IL-4 separately, we observe that this holds (**Fig 2.11D**). Surprisingly, we observed an increase in secreted IFN-γ in these mice compared to controls, but that this increase was not VEGFR-3 dependent (**Fig 2.11C**). Thus, MHC II on LECs is required for this

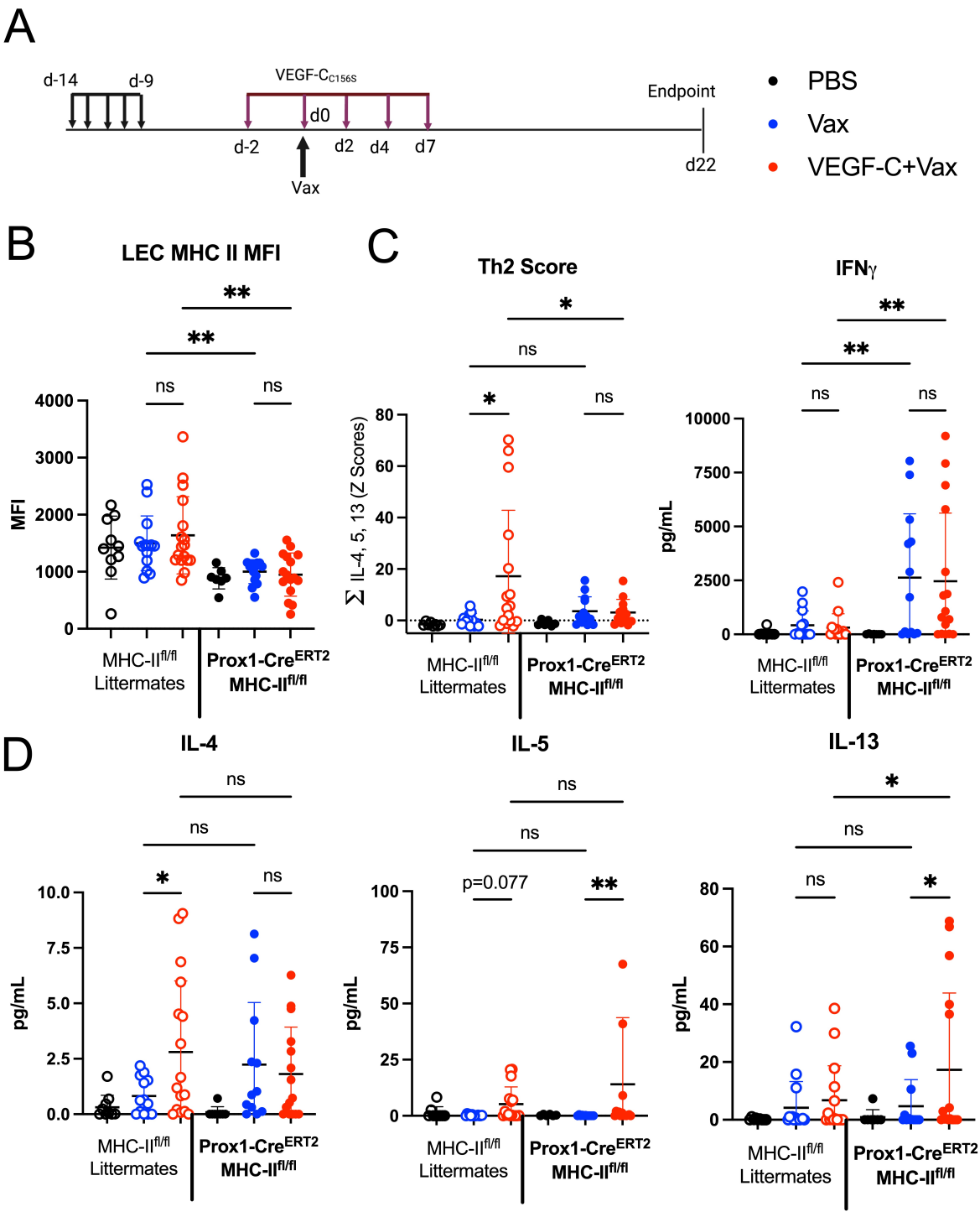

Figure 2.11: **MHC II on LECs restrains IFN-γ secretion by CD4 T cells and is required for the VEGFR-3 dependent upregulation of Th2 cytokines**| Prox1CreER^{T2}-MHC II$^{lox/lox}$ or MHC II$^{lox/lox}$ littermate control mice were treated as shown in Fig 2.4A. (A) Experimental schematic. (B) MHC II MFI on LECs quantified via flow cytometry (C-D) Quantification by ELISA of cytokine secretion by OVA restimulated lymph node cells

VEGFR-3 dependent increase in Th2 cytokines, particularly IL-4, and furthermore suppressed IFN-γ secretion in a non-VEGFR-3 dependent manner.

2.3.11 LEC MHC II is necessary in vitro for optimal Th2 polarization in LEC:DC:OT-II tri-cultures

Lastly, we tested this MHC II on LEC requirement in vitro. Due to their low levels of costimulation, LECs are not sufficient in vitro to activate naïve CD4 T cells [92]. Thus we used tricultures of bone marrow dendritic cells (BMDCs), LECs, and OT-IIs to determine the role of MHC II on LECs in vitro in modulating DC activation of CD4 T cells. Briefly, we first isolated lymph node stromal cells from WT and MHC II KO mice. After expanding the cells ex vivo, LECs were enriched through negative selection and seeded. LECs were then pre-treated with $OVA_{323-339}$ with and without IFN-γ, to upregulate MHC II.

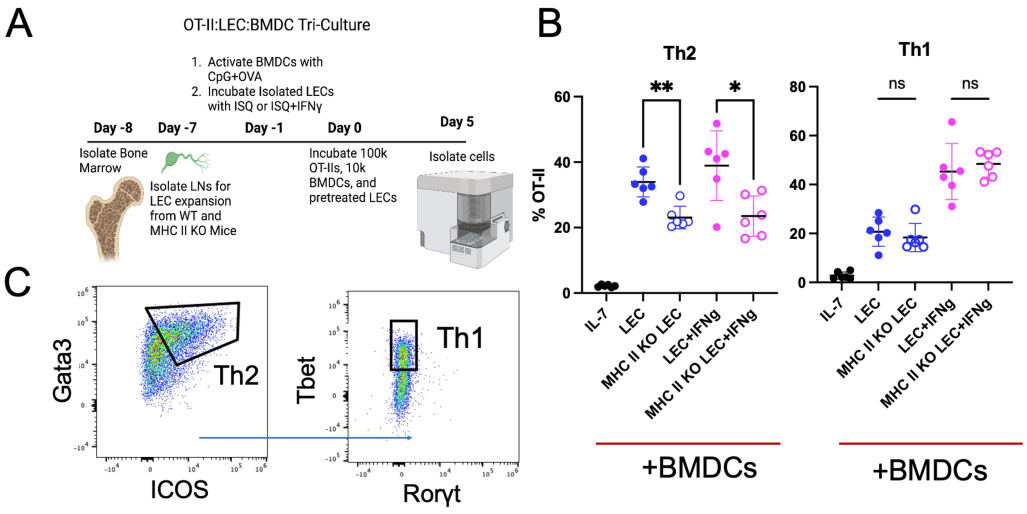

Figure 2.12: **In vitro LEC MHC II is necessary for Th2 polarization of α-OVA CD4 T Cells|** (A) Experimental schematic of in vitro LEC:DC:OT-II triculture (B) Sample gating of Th2 and Th1 cells by flow cytometry (pregated on CD45.1+CD3e+CD4+) (C) Quantification of Th2 and Th1 cells by flow cytometry

Concurrently, BMDCs were matured using CpG and OVA overnight. BMDCs were washed

and added to LEC coated wells. Isolated OT-II CD4 T cells specific for the $OVA_{323-339}$ epitope were lastly added. After 5 days, cells were harvested for analysis by flow cytometry of Th1 and Th2 polarization (**Fig 2.12A-B**). We observed that MHC II on LECs has no effect on Th1 polarization, though Th1 polarization was increased in the condition pretreated with IFN-γ; however, we observed that in LECs that lacked MHC II, maximal formation of Th2 cells was hindered and this effect was not dependent on IFN-γ pretreatment (**Fig 2.12C**). Thus, in vitro, MHC II is necessary for optimal Th2 conversation of OT-II CD4 T cells.

2.3.12 VEGFR-3 stimulation selectively decreases IgG2c, but not other subclasses, in an MPLA-based vaccine model

Lastly, we wanted to assess whether this VEGFR-3 dependent modulation of type 2 immunity was adjuvant dependent. Thus we used the exact experimental schedule as we have previously, but used monophosphoryl-lipid A (MPLA) as an adjuvant. MPLA is a TLR4 agonist, and as opposed to CpG which binds TLR9 expressed in the endosome of the cell, TLR4 is expressed on the surface and is more representative of a bacterial rather than viral pathogen. After assessing plasma antibody levels, we did not observe a phenocopy of CpG as there was no VEGFR-3 dependent increase in antigen-specific IgG1. However, we did observe a decrease in α-OVA IgG2c, which we have previously never observed (**Fig 2.13**). IgG2c is one of the subclasses associated with the type 1 immune response, so as opposed to promoting the type 2 immune response directly through increase in IgG1, VEGFR-3 stimulation in this different model slightly antagonizes the type 1 response.

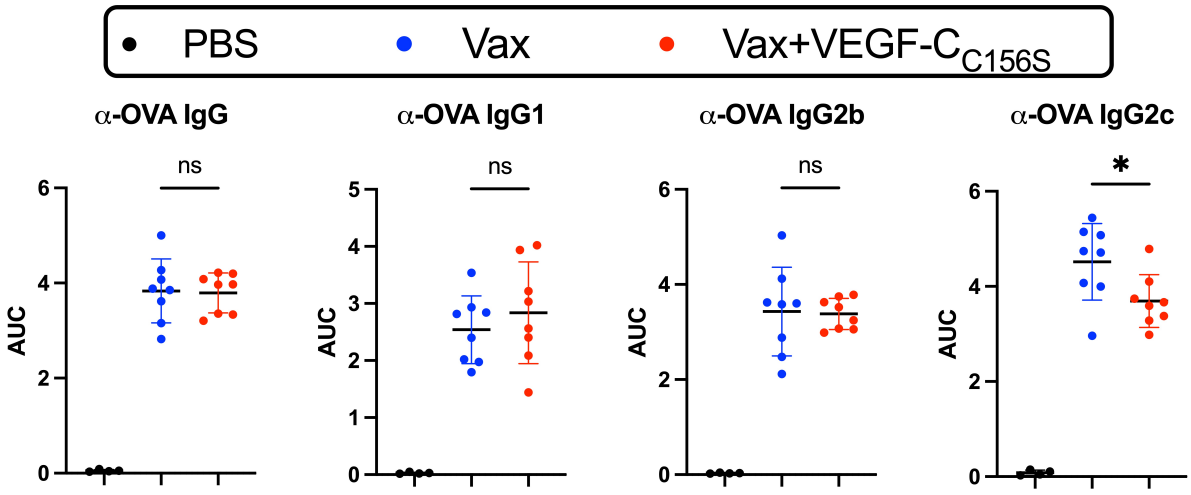

Figure 2.13: **VEGFR-3 stimulation selectively decreases IgG2c, but not other subclasses, in an MPLA-based vaccine model**| Experimental timeline was followed as shown in Fig 2.4A, using 5 μg of MPLA and 10 μg of OVA was used as the immunization. Quantification of area under the dilution curve (AUC) of α-OVA IgG, IgG1, IgG2b, and IgG2c

2.4 Discussion

In this present study, we uncovered a novel role of LECs as immunological players due to their ability to alter CD4 T cell polarization. Our data demonstrated that upon VEGFR-3 blockade during immunization, antigen-specific IgG1 is selectively antagonized and that restimulated lymph nodes secrete more IFN-γ. IFN-γ antagonizes IgG1 class switch and thus we find it is likely this increase IFN-γ, without increases in cytokines which may promote IgG1 class-switch, drives this decrease in IgG1. Conversely, when stimulating VEGFR-3 during immunization, we see a selective increase in antigen-specific IgG1. In the restimulated lymph node, we observe an increase in type 2 cytokines, which could explain the increased IgG1 as all three of the type 2 cytokines, especially IL-4, can induce IgG1 class-switch in various contexts. We then demonstrated through an inducible, conditional knock-out of VEGFR-3 on LECs, that it was VEGFR-3 expression by LECs that was required for maximal IgG1 class-switch. Using an IL-4 reporter mouse, we observed that VEGFR-3 stimulation

led to an increased accumulation of IL-4 expressing effector-memory CD4 T cells and that IL-4 expressing CD4 T cells were in close association with LECs. We lastly showed that MHC II expression by LECs is required for this VEGFR-3 induced Th2 cytokine secretion, and that it further suppressed IFN-γ in a VEGFR-3 independent manner.

Our work grows upon the increasing body of work demonstrating the key role LECs have as immunological players and in interacting with CD4 T cells. Previous work highlights the important of LECs in maintaining peripheral tolerance towards CD4 T cells, by serving as antigen reservoirs [113] while other work has shown that LECs can acquire peptide-MHC II complexes from dendritic cells, which also induces CD4 T cell tolerance [100]. Tumoral LEC MHC II promotes T_{Reg}-mediated suppression, and in mice that lacked MHC II in LECs, tumor growth was substantial impaired [102]. Another publication demonstrates that the absence of MHC II on lymph node-stromal cells (which include LECs) leads to autoimmunity [33]. Thus our work demonstrates a new role for LECs, not as "suppressors", but as "polarizers", as it had not been shown that LECs can polarize CD4 T cells.

It remains an open question what specifically about LECs make them able to polarize CD4 T cell responses in this way. One hypothesis is that LEC expression of PD-L1 with the low levels of costimulation polarizes away from the Th1 response induced by CpG [35]. ILC2s that lack PD-L1 lead to defective Th2 priming [114]. Thus, potentially this MHC II dependent interaction in the context of PD-L1 expression by LECs may be sufficient to alter this polarization. Other studies highlight the role of PD-L1 in promoting M2 macrophage infiltration, which could promote a type 2 permissive environment for Th2 polarization [115, 116]. Thus potentially PD-L1 may directly promote Th2 polarization or indirectly promote a Th2 permissive environment, but whether LEC PD-L1 is actually the mechanism remains and interesting avenue for future exploration.

While we did not observe a direct phenocopy using MPLA as an alternative adjuvant, we did still observe a slight antagonism in IgG2c, a type 1 associating subclass. It is relevant

to note that this dose of MPLA used (5 μg) induces a much more robust antibody response compared to our CpG dose, and MPLA also induces much higher levels of total α-OVA IgG compared to CpG. Since the effects of LECs are relatively subtle, it may be worth further exploration by lowering the dose of MPLA to match the levels of antibodies induced by CpG, and to see if this case VEGFR-3 stimulation could also promote IgG1 increases. It may be that the adjuvant dose is too high compared to the ability of LECs to assert their immunomodulatory affect and thus no change above the much higher baseline can be detected.

In human, there is substantial variability in plasma and serum VEGF-C levels. In healthy women, VEGF-C levels ranged from 700 pg/mL to 2800 pg/mL [117], while a separate study demonstrated that serum VEGF-C levels ranged from 2500 to 13000 pg/mL [118]. Thus even at steady-state there is a wide range of VEGF-C that would be available in various contexts. Furthermore, various inflammatory pathologies such as lymphedema and septic shock are associated with increased circulating VEGF-C levels [119, 120]. There is already evidence that links increased VEGF-C with increased IL-4 and IL-13 in lymphedema [119]. More than simply showing this association, our work directly links LECs with this type 2 polarization. Thus, our work has elucidated the mechanism to a previously unstudied association in lymphedema, which highlights the importance of LECs as an immunological player and demonstrates that this ability seems to be relevant in human, and not only in mice. It remains to be seen if this association is preserved across other inflammatory pathologies upon which VEGF-C is upregulated, but it is worth further exploration.

In conclusion, our study broaden the role of LECs as immunological players, highlighting their ability to alter CD4 T cell polarization in an immunization model, and that this polarization can functionally alter antibody class-switch towards IgG1.

2.5 Materials and Methods

2.5.1 Animals

Wild-type (WT) mice (C57BL/6J) were purchased from The Jackson Laboratory. IL-4 reporter (4get, C.129-Il4tm1Lky/J) were purchased from The Jackson Laboratory and then bred in house. MHCII-/- mice (B6.129-H2-Ab1tm1Gru) were bred in house. Prox1Cre-ER^{T2}-VEGFR-3$^{lox/lox}$ mice (or referred to as Prox1-VEGFR-3 mice) were generated through crossing of Prox1-Cre-ER^{T2} mice [121] to with VEGFR-3$^{lox/lox}$ mice [91]. Mice were maintained homozygous for the floxed allele, and heterozygous for the Prox1 transgene (i.e. Prox1-Cre-ER^{T2} Tg/0-VEGFR-3$^{lox/lox}$). Littermate controls are homozygous for the VEGFR-3 floxed sequences but with no Prox1 transgene. For phenotypic induction, mice were injected intraperitoneally with 1 mg tamoxifen (Sigma Aldrich) daily for seven days, and mice were enrolled in experiments 1 week after the last injection. Prox1Cre-ER^{T2}-MHCII$^{lox/lox}$ mice (or referred to as Prox1-MHC II mice) were generated through crossing of Prox1-Cre-ER^{T2} mice (Prox1tm3(cre/ERT2)Gco/J) with MHCII$^{lox/lox}$ mice (B6.129-H2-Ab1tm1Koni/J) [121]. Prox1-MHC II mice were maintained heterogeneous for the Prox1 transgene and homozygous for the MHC II floxed sequences (i.e. Prox1-Cre-ER^{T2} Tg/0-MHCII$^{lox/lox}$). Littermate controls are homozygous for the floxed alleles. For phenotypic induction, mice were injected intraperitoneally with 1 mg tamoxifen (Sigma Aldrich, St. Louis, Missouri, USA) daily for five days, and mice were enrolled in experiments 1 week after the last injection. All mice were used at age 8-16 weeks at the beginning of experiments. All animal experimentation was approved by the Institutional Animal Care and Use Committee of the University of Chicago (72551).

2.5.2 Genotyping

DNA was extracted from tail clips or ear punch biopsies. PCR was carried out Prox1-CreER^{T2} transgene. For the Prox1 transgene, primers used were 5'-TGT CTG TGC CTC CAT CTC AG-3‘ and 5'-AGG CAA ATT TTG GTG TAC GG-3' for forward and reverse, respectively. The transgene band yields a 730 bp long amplicon. Since the MHC-II and VEGFR-3 floxes were maintained homozygously in all mice (conditional knockout and littermate), no genotyping was necessary.

2.5.3 Immunization and VEGFR-3 modulation

Mice were immunized subcutaneously in all for hocks with a total with 10 μg of CpG-B and 10 μg of EndoFit chicken ovalbumin (Invivogen) split evenly between all four hocks. Alternatively, instead of CpG, 5 μg of MPLA (Invivogen) with 10 μg of OVA could be used to assess the effect of another adjuvant. To stimulate VEGFR-3, mice were injected with VEGF-C$_{C156S}$ at a dose of 50 ng per hock in all 4 hocks. To block VEGFR-3, 500 μg of α-VEGFR-3 (clone mF4-31C1, Eli Lilly) or Rat IgG (Sigma) as a control in 100 μL of PBS was administered intraperitoneally (i.p.) and is given every 4 days up until Day 6 post immunization.

2.5.4 Lymph node digestion

Lymph nodes were dissected from euthanized animals and digested with following a protocol adapted from Broggi et al [122]. Briefly, lymph nodes were cut with scissors and digested in 1 mg/mL collagenase IV (Worthington-Biochem) and 40 μg/mL DNAse I (Worthington-Biochem) for 30 min at 37°C with magnetic stirring. 3.3 mg/mL collagenase D (Sigma) was then added to the mix for an additional 15 min. After repeated pipetting, enzymatic digestion was quenched with EDTA at a final concentration of 5 mM followed by addition of full media. Cells were then filtered twice through a 70 μm strainer to obtain single cell

suspensions for subsequent processing.

2.5.5 Flow cytometry

Single cell suspensions were stained in 96-well round bottom plates. Live/dead staining along with CD16/32 Fc (93, Biolegend) receptor blocking was performed in PBS for 15 min on ice at 1:100 dilution, simultaneosly cells were viability stained using Live/Dead Blue (Thermo Fisher)at 1:500 dilution. CXCR5 was stained separately for 1 hr at 37 °C in FACs Buffer (PBS supplemented with 2% FBS). Surface staining was performed in Brilliant Stain Buffer (BD) for 15 min on ice. Fixation performed using the FoxP3 fixation/permeabilization kit (eBioscience) for 30 min at 50 μL. For nuclear transcription factor and IgG subclass staining, staining was performed in permeabilization buffer (eBioscience). Cells were then washed one last time in FACs Buffer and resuspended in 100 μL FACs buffer before samples were run on the Cytek Aurora. Data analysis was performed using FlowJo (TBD) and statistical analysis performed using Prism v9 (Graphpad). To see flow panels, refer to **Tables 2.1-2.4** below for further information.

Fluorophore	Specificity	Clone	Purpose	Dilution
CD45	AF532	30-F11	Pan-Immune	400
CD31	BUV615	1D3	LECs	400
gp38	APC-Cy7	8.1.1	LECs	200
F4/80	AF647	BM8	Macrophages	400
CD169	BV605	3D6.112	SCS Macrophages	150
CD49b	PE	DX5	NK Cells	400
CD3e	BUV395	145-2C11	T Cells	100
CD4	BUV496	GK1.5	CD4 T Cells	400
CD8a	BUV805	53-6.7	CD8 T Cells	400
CD44	PerCp-Cy5.5	IM7	Antigen experience	400
CD62L	BUV737	MEL-14	Naive/Memory T Cells	400

Table 2.1: Flow cytometry panel for identification of IL-4 expressing cells

Fluorophore	Specificity	Clone	Purpose	Dilution
CD45	AF532	30-F11	Pan-Immune	400
CD31	BUV615	1D3	LECs	400
gp38	APC-Cy7	8.1.1	LECs	200
F4/80	AF647	BM8	Macrophages	400
CD169	BV605	3D6.112	SCS Macrophages	150
CD11b	BV785	M1/70	CD11b Subsets	400
CD19	BUV395	1D3	B Cells	300
B220	BUV496	RA3-6B2	B Cells	400
IgM	BUV563	II/41	B Cell Subsets	150
IgD	AF700	11-26c.2a	B Cell Subsets	200
GL-7	PacBlue	GL7	GC B Cells	200
CD95	BUV737	JO2	GC B Cells	200
IgG1	BV421	RMG1-1	IgG1+ B Cells	400
IgG2b	AF594	RMG2b-1	IgG2b+ B Cells	200
CD8a	BUV805	53-6.7	CD8 T Cells	400
CD11c	BV480	N418	APCs	400
I-A/I-E	PerCp-Cy5.5	M5/114	Naive/Memory T Cells	400

Table 2.2: Flow cytometry panel for identification of IgG1+ GC B Cells and Stromal Cells

Fluorophore	Specificity	Clone	Purpose	Dilution
CD45	AF532	30-F11	Pan-Immune	400
CD3e	BUV395	145-2C11	T Cells	100
CD4	BUV496	GK1.5	CD4 T Cells	400
CD62L	BUV737	MEL-14	Naive/Memory T Cells	400
Rorγt	BV421	C9B7W	Th17	400
CD8a	BV480	53-6.7	CD8 T Cells	400
PD-1	BV605	29F.1A12	Activation/Exhaustion	200
ICOS	BV650	C398.4A	Activation	200
CD25	BV785	PC61	Activation/T_{Reg}	200
Foxp3	AF488	MF23	T_{Reg}s	200
CD44	PerCp-Cy5.5	IM7	Antigen experience	400
Gata3	PE/Dazzle-594	L50	Th2 Polarization	400
Tbet	PE-Cy7	4B10	Th1 Polarization	400
CXCR5	AF647	L138D7	Tfh	400
CD45.1	AF700	A20	Congenic Marker	400
Bcl6	APC-Cy7	K112-91	Tfh	400

Table 2.3: Flow cytometry panel for OT-II Analysis In Vivo

Fluorophore	Specificity	Clone	Purpose	Dilution
CD45	AF532	30-F11	Pan-Immune	400
CD3e	BUV395	145-2C11	T Cells	100
CD4	BUV496	GK1.5	CD4 T Cells	400
Gata3	PE/Dazzle-594	L50	Th2 Polarization	400
Tbet	PE-Cy7	4B10	Th1 Polarization	400
CD45.1	AF700	A20	Congenic Marker	400
CD44	PerCp-Cy5.5	IM7	Antigen experience	400

Table 2.4: Flow cytometry panel for OT-II Analysis In Vitro

2.5.6 Flow cytometry clustering

After spectral unmixing and conventional compensation was performed using a combination of single stained cells and compensation beads (Cat 01-3333-42, Thermo Fisher Scientific), OT-IIs were gated as shown (**Fig 2.15**). Samples of all OT-IIs from each sample were then concatenated together into one file, and all subsequent analysis was performed. Individual samples could be identified from the concatenated file due to unique keyword identifiers added to the individual samples before concatenation. At first, unsupervised clustering using Flowsom was performed, but as the number of clusters was deemed too small to reflect the diversity of the system (4), supervised clustering was then performed where the number of clusters was manually selected. Clustering was performed using the default number of clusters to start (8), and the quality of the cluster was assessed using Cluster Explorer. The number of clusters was found satisfactory when the expression patterns of each clusters was unique and that when increasing the number of clusters led to overclustering while decreasing the number of clusters led to losing the diversity of the populations. In the end, 8 clusters was chosen. Both FlowSom and Cluster Explorer are available as plugins to FlowJo and freely downloadable through the FlowJo Exchange. Clustering were performed using the following markers: CD44, CD62L, PD-1, ICOS, CD25, Foxp3, Gata3, Tbet, Rorγt, CXCR5, and Bcl6.

2.5.7 Microscopy

Immunization draining lymph nodes were fixed in 1% paraformaldehyde (PFA), embedded in paraffin and cut into 6 μm sections using a microtome (Leica). After deparaffinization in xylene and re-hydration in decreasing concentrations of ethanol, slides were incubated for 40 min in citrate buffer (10 mM citric acid, 0.05 % Tween 20, pH 6.0) at 95 °C. Slides are then incubated for 10 min in tris-buffered saline (TBS) 10 % DMSO, 10 min in TBS 0.1 % Triton, 30 min in TBS 0.5 % casein prior to immunostaining. Slides were incubated with rat anti-mouse CCL21 (R&D, 59106) and goat anti-Lyve1 (R&D, AF2125) in TBS 0.5 % casein overnight at 4 °C, followed by matching secondary antibodies (Invitrogen) for 1 hr at room temperature. After vigorous washing, slides were lastly stained with AF647 anti-I-A/I-E (BioLegend, M5/114.15.2) overnight at 4°C. Sections were mounted with Prolong Gold Antifade Reagent with DAPI (Invitrogen) and imaged using a Leica DMi8 fluorescent microscope and 25x oil objective. Image processing was performed with ImageJ (NIH).

For the IL-4 reporter mice (4get), lymph nodes were fixed in 1 % PFA for 1 day, and were subsequently incubated for at least 2 days in 15 % sucrose in TBS followed by 30 % sucrose in TBS. Tissues were embedded in Tissue-Tek® OCT Compound (Electron Microscopy Sciences) and frozen before being cut into 9 μm sections using a cryostat (ThermoFisher). All sections were incubated for 10 min in TBS 10 % DMSO, 10 min in TBS 0.1 % Triton, 30 min in TBS 0.5 % casein prior to immunostaining. Slides were incubated with goat anti-Lyve1 (R&D, AF2125), CD4 (BioLegend, GK1.5) and lastly rabbit anti-EGFP (Invitrogen) for signal amplification in TBS 0.5 % casein overnight at 4°C, followed by matching secondary antibodies (Invitrogen) for 1 hr at room temperature. After vigorous washing, slides were lastly stained with AF647 anti-B220 (BD, RA3 6B2) in TBS 0.5 % casein overnight at 4°C. Sections were mounted with Prolong Gold Antifade Reagent (Invitrogen) and imaged using a Leica SP8 laser-scanning confocal microscope and 25x oil objective. Image processing was performed with ImageJ (NIH).

2.5.8 Restimulation

To assess cytokine secretion by T cells through antigen-specific restimulation. Briefly, single cell suspensions of LNs were seeded in 96- well round bottom plates at 5 x 10^5 cells per well, and restimulated or not with $OVA_{323-339}$ (1 μg/mL) or full protein OVA (100 μg/mL) depending on the experiment for a total of 4 days. After 4 days, the supernatant was collected and frozen for subsequent analysis. For supernatant analysis, LEGENDplex™ Mouse Th1/2 Cytokine Panel kit (BioLegend) was performed according to the manufacturer's instruction. Approximately 300 events per cytokine was acquired using Fortessa 4-15 flow cytometer (BD), and analyzed with LEGENDplex v8.0 software.

2.5.9 α-OVA Antibody ELISA

Blood was collected from immunized EDTA-K2-coated tubes (BD). Plasma was separated by centrifugation at 15000xg for 10 min and stored at −80 °C. Plasma was assessed for anti-OVA IgG as well as IgG subclasses IgG1, IgG2b, and IgG2c by ELISA. 96-well ELISA plates (MaxiSorp Immuno plates, Thermo Scientific) were coated with 10 μg/mL OVA in PBS overnight at 4 °C. The following day, plates were washed in PBS with 0.05 % Tween 20 (PBS-T) and then blocked with 1x casein (Sigma) diluted in PBS for 2 h at room temperature. Then, wells were washed with PBS-T and further incubated with various dilutions of plasma for 2 h at room temperature. Plasma was first diluted 100-fold for the initial dilution and then serially in 10 fold increments up to 6 times to create a dilution curve. After 6 washes with PBS-T, wells were incubated for 1 h at room temperature with horseradish peroxide (HRP)-conjugated antibody against mouse IgG, IgG1, IgG2b, IgG2c, (Southern Biotech). After 5 washes with PBS-T, bound anti-OVA antibodies were incubated with tetramethylbenzidine substrate for 30 min. 3 % H2SO4 with 1 % HCl was added at that time, and the absorbances at 450 nm and 570 nm were immediately measured (Epoch Microplate Spectrophotometer, BioTek). For all subsequent analysis, the absorbance at 570

nm was subtracted from the absorbance at 450 nm. For AUC analysis, the Reimann's sum (trapezoidal rule) was calculated using the log transformed dilution versus the absorbance for each sample.

2.5.10 Bone marrow-derived DC (BMDC) generation

BMDCs were generated as previously described [100]. Briefly, mouse femurs and tibiae were harvested, and bone marrow was flushed out using a 27-gauge syringe needle or finer, loaded with RPMI-1640 media. Bone marrow cells were seeded and expanded with GM-CSF (2 ng/mL, Peprotech) and used between 7 and 9 days after seeding. BMDCs were then matured with 1 μg/mL CpG-B (ODN-1826, Trilink) and 10 μg/mL OVA overnight.

2.5.11 Isolation of lymph node lymphatic endothelial cells

Axillary, brachial, inguinal and popliteal lymph nodes (LNs) were harvested from WT and MHC II-/- mice and digested as previously described [123]. Briefly, LNs were mechanically disrupted and digested in IMDM (Gibco) containing Liberase DH (Roche, 250 μg/mL) and DNase I (Sigma, 100 μg/mL). After 1 hr of digestion at 37 °C, the mixture was homogenized by repeated pipetting. Cells were then passed through a 70 μm cell strainer and the enzymatic digestion was quenched with IMDM containing 10% FBS, penicillin (100 U/mL), streptomycin (100 μg/mL), and EDTA at a final concentration of 5 mM. Cells were washed and seeded on plates that were pre-coated with PBS containing human fibronectin (10 μg/mL, Fisher Scientific) and bovine type-I collagen (PureCol; 10 μg/mL, Advanced Biomatrix) for 30 min at 37 °C. Cells were cultured in αMEM (Gibco) supplemented with 10% FBS, penicillin (100 U/mL) and streptomycin (100 μg/mL). 24 hr after seeding, cells in suspension were removed and replaced with fresh medium. After reaching around 80% confluency, cells consisting mainly of LECs (CD45-CD31+gp38+CD140a-) and fibroblastic reticular cells (FRCs; CD45-CD31-gp38+CD140a+) were harvested and used directly or

sorted for LECs using a negative selection approach. For sorting, cells were incubated with biotinylated antibodies against CD45, EpCam, and CD140a for negative selection and sorted with streptavidin beads/magnet from EasySep, yielding a fraction enriched for LECs.

2.5.12 CD4+ T cell isolation

Spleens were harvested from OT-II transgenic mice and mechanically disrupted on a pre-wet 70 μm strainer using a syringe plunger. Red blood cells were lysed using ACK buffer (Gibco) for 3-4 minutes. CD4+ T cells were then isolated using the negative selection kit for mouse CD4+ T cells from Biolegend, yielding purity greater than 85%. For carboxyfluorescein succinimidyl ester (CFSE) labeling, cells were washed with PBS and resuspended in PBS at 10^7 cells/mL. CFSE was diluted at 2 μM in PBS, and was mixed with the cell suspension at 1:1 for 7 minutes at room temperature in the dark. The labeling reaction was quenched with FBS-containing medium on ice for several minutes before washing. For adoptive transfer, cells were resuspended in PBS.

2.5.13 In vitro MHC II necessity

One day before the start of the tri-culture, BMDCs were matured with OVA and CpG-B as described. Isolated LECs from the primary LNSC cultures were counted and seeded at a density of 10,000 cells per well in a flat bottom TC-treated 96 well plates that were pre-coated with PBS containing human fibronectin (10 μg/mL, Fisher Scientific) and bovine type-I collagen (PureCol; 10 μg/mL, Advanced Biomatrix) for 30 min at 37 °C. Isolated LECs were either treated with $OVA_{323-339}$ (1 μg/mL) or $OVA_{323-339}$ (1 μg/mL) and IFN-γ (50 ng/mL). The next day, OT-II isolation was performed and cells were CFSE labelled as described. Cells were counted and seeded at 100,000 cells/well into the wells that already contained the seeded LECs from the day before. Matured BMDCs were then added to each well at an amount of 10,000 cells/well giving a OT-II:DC:LEC ratio of 10:1:1. As a negative

control, OT-IIs were incubated with IL-7 (10 ng/mL) without any LEC or BMDCs. Cells were then incubated for 5 days and analyzed by flow cytometry at endpoint.

2.5.14 Statistics

For data in which there are three or more experimental groups of comparison, parametric data were analyzed using one-way analysis of variance (ANOVA) Dunnett's or Bonferroni's post hoc test for multiple comparisons. Non-parametric data was analysis using Kruskal-Wallis with Dunn's test for multiple comparisons. For data in which there are only two experimental groups, an unpaired 2-tailed Student's t test is performed for parametric data while non-parametric data was tested using Mann-Whitney. The difference was considered significant when $P < 0.05$. P values were classified as follows: ns, not significant; *$P < 0.05$; **$P < 0.01$; and ***$P < 0.001$.

2.5.15 Supplemental Figures

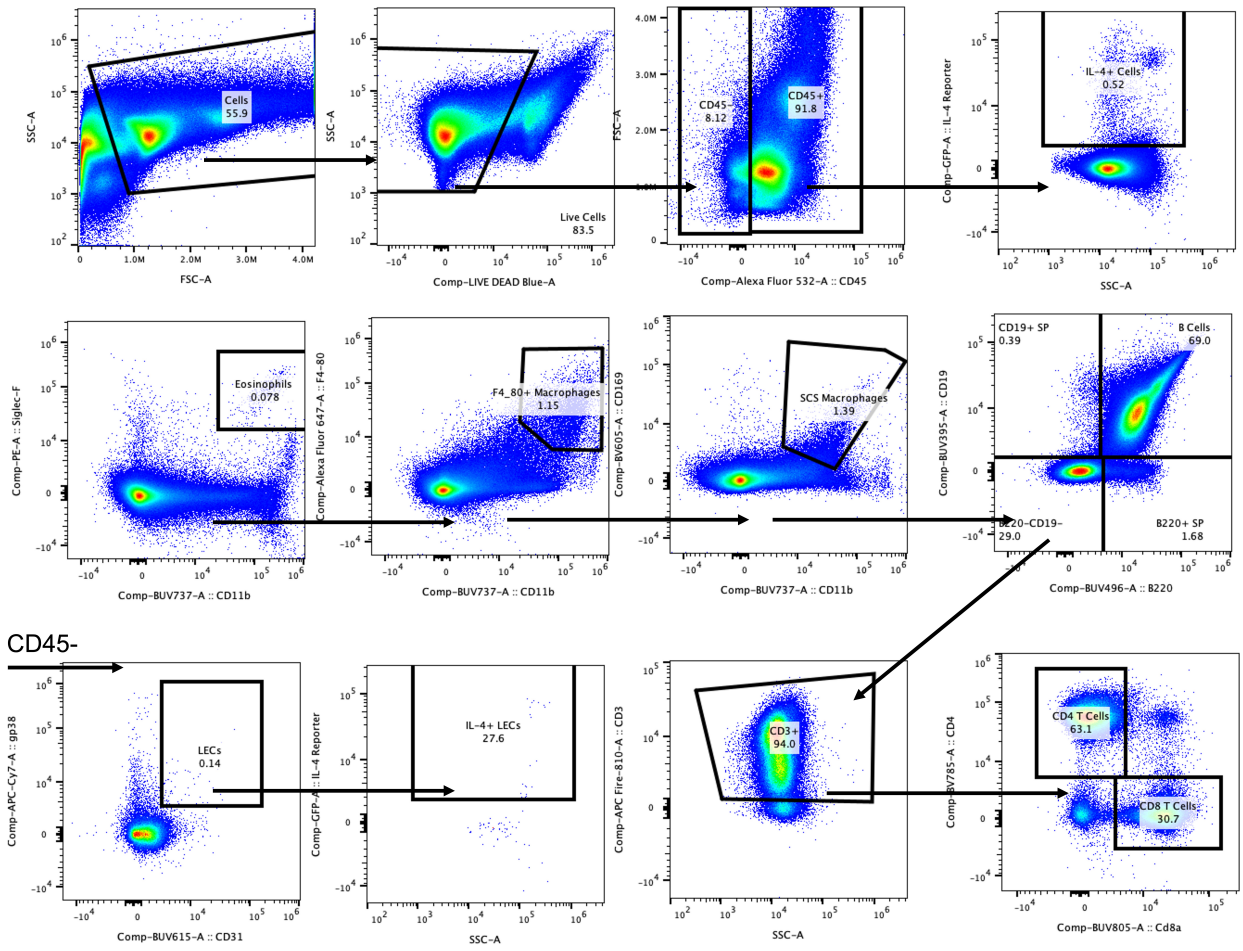

Figure 2.14: **Gating strategy for the identification of IL-4 (EGFP) expressing Cells**

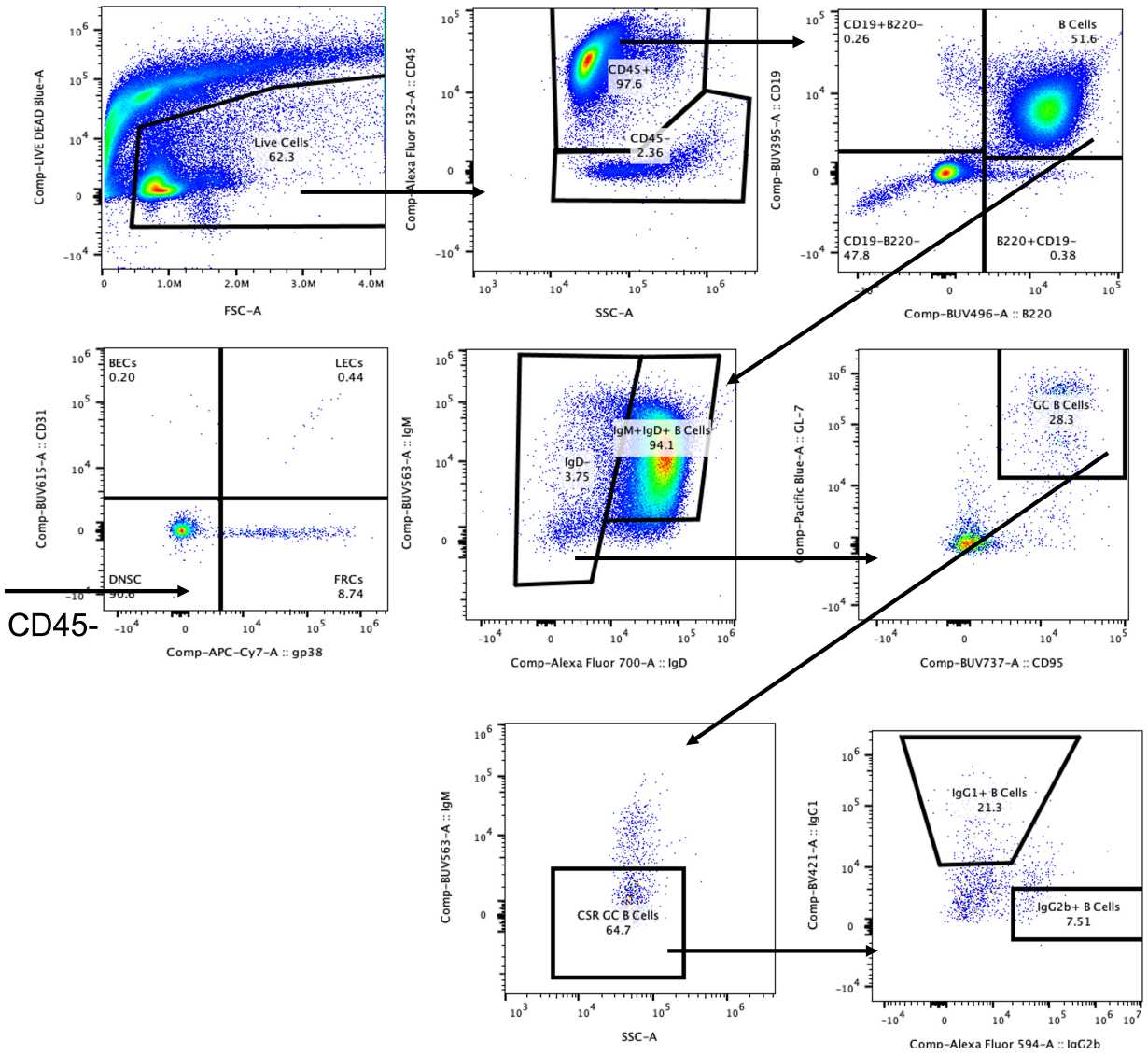

Figure 2.15: **Gating strategy for the identification of immune and stromal populations in the lymph node after vaccination**

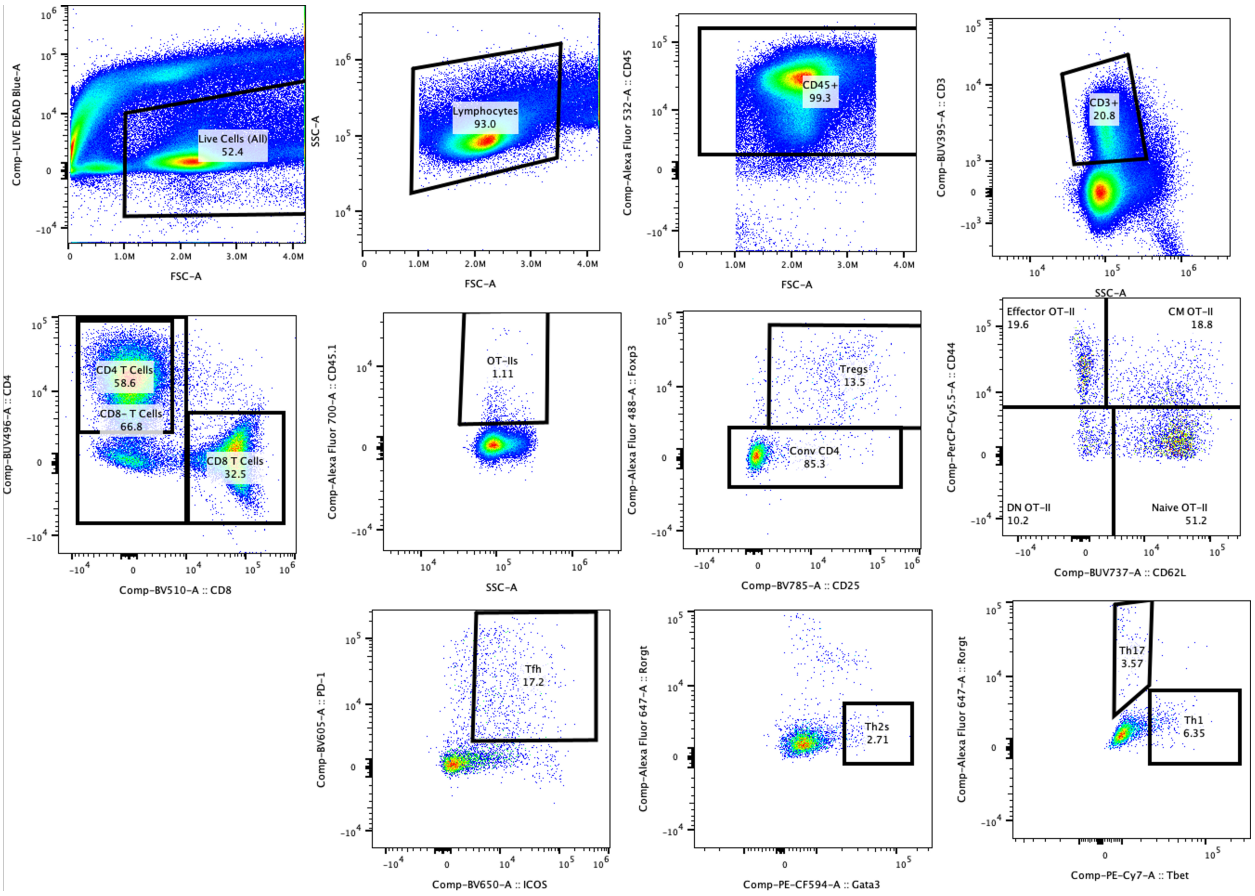

Figure 2.16: **Gating strategy for the phenotyping of OT-IIs in the lymph node**

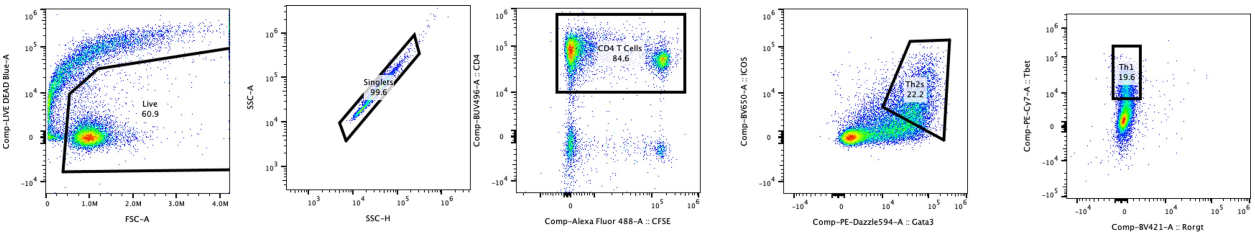

Figure 2.17: **Gating strategy for the analysis of Th1/Th2 polarization in vitro**

CHAPTER 3

THE VEGFR-C/VEGFR-3 AXIS MODULATES CD8 T CELLS AND POTENTIATES IMMUNOTHERAPY IN A CXCR3 DEPENDENT MANNER

3.1 Abstract

Vascular endothelial growth factor-C (VEGF-C) expression and subsequent lymphangiogenesis in the tumor microenvironment are associated with metastasis and poor prognosis in melanoma. We have demonstrated that while VEGF-C promotes a highly immunosuppressive microenvironment in the tumor, it paradoxically renders immunotherapy more effective in mouse models and correlates with improved survival after checkpoint blockade therapy in patients, a phenomenon we termed lymphangiogenic potentiation. We first queried whether the T cells in the tumor immune microenvironment were altered in lymphangiogenic tumors, and we observed that not only are lymphangiogenic tumors more T cell inflamed, but that the phenotype of these immune infiltrates is also altered. Thus before immunotherapy, the T cell infiltrates are already distinct. We utilized an adoptive cell transfer therapy model upon which activated antigen specific CD8 T cells (OT-Is) were transferred as an immunotherapy. We found that lymphangiogenic melanomas after adoptive transfer had increased CXCL9 levels, and that blocking CXCR3 reduced the benefit of immunotherapy efficacy on lymphangiogenic melanomas, suggesting that lymphangiogenic potentiation was partly dependent on endogenous T cell recruitment. Taken together, our data demonstrates that intratumoral lymphangiogenesis enhances the efficacy of immunotherapy by boosting immune infiltration via enhanced T cell recruitment and priming.

3.2 Introduction

Historically, lymphatics have correlated poorly with survival in cancer. Tumors with higher lymphatic vessel density are more metastatic and VEGFR-3 dependent lymphangiogenesis has been reported to be required to initiate the early events of metastasis in a VEGF-D overexpressing tumor model as lymphatics serve as routes of escape for tumor cells [60]. Furthermore, LECs themselves have many immunosuppressive functions restricting recruit-

ment of inflammatory cells and decreasing levels of pro-inflammatory cytokines such as TNF and IL-1β [64].

Current work highlights the more direct role lymphatics have as immunological players in the tumor context. IFN-γ activation of dermal LECs was seen to inhibit cytotoxic T cells in melanoma [124], and LEC PD-L1 has been shown to suppress CD8 T cells by inducing their apoptosis in the draining LNs [125]. On the CD4 T cell side, LEC MHC II promoted increased Treg suppressive function in the tumor [34]. As highlighted previously, LECs secrete multiple inhibitory enzymes, including nitric oxide (NO) and indoleamine-2,3-dioxygenase (IDO) and can suppress DC mediated T cell activation [65–67]. However, despite these many negative associations, more recent research highlights that lymphatics actually are critical in many contexts for immune cell trafficking to the tumors and their ability to respond to various therapies. Meningeal lymphatics that surround the brain are critical for regulating radiotherapy efficacy by regulating immune cell trafficking and CD8 T cell activation [126], and VEGF-C promotes immune-surveillance and immunotherapy efficacy in glioblastoma [70].

It is not only meningeal lymphatics that have been shown as beneficial in this regard. We have shown that in melanoma, dermal lymphatic vessels are required to elicit a potent adaptive immune response [127]. Moreover, we demonstrated that the blockade of the VEGF-C/VEGFR-3 signaling axis resulted in a reduction of cancer immunotherapy efficacy in several immunotherapy models including adoptive cell transfer (ACT) and tumor peptide vaccines, indicating that tumor lymphangiogenesis plays beneficial roles in eliciting antitumor immunity [69], an effect we refer to as lymphangiogenic potentiation of immunotherapies. We observed that lymphangiogenic murine melanomas are more inflamed with immune cells, but particularly T cells. These tumors were enriched for naïve T cells prior to immunotherapy, and that the CCL21-CCR7 signaling pathway was involved in this process. Importantly, CCR7 inhibition reduced the therapeutic benefit provided by tumor

VEGF-C signaling, indicating that the chemokine CCL21, which LECs are a main source of citegunn1998chemokine, contributes to the therapeutic benefit of VEGF-C. This association between lymphangiogenesis and immunotherapy outcome was also observed in melanoma patients, where higher levels of serum VEGF-C prior to immunotherapy correlated with a better clinical response in two independent clinical trials [69]. However, it remains unclear whether other pathways besides the CCL21:CCR7 axis are relevant in the generation of lymphangiogenic potentiation in melanoma. Here, we address further mechanisms by which the tumor lymphangiogenesis shapes antitumor immunity and affects the response to immunotherapy.

3.3 Results

Previous work from the lab has demonstrated that lymphangiogenic tumors are more T cell inflamed, with an increase in overall CD4 and CD8 T cell infiltration. However, we wanted to probe whether lymphangiogenic tumors had altered phenotype of their T cell infiltrates. To achieve this we used unbiased clustering approaches to use a broad array of markers to assess the quality of the CD8 T cell compartment. To assess activation and exhaustion we used CD44, ICOS, PD-1, Lag3, Tbet, and Tim3; Tox for terminal exhaustion, Ki67 for proliferation; TCF1 and CXCR5 for T cell stemness; and CCR7, CD127, and CD62L to assess memory phenotype. We identified 10 unique clusters using supervised clustering using FlowSom (**Fig 3.1A**). We removed Pop5 from analysis due to the extremely high autofluorescence, and thus is likely macrophage contamination. That leaves 9 bona fide clusters. We observed 3 clusters that were upregulated in lymphangiogenic tumors (Pop1, Pop3, Pop9) (**Fig 3.1B**). One cluster was downregulated (Pop2), while the rest were unaffected. (**Fig 3.1B**)

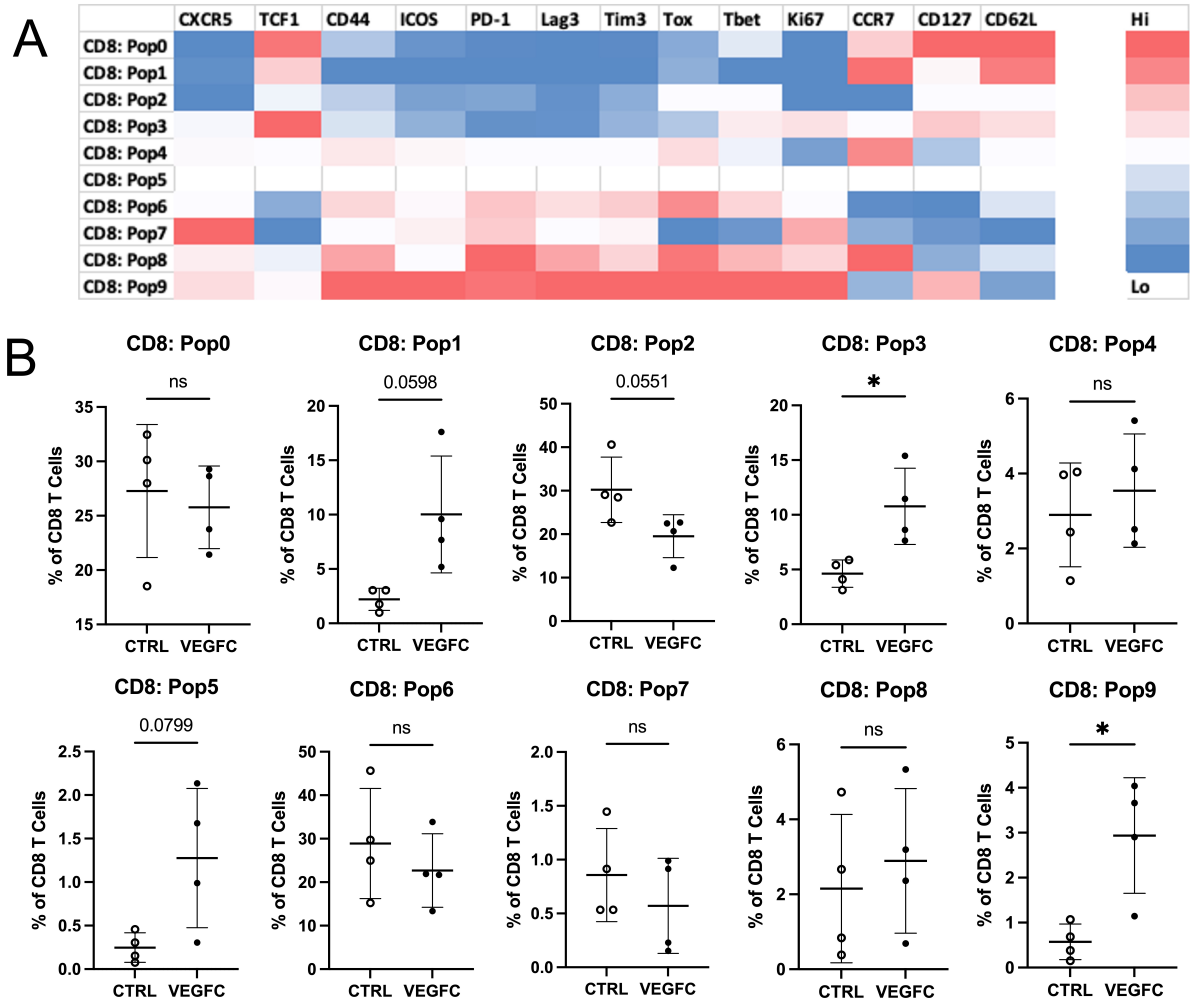

Figure 3.1: **Lymphangiogenic tumors have altered CD8 T cell populations** | 250e3 B16F10-CTRL or B16F10-VEGF-C tumor cells were inoculated and tumors were grown for 14 days. At endpoint, tumors were digested to a single cell suspension and stained for flow cytometry. (A) Heatmap of expression of FlowSom clusters of concatenated CD8 T cells (B) Proportions of each cluster as a fraction of total CD8 T cells

Annotations for all clusters can be viewed in (**Table 3.1**), but we will focus on the differentially regulated clusters for more in-depth analysis. Interestingly, of the three populations (Pop1, Pop3, and Pop9) that are enriched in the lymphangiogenic tumors, only one of them (Pop1) expressed high levels of CCR7 while Pop3 expressed low CCR7 while Pop9 the lowest expression. CCR7 is the receptor to CCL21, of which LECs are a key source. Pop1 are naive T cells expressing CD127, CD62L, CCR7, but not expressing activation markers

such as CD44 or PD-1. Pop3 are proliferating central memory phenotype cells expressing CD127, CCR7, and CD62L while also expressing low levels of the activation marker CD44 and effector transcription factor Tbet, but not expressing any exhaustion markers such as PD-1 or Tox. Pop9 are highly exhausted as they express the highest levels of most activation and exhaustion markers, including Tox for terminal exhaustion, but they also express CD127, which indicates they may be IL-7 responsive. This population does not express CCR7. Interesting, the only cluster that was downregulated was Pop2, which while having effector phenotype due to the expression of (low levels) of CD44, they did not express other activation or exhaustion markers. Thus lymphangiogenic tumors have altered CD8 T cell infiltrates compared to their non-lymphangiogenic counterparts.

Cluster	Annotation
CD8: Pop0	Non-proliferation central memory
CD8: Pop1	Naive
CD8: Pop2	non-activated effectors
CD8: Pop3	Proliferating central memory
CD8: Pop4	CCR7+ Effectors
CD8: Pop5	Autofluorescent contamination
CD8: Pop6	CCR7- Exhausted Effectors
CD8: Pop7	Proliferating Effectors
CD8: Pop8	CCR7+ Exhausted Effectors
CD8: Pop9	Highly-activated IL-7Rα+ effectors

Table 3.1: Cluster Annotation for CD8 TILs

3.3.1 T cells colocalize in lymphatic rich areas in lymphangiogenic tumors

While we began our analysis on lymphangiogenic and non-lymphangiogenic tumors without any treatment to assess baseline differences in the T cell phenotype, we next assessed the mechanism for "lymphangiogenic potentiation" that we have observed previously. We first assessed whether there was a more direct relationship between lymphatics and this T cell inflammation. We chose the adoptive transfer model using B16-OVA-VEGF-C, a modified

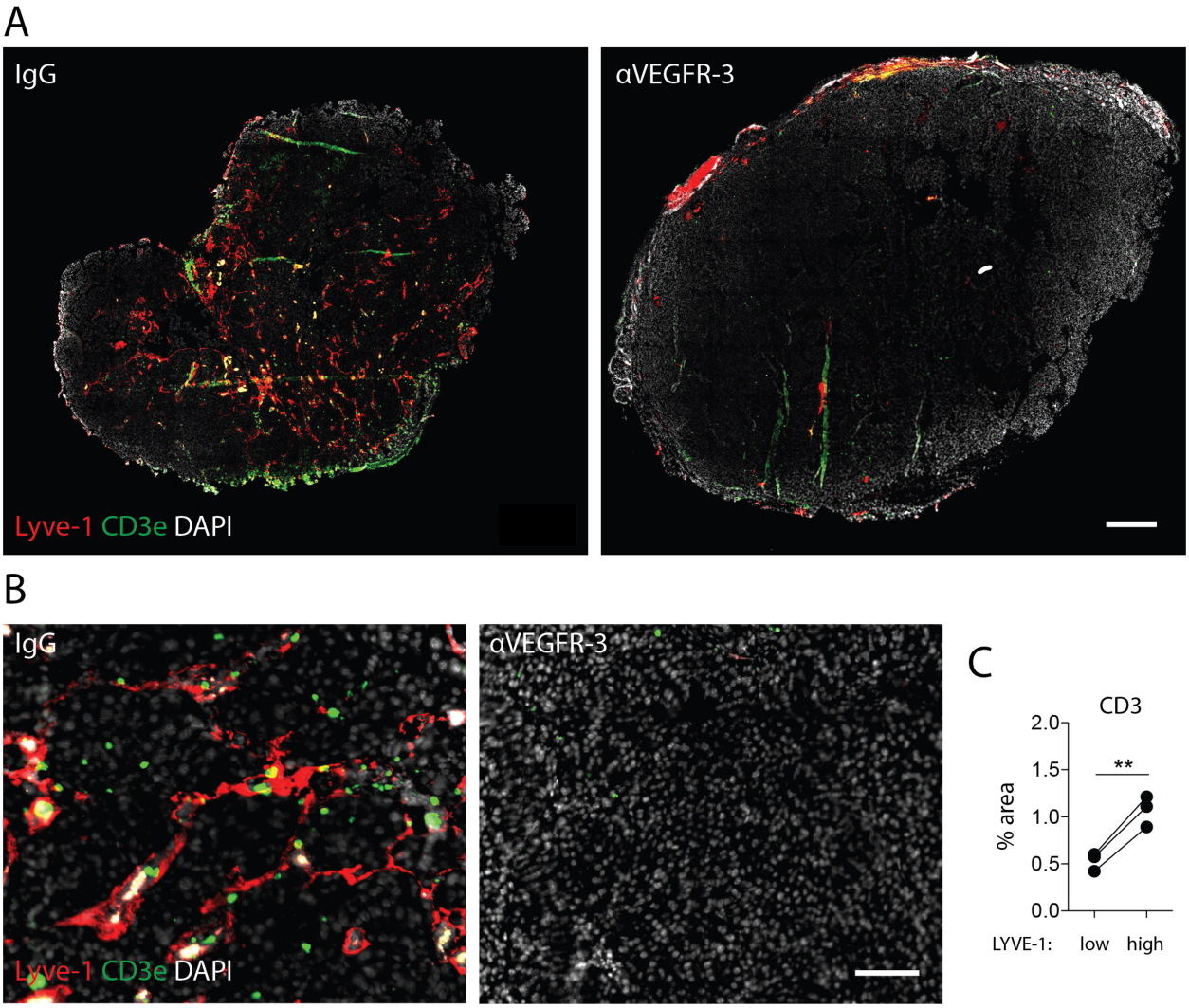

Figure 3.2: **Localization of T cells within lymphangiogenic tumors** |B16F10-OVA-VEGF-C tumors, after adoptive transfer of activated OT-I CD8+ T cells on day 8, treatment with IgG or α-VEGFR-3 and sacrifice at day 20. (A) Representative images of whole tumor sections. Grey: DAPI. Red: LYVE-1. Green: CD3. Scale bar: 500 μm. (B) Inset image of tumor sections. Grey: DAPI. Red: LYVE-1. Green: CD3. Scale bar: 100 μm. (C) Percentage CD3+ area in lymphatic-poor (LYVE-1 low) and lymphatic-rich (LYVE-1 high) regions in tumor sections of IgG-treated mice (n=3 mice, each n represents the average of 32 sub-images within the core of one tumor)

form of B16-VEGF-C that also express ovalbumin (OVA) protein to serve as an antigen. To block lymphangiogenesis, we utilized a VEGFR-3 blocking antibody (mF4-31C1, Eli Lilly). The use of OVA as a model antigen allows us to use OT-Is, which are transgenic CD8 T cells

that are specific to an SIINFEKL, the immunodominant CD8 epitope of OVA. We activate the OT-Is ex vivo and adoptive transfer them on Day 8. This therapy mimics other adoptive transfer therapy such as CAR T cells or TIL adoptive transfers. At endpoint, we stained paraffin sections for lymphatics (Lyve1) as well as T cells (CD3ϵ), and then assessed their colocalization. As expected, in lymphangiogenic tumors, lymphatics penetrate throughout the tumor, while after VEGFR-3 blockade, there is an almost entire absence of intratumoral lymphatics (**Fig 3.2A**). In lymphangiogenic tumors, there is also large CD3 T cell infiltration, while α-VEGFR-3 treated mice have substantially less infiltration (**Fig 3.2A-B**). We next quantified lymphatic rich and lymphatic poor regions, and we found that lymphatic rich areas of the tumor had increased T cell infiltration compared to lymphatic poor regions, even considering these tumors were all lymphangiogenic (**Fig 3.2C**). Qualitatively, the T cells are very closely colocalized to the lymphatics (**Fig 3.2B**) compared to distal regions. Together, this implies a direct relationship between lymphatics and T cells causing this colocalization.

3.3.2 Lymphangiogenic tumors are enriched in CXCL9, which is secreted by LECs under inflammatory conditions

Previously the lab has established that lymphangiogenic tumors were enriched for CCL21 and that blockade of the receptor for CCL21, CCR7, led to the loss of lymphangiogenic potentiation and decrease in naive and memory T cell accumulation in the tumor. Since we observed that there were still subsets of T Cells that did not express high levels of CCR7, we decided to probe if other chemokines from LECs could be involved [69]. To assess this, we inoculated B16-OVA-VEGF-C tumors into mice and either treated with α-VEGFR-3 blocking antibody, using OT-Is as immunotherapy as described previously. At endpoint, tumors were harvested and lysed for protein content, and chemokines were assessed via Legendplex (Biolegend). We observe that lymphangiogenic tumors had increased CXCL9 and CCL22 compared to their non-lymphangiogenic counterparts (**Fig 3.3A**). However,

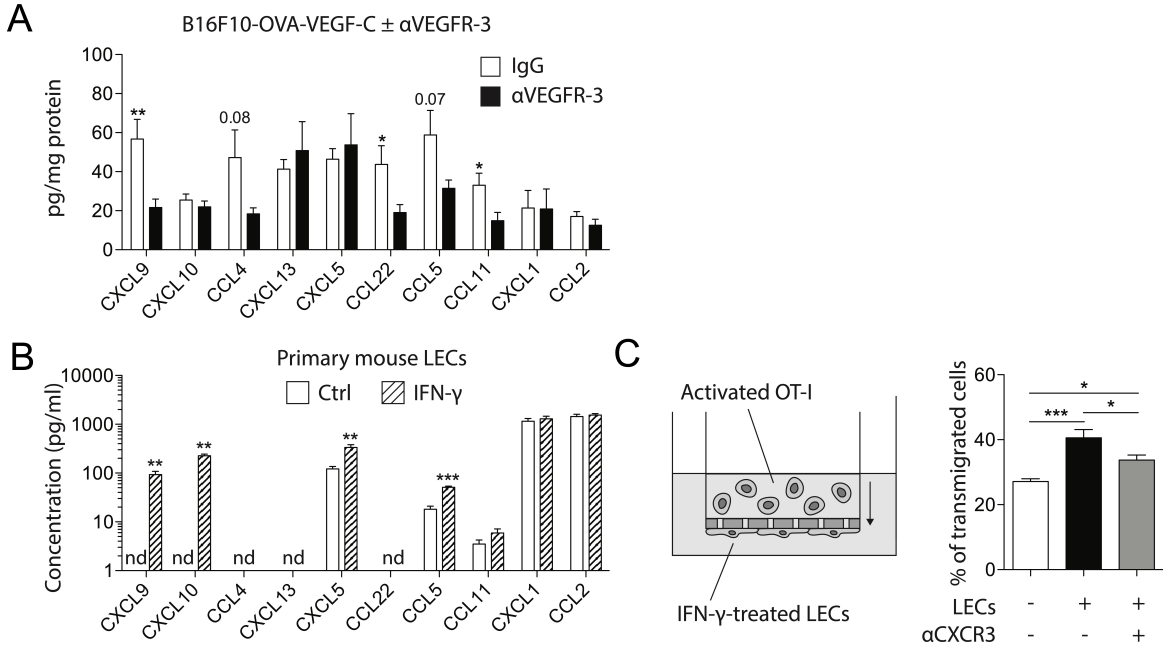

Figure 3.3: **Lymphangiogenic tumors are enriched with CXCL9, which LECs secrete upon IFN-γ stimulation**| B16F10-OVA-VEGF-C cells injected into WT mice, with adoptive transfer of activated OT-I CD8+ T cells on day 8. Mice treated with IgG or α-VEGFR-3 and euthanized at day 18 for analysis. Tumor protein analysis using LEGENDplex. Representative of 2 independent experiments. (B)Supernatant analysis of primary mouse LECs, stimulated or not with 50 ng/ml of recombinant murine IFN-γ. Data representative of 3 experiments. (C) T cell transmigration. Experimental setup (left), and quantification of transmigrated activated CD8+ T cells after 16 hr (right). Data representative of 3 experiments. Data represent mean±SEM.

this does not indicate whether LECs themselves are capable of making this chemokine. To assess this we took LN LECs, expanded them in vitro, and stimulated them with or without IFN-γ to assess their chemokine secretion at baseline and under inflammatory conditions. Interestingly we found that even though CCL22 is enriched in lymphangiogenic tumors, it was not found to be secreted by LECs either at baseline or after IFN-γ stimulation (**Fig 3.3B**). However, we did find that while CXCL9 was not produced at baseline by LECs, it was produced by IFN-γ stimulated LECs (**Fig 3.3B**). Thus lymphangiogenic tumors are enriched in CXCL9, which can be secreted by IFN-γ inflamed LECs. CXCL9 is the receptor

for CXCR3, which is expressed by effector T cells and is important for their migration [128]. To assess in vitro if the CXCL9/CXCR3 axis plays a role in functionally altering T cell migration in our setup, we utilized a transwell setup where we seeded IFN-γ stimulated LECs on one side of a transwell and added activated CD8 T cells onto the other side to assess their ability to transmigrate, and blocked CXCR3 using a blocking antibody (**Fig 3.3C**). We found that the addition of LECs significantly increased CD8 T cell transmigration, suggested that LECs can directly facilitate CD8 T cell transmigration (**Fig 3.3C**). We observed that upon CXCR3 blockade, there was a significant reduction in transmigration, which implicates LEC CXCL9 as being functionally relevant in its potential to alter CD8 T cell migration (**Fig 3.3C**). Interestingly, transmigration did not get reduced to baseline levels without LECs, which could indicate that there are other factors, potentially other LEC secreted chemokines can alter transmigration of effector T cells.

3.3.3 CXCR3 blockade reduces lymphangiogenic potentiation of immunotherapy

We next assessed whether CXCR3 had a functional role in vivo in altering lymphangiogenic potentiation. Here we treated B16-OVA ± VEGF-C tumor bearing mice that were were given OT-I ACT with α-CXCR3 or isotype control. However, since CXCR3 is so critical for effector T cell homing, which include the effector OT-Is we transferred, we waited for 3 days after therapy to allow for the T cells to traffic to the tumor properly. Here we confirmed that the lymphangiogenic B16-OVA-VEGF-C responded to the immunotherapy much better than their non-lymphangiogenic counterparts (**Fig 3.4A**). We found that by disrupting the CXCR3 axis through antibody blockade we lost this therapeutic benefit, and the growth curve for these mice looked almost identical to the non-lymphangiogenic counterparts without any CXCR3 blockade (**Fig 3.4A**). Interestingly, we observed that CXCR3 blockade in non-lymphangiogenic tumors did not effect the tumor growth (**Fig 3.4A**). To confirm the efficacy

of the blockade, we assessed immune infiltration by flow cytometry. We observed that CXCR3 blockade reduced CD4 T cell, CD8 T cell, NK, and NKT cell infiltration, and that this affect was independent the tumor type, but that it did not effect LEC numbers (**Fig 3.4B-C**). CD4 T cells [129], CD8 T cells [128], NK cells [130], and NKT cells all can express CXCR3, which is important for their trafficking to inflammatory sites [131]. Thus phenotypically, the CXCR3 blockade alters the infiltration in both lymphangiogenic and non-lymphangiogenic tumors, but only has a functional effect on the therapeutic efficacy of the lymphangiogenic tumors. Thus, the CXCR3 axis reduces lymphangiogenic potentiation of immunotherapy, but does not alter therapeutic efficacy in non-lymphagnigogenic tumors.

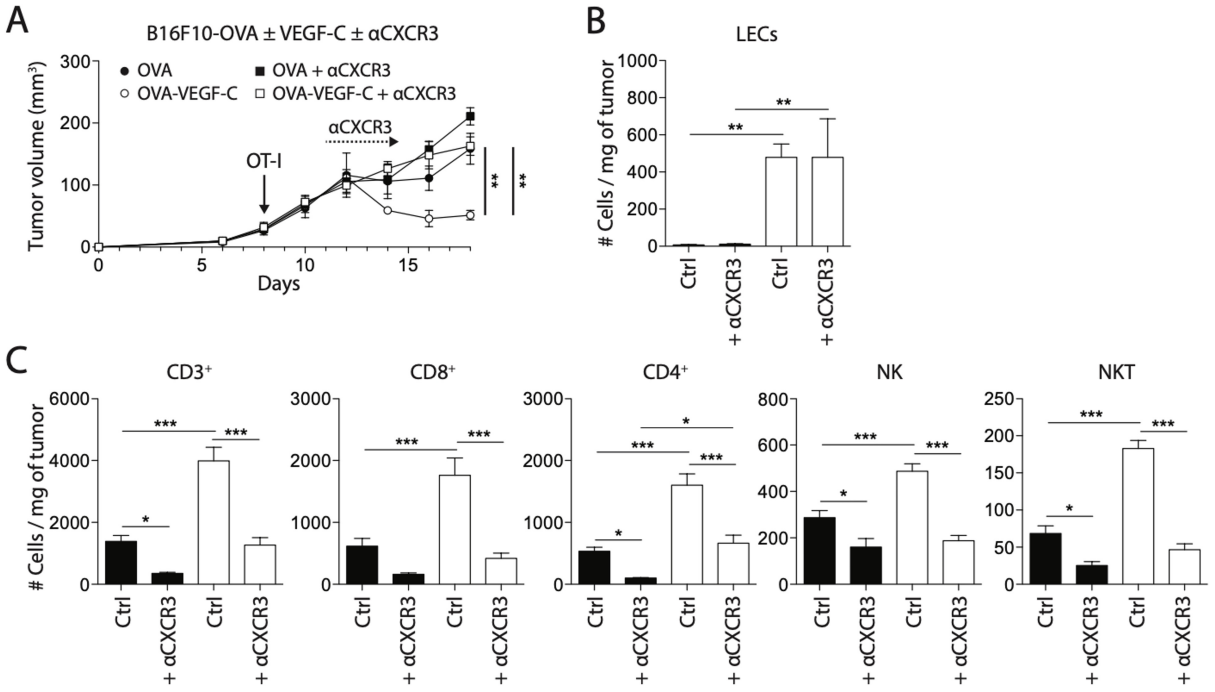

Figure 3.4: **CXCR3 blockade reduces lymphangiogenic potentiation of immunotherapy** |B16F10-OVA ± VEGF-C cells injected into WT mice, with adoptive transfer of activated OT-I CD8+ T cells on day 8. Mice treated or not with α-CXCR3 from day 11 and analyzed at day 18. (A) Tumor growth curves. Flow cytometry analysis of (B) LECs, (C) CD3+ T cells, CD8+ T cells, CD4+ T, NK and NKT cells. Quantification of cells per mg of tumor. B16F10-OVA ± VEGF-C cells injected into WT mice, with adoptive transfer of activated OT-I CD8+ T cells on day 8.

3.3.4 Immunotherapy efficacy in lymphangiogenic tumors is dependent on early presence of intratumoral T cells

Due to the specificity of CXCR3 blockade in abrogating the therapeutic efficacy in lymphangiogenic tumors, we next asked whether intratumoral T cells were sufficient for therapeutic efficacy, or if there was a requirement for the continuous recruitment of new effector T cells from the lymph node. This is not addressed by CXCR3 blockade alone as T cells are able to leave the tumor under normal conditions and then CXCR3 blockade would prevent rehoming of T cells to the tumor as all T cell infiltrates decrease (**Fig 3.4C**). This does not ellucidate whether new populations of T cells must be recruited from the lymph node or whether the populations in the lymph node would be sufficient on their own, were they not allowed to exit the tumor. To ascertain which population of T cells is critical, we utilized FTY720 that prevents T cell egress from the lymph node [132]. We can then give FTY720 in combination with CXCR3 blockade to address this question.

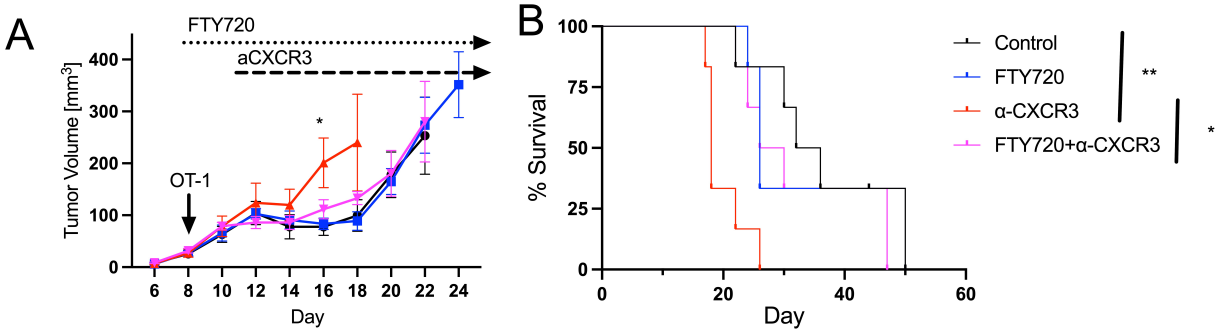

Figure 3.5: **Therapeutic efficacy of ACT in lymphangiogenic tumors is dependent on intratumoral T cells** |B16F10-OVA ± VEGF-C cells injected into WT mice, with adoptive transfer of activated OT-I CD8+ T cells on day 8. Mice treated or not with α-CXCR3 from day 11 every 3 days or FTY720 from day 8 and given daily (A) Tumor growth curve. (B) Survival curve.

We observed that, as expected, CXCR3 substantially interfered with therapeutic efficacy of ACT in B16-OVA-VEGF-C tumors (**Fig 3.5A-B**). As we have observed previously, FTY720 alone does not affect therapeutic efficacy compared to the ACT only mice (**Fig**

3.5A-B) [69]. Interestingly we found that the addition of FTY720 rescued the antagonistic effect of CXCR3 blockade and the combination treated mice look identical to the control mice that received only ACT (**Fig 3.5A-B**). This would indicate that therapeutic efficacy of ACT in lymphangiogenic tumors is dependent on the intratumoral T cell population and not on the CXCR3-dependent circulation of new effector T cells, as long as the tumors are initially unable to leave the tumor with FTY720.

3.4 Discussion

In this present study we demonstrate more of the mechanisms of lymphangiogenic potentiation. While it is known that lymphangiogenic tumors are more T cell inflamed, we further identified that the T cell infiltrates themselves are altered as we saw an increase in clusters identified as naive, proliferating central memory, and high-activated IL-7Rα+ effectors as well as a decrease in non-activated effectors. While previously it has been established that CCL21 from LECs is important for the recruitment of CCR7+ T cells to the tumor in lymphangiogenic tumors, only one of the identified clusters that was enriched in lymphangiogenic tumors expressed high levels of CCR7. This motivated us to look more into other chemokines in the tumor microenvironment that may be involved in recruiting these other clusters. We found that CXCL9 was upregulated in lymphangiogenic tumors and that in vitro primary murine LECs produced CXCL9 upon IFN-γ stimulation. In vitro, we demonstrated that LECs were able promote transmigration of activation CD8 T cells and that this effect was partially CXCR3 dependent. In vivo we demonstrates that lymphangiogenic potentiation was CXCR3 dependent. Lastly, we demonstrated that the TILs in the tumor upon the onset of ACT were required for immunotherapy efficacy in lymphangiogenic tumors, and not on the entry of new T cells from the lymph node as long as the TILs are unable to leave the tumor, otherwise the CXCR3 dependent recirculation of T cells is required for efficacy.

Our work grows on the increasing body of work showing that as opposed to their classi-

cal role associated with metastasis, that lymphatics also have an important role in immune trafficking through the secretion of various chemokines. In some cases as we have found, it is beneficial, and this has also been demonstrated in glioblastoma that VEGF-C drives immunosurveilance and immunotherapy responsiveness [70]. Furthermore, LEC secreted CXCL12 restricts CD8 T cells into the periphery of the tumor in the ICB responsive Yummer1.7 melanoma cell line [133, 134]. It remains unclear what about these different models would induce such different responses, but either way these implicates lymphatics as having a direct role in modulating T cell trafficking to alter, either for better or worse, immunotherapy responsiveness.

In short, we have demonstrated that lymphangiogenic tumors have altered CD8 T cell infiltration, that LEC CXCL9 is important for CD8 T cell transmigration, and that the CXCR3 axis is required for lymphangiogenic potentiation. Thus, lymphangiogenic tumors can directly promote recruitment of relevant T cell populations through CXCL9 and CCL21, thus opposed to their normally negative association with metastasis, there are benefits to increased lymphatics in the tumor, in the context of immunotherapy.

3.5 Materials and Methods

3.5.1 Mice

Wild-type mice (WT, C57BL/6J) were purchased from the Jackson Laboratory (Bar Harbor, Maine, USA). OT-I CD45.1.2 mice were crossed between CD45.1 mice (B6.SJL-Ptprc^{a}Pepc^b/BoyJ) and OT-I mice (C57BL/6-Tg(TcraTcrb)1100Mjb/J), both from the Jackson Laboratory. All mice were used at age 8-16 weeks at the beginning of experiments. All animal experimentation was approved by the Institutional Animal Care and Use Committee of the University of Chicago (72414 and 72551).

3.5.2 Tumor experiments

For the B16F10 experiments, recipient mice were anesthetized and shaved on the back. For T cell analysis B16F10 ±VEGF-C was used while for ACT experiments B16F10-OVA ± VEGF-C cells were maintained in DMEM high glucose (Gibco) supplemented with 10% FBS (Gibco), as previously described [135]. Tumor cells were harvested around 80% of confluence, washed three times with PBS, and 250,000 cells in 30 μL PBS were injected intradermally in the mouse skin under anesthesia. Tumors were measured in 3 dimensions (x, y and z) with a digital caliper and volume was computed as Volume = 4π*(x/2)*(y/2)*(z/2)/3. Tumor cells were tested negative for mycoplasma.

3.5.3 Adoptive cell transfer

For the adoptive T cell transfer, spleens from OT-I mice were dissociated on a 70 μm strainer. Red blood cells were lysed using ACK buffer (3 min at room temperature). After washing, cells were seeded on non-tissue culture-treated 24- well plates in IMDM medium supplemented with 10% FBS, penicillin (100 U/mL), streptomycin (100 μg/mL), murine IL-2 (20 U/mL, Peprotech) and 1 μg/mL SIINFEKL peptide (GenScript). After 2 days, cells were split 1:2 and IL-2-containing fresh medium was added. 2 days later, cells were harvested, and washed several times with large volumes of PBS. 10^6 cells in 100 μL PBS were injected in the tail vein.

3.5.4 Antibody treatment

500 μg of αVEGFR-3 antibody (clone mF4-31C1, Eli Lilly) or rat IgG control (Sigma) was administered i.p. in 100 μL PBS every 4 days from day 0 (time of B16F10 cell injection). 200 μg of αNK1.1 (clone PK136, BioXCell) was administered i.p. with PBS every 3 days from day 8. 200 μg of αCXCR3 (clone CXCR3-173, BioXCell) was administered i.p. with PBS every 3 days from day 11 (3 days after the adoptive T cell transfer).

3.5.5 FTY720

FTY720 (Sigma) was dissolved in sterile DI water at a concentration of 250 μg/mL. Mice were injected at 1 mg/kg (25 μg per mouse) at each timepoint. FTY720 was injected i.p. daily starting day 8 (the day of ACT) until mouse reached endpoint. Non-FTY treated mice were injected with an equal volume of DI water for control. For mice that received CXCR3 blockade and FTY720, CXCR3 blockade was given via a separate i.p. injection every 3rd day as described above.

3.5.6 Tumor digestion

Tumors were dissected from euthanized animals and digested with following a protocol adapted from Broggi et al [122]. Briefly, tumors were cut with scissors and digested in 1 mg/mL collagenase IV (Worthington-Biochem) and 40 μg/mL DNAse I (Worthington-Biochem) for 30 min at 37°C with magnetic stirring. 3.3 mg/mL collagenase D (Sigma) was then added to the mix for an additional 45 min. After repeatedly pipetting, enzymatic digestion was quenched with EDTA at a final concentration of 5 mM, followed by addition of full media. Cells were then filtered twice through a 70 μm strainer to obtain single cell suspensions for subsequent processing.

3.5.7 Flow cytometry

Single cell suspensions were stained in 96-well round bottom plates. Live/dead staining along with CD16/32 Fc (93, Biolegend) receptor blocking was performed in PBS for 15 min on ice at 1:100 dilution, simultaneosly cells were viability stained using Live/Dead Blue (Thermo Fisher) at 1:500 dilution. Surface staining was performed in Brilliant Stain Buffer (BD) for 15 min on ice. Fixation was performed using the FoxP3 fixation/permeabilization kit (eBioscience) for 30 min at 50 μL. For nuclear transcription factor staining, staining was performed in permeabilization buffer (eBioscience). Cells were then washed one last time

in FACs Buffer and resuspended in 100 μL FACs buffer before samples were run on the Cytek Aurora. Data analysis was performed using FlowJo (BD) and statistical analysis performed using Prism v9 (Graphpad). To see flow panel, refer to **Table 3.2** below for further information.

Fluorophore	Specificity	Clone	Purpose	Dilution
AF532	CD45	30-F11	Pan-Immune	400
CD3e	BUV395	145-2C11	T Cells	100
CD4	BUV496	GK1.5	CD4 T Cells	400
CD62L	BUV737	MEL-14	Naive/Memory T Cells	400
CD8a	BUV805	53-6.7	CD8 T cells	400
Lag3	BV421	C9B7W	Exhaustion	200
TCF1	Pacific Blue	C63D9	Stemness	100
Tim3	BV480	5D12	Exhaustion	400
PD-1	BV605	29F.1A12	Activation/Exhaustion	200
ICOS	BV650	C398.4A	Activation	200
CD127	BV711	A7R34	IL-7R	200
CD25	BV785	PC61	Activation/Treg	200
Foxp3	AF488	MF23	Tregs	200
CD44	PerCp-Cy5.5	IM7	Antigen experience	400
Tbet	PE	4B10	Effector Function	400
CCR7	PE/Dazzle594	4B12	CCL21 Responsiveness	400
Ki67	PE-Cy7	B56	Proliferation	400
Tox	e660	TXRX10	Terminal Exhaustion	200
NK1.1	AF700	PK136	NK Cells	75
CXCR5	APC-Cy7	L138D7	Stemness	400

Table 3.2: Flow cytometry panel for TIL Analysis

3.5.8 Flow cytometry clustering

After spectral unmixing and conventional compensation was performed using a combination of single stained cells and compensation beads (Cat 01-3333-42, Thermo Fisher Scientific), cells were gated for viability then CD45+, CD3+, CD8+ to gate on CD8 T cells. Samples of an equal number of downsampled CD8 T cells from each sample were then concatenated together into one file, and all subsequent analysis was performed on this concatenated file.

Individual samples could be identified from the concatenated file due to unique keyword identifiers added to the individual samples before concatenation. At first, unsupervised clustering using Flowsom was performed, but as the number of clusters was deemed too small to reflect the diversity of the system (4), supervised clustering was then performed where the number of clusters was manually selected. Clustering was performed using the default number of clusters to start (8), and the quality of the cluster was assessed using Cluster Explorer. The number of clusters was found satisfactorily when the expression patterns of each clusters was unique and that when increasing the number of clusters led to overclustering while decreasing the number of clusters led to losing the diversity of the populations. In the end, 10 clusters was chosen. One cluster was identified to be contamination (Pop 5) due to its extremely high autofluorescence, and was excluded from analysis. Both FlowSom and Cluster Explorer are available as plugins to FlowJo and freely downloadable through the FlowJo Exchange. Clustering were performed using the following markers: CXCR5, TCF1, CD44, ICOS, PD-1, Lag3, Tim3, Tox, Tbet, Ki67, CCR7, CD127, and CD62L.

3.5.9 CXCR3 Transwell Assay

30,000 sorted primary LECs were seeded on the outer side of 5-μm porous inserts (Fisher Scientific). 2 hr after seeding, the inserts were flipped and transferred into a 24-well plate. 600 μL and 100 μL of medium were added in the bottom and top chambers, respectively. The next day, the medium was replaced with fresh medium, containing 50 ng/mL of recombinant murine IFN-γ. After 24 hr of stimulation, 500,000 activated OT-I CD8+ T cells were added to the top chamber. 16 hr after the addition of T cells, the medium in the bottom chamber was collected and T cells were counted on a cell counting chamber. To block CXCR3 signaling, 2 μg/mL CXCR3 antibody (clone CXCR3-173) was added to the culture medium for the duration of the transmigration assay.

3.5.10 Microscopy

B16F10 tumors were fixed in 10% formalin, embedded in paraffin and cut into 6 μm sections using a microtome (Leica). After deparaffinization, slides were incubated for 40 min in citrate buffer (10 mM citric acid, 0.05% Tween 20, pH 6.0) at 95 °C . All sections were incubated for 10 min in TBS 10% DMSO, 10 min in TBS 0.1% Triton, 30 min in TBS casein 0.5% prior to immunostaining. They were then incubated with rat anti-Lyve-1 (ALY7, eBioscience), rabbit anti-CD3ϵ (SP7, Abcam) in TBS Casein 0.5% overnight at 4°C, followed by matching secondary antibodies (Invitrogen) for 1 hr at room temperature. Slides were mounted with Prolong Gold Antifade Reagent with DAPI (Invitrogen) and imaged using a Leica DMi8 fluorescent microscope and 25x oil objective. Image processing was performed with ImageJ (NIH).

3.5.11 Statistics

Unless otherwise stated, statistical significance was analyzed by unpaired, 2- tailed Student's t test or by ANOVA followed by Tukey's post- hoc test for group analysis using Prism (GraphPad). Differences in survival curves were assessed using the log- rank (Mantel-Cox) test. P-value < 0.05 was considered statistically significant.

3.6 Acknowledgments

Special thanks to Dr. Lambert Potin for his close collaboration and mentorship for the work enclosed in this chapter. The work on CXCL9 and the CXCR3 axis was done in collaboration with Lambert while the in-depth phenotyping of T cells was performed by me.

3.7 Supplementary Figures

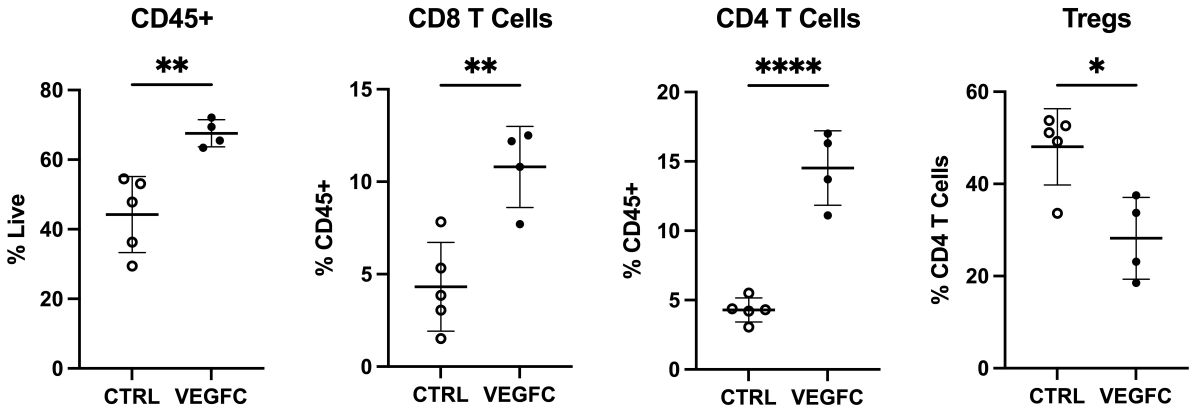

Figure 3.6: **Lymphangiogenic tumors are more T cell inflamed than their non-lymphangiogenic counterparts, and have less Tregs** |250e3 B16F10-CTRL or B16F10-VEGF-C tumor cells were inoculated and tumors were grown for 14 days. At endpoint, tumors were digested to a single cell suspension and stained for flow cytometry. Flow cytometry plots demonstrating CD45+ cells, CD8 T cells, CD4 T cells, and Tregs as quantified

CHAPTER 4

CHARACTERIZING MECHANISMS OF ANTI-TUMOR EFFICACY FOR CBD-CYTOKINE IMMUNOTHERAPIES

4.1 Abstract

Checkpoint-inhibitor (CPI) immunotherapy has achieved remarkable clinical success, yet it only remains effective for a subset of patients. Interleukin-12 (IL-12) is a powerful cytokine that activates the innate and adaptive arms of the immune system; however, the administration of IL-12 has been associated with immune-related adverse events. Even a collagen binding (CBD) variant that accumulates preferentially in the tumor has significant cytotoxic potential due to the effective dose. However, the use of two distinct combination approaches of less toxic therapeutic agents, CBD-GM-CSF and IL-7-CBD, led to to equivalent, if not enhanced efficacy, and lowered toxicity due to the ability to reduce the total dose of IL-12 needed. However, it was unclear the exact mechanism of action for these distinct combination therapeutics. Here we assessed, using high-dimensional flow cytometry, the T cell immune infiltrates in the IL-7-CBD and CBD-IL-12 therapeutics regimen. We observed an increase in overall CD8 T cells infiltration in the CBD-IL-12 and combination therapy. We further identified a specific decrease in terminal exhaustion and in increase in effector CD8 T cell subsets in the tumor in combination therapy. We posit these higher quality T cell are responsible for the enhanced therapeutic efficacy and immunological memory. GM-CSF, on the other hand acts on myeloid cells and thus, in combination with the CBD-IL-12, activates both the myeloid and T cell arms of the immune system. As such, we assessed how both T cells and myeloid cells change in the lymph node and tumor. In both the lymph node and tumor we observed that GM-CSF and combination with IL-12 antagonizes M2 macrophage polarization and increased cDC1 activation, without altering total DC numbers. On the T cell side, we see that uniquely the combination therapy has an increased CD8 T cell infiltration compared to either monotherapies in the tumor (though there was no change in the phenotype), and an increase in memory phenotype CD8 T cells in the draining LN. Thus we have demonstrated two distinct mechanisms of action for two therapeutics that both synergize with CBD-IL-12 to limit toxicity and increase efficacy.

4.2 Introduction

The development of checkpoint inhibitors (CPI) into potent immunotherapeutics has dramatically altered the treatment regimen for patients with metastatic melanoma. For what used to have a median survival of less than 6 months, now a fraction of patients can have a longlasting, durable benefit [136]. The success of CPI has highlighting the importance of the immune system in the anti-cancer response, but the challenge remains that only a small fraction of cancer patients have a durable benefit among those who are treated. Thus over the past decade there has been an explosion of immunotherapeutics that are being developed to try to utilize the power of the immune system, but with more potency for a larger fraction of people [47]. Over the years, it has been shown that patients needs to have infiltration of immune cells to respond to CPI [137]. Without this pre-existing infiltration, patients are unlikely to respond. Thus, novel immunotherapies aim to increase immune infiltration in these tumors, or in more colloquial terms to "make a cold tumor hot", either to be used in combination with CPI or as a monotherapy [138].

The laboratory of Jeffrey Hubbell has worked to develop one such immunotherapy: IL-12. IL-12 is a cytokine, produced by dendritic cells, and canonically promotes Th1 polarization and IFN-γ secretion by CD4 T cells while also activating cytotoxic CD8 T cells [52, 53]. Furthermore, IL-12 can also stimulate antigen presentation which could further enhance CD4 and CD8 T cell activation and function [54, 55]. However, the use of IL-12 in it's native form has a two-fold issue: toxicity and a requirement for a high-enough local concentration to have efficacy [54]. Especially in human, the severity of the toxicity supercedes its therapeutic efficacy, and several human trials were discontinued for this reason. One of the major reasons for IL-12's high toxicity, is the strong induction of IFN-γ by T cells and NK cells [139]. While IFN-γ has powerful anti-tumor effects, too much is highly toxic [140, 141].

Therefore to better utilize IL-12 safely, there needs to be a way to minimize the toxicity without reducing efficacy. One potential method to achieve this is to modify IL-12 to localize

preferentially to the tumor, concentrating the effect in the target site while minimizing systemic side effects. Targeting the tumor site directly could allow for a lower therapeutic dose since the dose in the tumor will be substantially higher than in off-target sites. The Hubbell lab has previously published a collagen binding domain (CBD) CPI which fused the A3 domain of Von-Willibrand factor (which naturally binds collagen) to α-PD-L1 and α-CTLA-4 [142]. This demonstrated increased efficacy and preferentially targeted to the tumor compared to the unmodified antibody. Subsequent to these findings, the Hubbell lab then modified IL-12 with this collagen binding domain to make CBD-IL-12. They found that CBD-IL-12 had remarkable antitumor efficacy, and reduced toxicity compared to the wild-type IL-12 [143]. However, in spite of this progress, the therapeutic dose used was 25 μg per mouse, and in human trials repeated administration of a dose as low as 500 ng/kg of IL-12 led to severe toxicities [139]. Thus while this modification was necessary for increased efficacy, this dose is still too toxic. This led to the next phase of development for the IL-12 therapeutic: combination therapy strategies. The key idea being to lower the required dose of IL-12 in combination with another, less toxic therapeutic cytokine. This led to the development of two promising combination therapy strategies: IL-7-CBD and CBD-GM-CSF.

Interleukin-7 (IL-7) is a common gamma chain (γ_c) cytokine that plays a crucial role in T cell survival and homeostasis of both memory and naive T cells [144, 145]. Due to its important role in T cell survival, IL-7 was tested as a monotherapy in a clinical trial. At a dose of 60 μg/kg, IL-7 expanded peripheral CD8 T cells, but not Tregs or NK cells; however, it did not demonstrate clinical benefit [146]. However, due to its immunomodulatory ability, it still had potential to be paired with another immunomodulatory molecule and demonstrate therapeutic efficacy. Due to the role of IL-7 as a T cell survival factor, it seemed a promising candidate for rational combination immunotherapy design with IL-12. IL-12 can activate T cells while IL-7 is important for survival, and can potentially promote memory. Thus,

combined they may demonstrate a particularly potent synergy.

Granulocyte-monocyte colony stimulation factor (GM-CSF) was first identified as a growth factor, but is now known to have a wide range of effects including promoting activation, differentiation, and mobilization of various myeloid populations [147]. The receptor of GM-CSF, GM-CSFR, is expressed on many myeloid cell types including DCs, macrophages, and monocytes, but furthermore is not expressed by lymphocytes such as T cells [148]. In terms of anti-tumor immunity, GM-CSF can promote M1 macrophage polarization [147], which are classically activated "pro-inflammatory" macrophages that can have anti-tumor effects, especially compared to M2-macrophages which can help support tumor growth [149, 150]. Furthermore, GM-CSF is able to activate DCs and potentially enhance T cell activation [151], and the presence of Batf3 DCs, which are mostly cross-presenting cDC1s, is required for immunotherapy responsiveness in an genetically engineered mouse model of melanoma [137, 152]. Thus, GM-CSF has the potential to activate the myeloid arm of the anti-tumor response and bridge the gap towards the adaptive arm through increased DC activation. Our particular interest in GM-CSF lies in the fact that instead of acting on T cells like IL-12, it would act on the macrophages and DCs and would thus activate both the innate and adaptive arms of the anti-tumor immune response and could demonstrate synergy in that manner. CBD-IL-12 can activate the T cells directly and the CBD-GM-CSF may activate and/or recruit DCs to the tumor, which could downstream promote further activation and accumulation of T cells.

For this chapter, we will restrict our analysis to B16F10 melanoma, which is an injectible melanoma cell line of C57BL/6 background that does not respond to α-PD-L1, but that does respond to CBD-IL-12. Thus, we think it is the ideal model for our studies.

4.3 Results

4.3.1 CBD-IL-12 and IL-7-CBD combination therapy is a potent therapeutic that induces CD8 T cell memory

Using the CBD platform for tumor targeting, IL-7-CBD was tested in combination with CBD-IL-12, using a 2 μg dose (over 10 fold lower than the dose used by Mansurov et al.). As a monotherapy at this low dose CBD-IL-12 does demonstrate therapeutic effect by extending survival, but when combined with IL-7-CBD this anti-tumor effect is even more dramatic and led to tumor clearance in 20% of the mice (**Fig 4.1A**). Also, compared to the non-modified version of the cytokines, the efficacy was substantially improved, as the combination therapy of the unmodified versions of the cytokines only maintained similar efficacy as the CBD-IL-12 monotherapy (**Fig 4.1A**). Next, a high dose of CBD-IL-12 (10 μg) was used as a monotherapy to determine if the low dose of IL-12 used in the combination therapy still allowed for similar efficacy of the high dose, without the associated toxicity of the higher dose of IL-12. Furthermore, this was only using a single dose of therapy. With just this

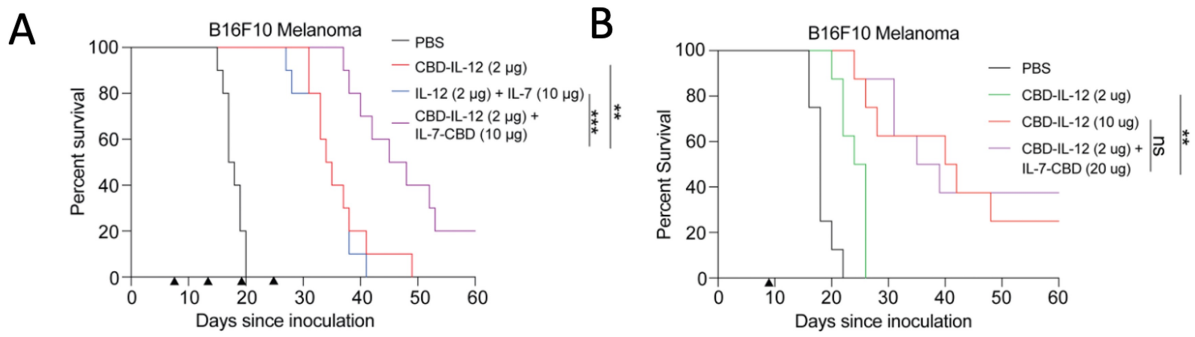

Figure 4.1: **CBD-IL-12 and IL-7-CBD combination therapy exhibit synergistic anti-titumor effect and reduce toxicity compared to high dose of CBD-IL-12 |** C57BL/6 mice were inoculated with 5 x 10^5 B16F10 melanoma cells intradermally on day 0 and treated with either i.v. with PBS, IL-12 + IL-7, CBD-IL-12 or with CBD-IL-12 + IL-7-CBD on day 7, 13, 19, and 25. Survival curves (A) are shown. B. C57BL/6 mice were inoculated with 5 x 10^5 B16F10 melanoma cells intradermally on day 0 and treated with either i.v. with PBS, 2 μg CBD-IL-12, 10 μg CBD-IL-12, or with 2 μg CBD-IL-12 + IL-7-CBD on day 9. Survival curves (D) are shown. **Data Provided by Dr. Seounghun Kang**

single dose, the low dose of CBD-IL-12 does not demonstrate much therapeutic benefit (**Fig 4.1B**). However, the combination therapy using the same dose has a very similar therapeutic benefit to that of the high dose of CBD-IL-12 used (**Fig 4.1B**). Thus the addition of IL-7-CBD allows for a dramatic reduction in the required dose of IL-12, without compromising on efficacy.

Next, it was assessed if this therapeutic could induce bona-fide immunological memory. Using intratumoral injections of the combination therapeuic and high-dose CBD-IL-12, tumor free mice were re-innoculated with tumors that were let to grow untreated, to see if they had developed memory and would reject the tumor (**Fig4.2A**). Even though high dose CBD-IL-12 mice could reject the primary tumor, they were unable to reject the secondary tumor; however, all the combination therapy treated mice were able to reject the re-challenge, even in the absence of additional therapeutic (**Fig4.2B**). To ascertain which key factor led to this protection from rechallenge, mice from the combination therapy treatment that had rejected their primary tumor were depleted of either CD4 or CD8 T cells, or treated with an IFN-γ neutralizing antibody both before and during the early phase of tumor implantation. It was only the mice treated with the α-CD8 depleting antibody that lost almost all benefit of the combination therapy treatment, and all mice succumbed to the tumor while CD4 depletion and IFN-γ neutralization only had modest effects (**Fig4.2C**). Thus, combination therapy leads to an induction of memory largely mediated by CD8 T cells.

4.3.2 CBD-IL-12 and IL-7-CBD induce differential changes in intratumoral immune cell infiltration

Due to the induction of immunological memory by combination treatment, changes in the immmune infiltrates in the tumor were analyzed to better understand the mechanism of action for this therapeutic benefit. B16F10 tumor-bearing mice were treated with a single dose intratumorally of PBS, IL-7-CBD, CBD-IL-12, and IL-7-CBD+CBD-IL-12 combina-

tion. After 6 days, tumors were harvested, digested to a single cell suspension, stained and then analyzed by flow cytometry. IL-7-CBD monotherapy did not alter total CD45+ immune cell infiltration, but CBD-IL-12 strongly induced an increase in total CD45+ immune cell infiltration (**Fig. 4.3**), but the addition of IL-7-CBD did not further increase this. CBD-IL-12 increases conventional (Foxp3-) CD4 T cell counts, though not significantly, and decreases Treg infiltration, but IL-7-CBD did not further alter either of these populations in the combination therapy or as a monotherapy compared to PBS (**Fig. 4.3**). Interestingly, the addition of IL-7-CBD did not alter CD8 T cell infiltration either as a monotherapy, compared to untreated mice, or as a combination therapy when compared to the CBD-IL-12 monotherapy (**Fig. 4.3**).

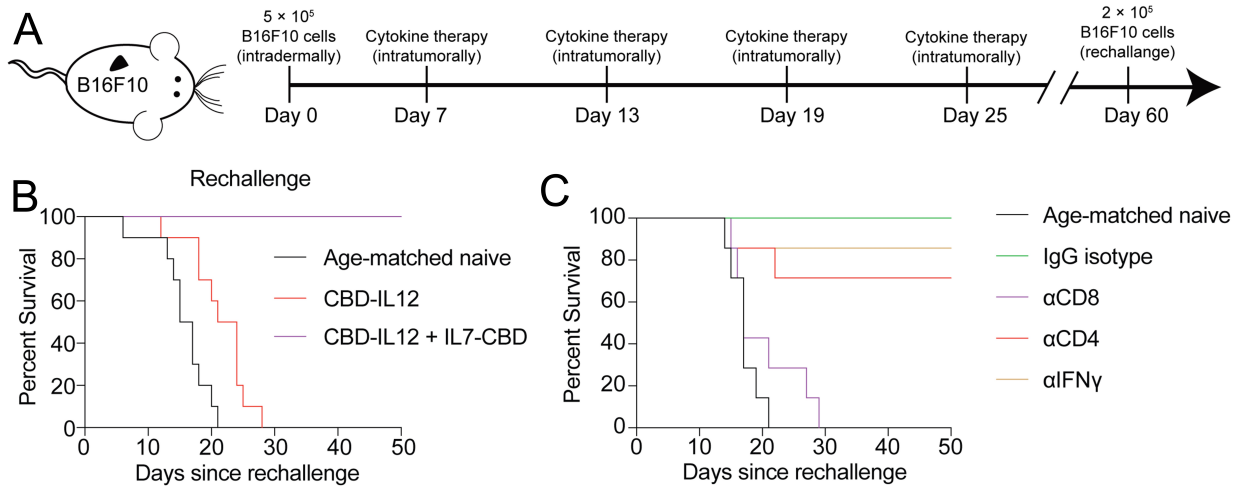

Figure 4.2: **IL-7-CBD and CBD-IL-12 combination promotes CD8 T cell memory** | C57BL/6 mice were inoculated with 5 x 10^5 B16F10 melanoma cells intradermally on day 0 and treated with either CBD-IL-12, or with CBD-IL-12 + IL-7-CBD as shown. After 60 days of the melanoma inoculation, tumor-free mice were rechallenged with 2 x 10^5 B16F10 melanoma (A). Overall survival shown of the rechallenged mice with no subsequent therapeutic intervention (B) The tumor-free mice due to CBD-IL-12 + IL-7-CBD combination therapeutic schedule, were rechallenged with 2 x 10^5 B16F10 melanoma and injected i.p with either 300 μg IgG isotype,α-CD8 depleting antibody, 300 μg α-CD4 depleting, or 300 μg α-IFN-γ blocking on day -1, 2, 5, and 8. The overall survival rate (C) is shown. **Data Provided by Dr. Seounghun Kang**

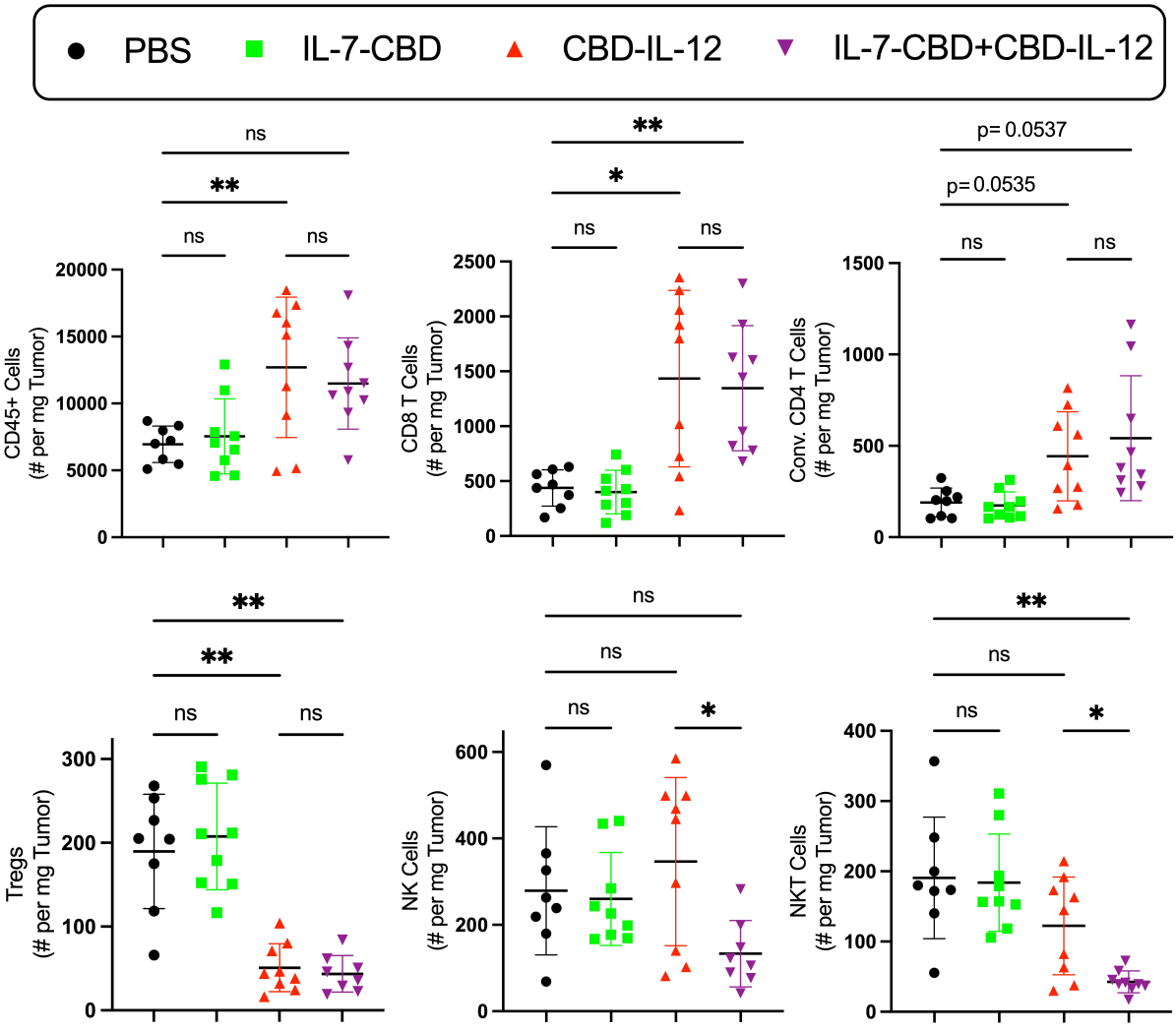

Figure 4.3: **Combination therapy reduces NK and NKT cell numbers compared to CBD-IL-12 monotherapy, but does not alter T cell population numbers** | B16F10 bearing mice were treated i.t. with either PBS, 33.3 pmol CBD-IL-12, 333 pmol IL-7-CBD, or 33.3 pmol CBD-IL-12 + 333 pmol IL-7-CBD, on day 7 and tumors were harvested day 13. Cells were digested into a single cell suspension, stained, and run by flow cytometry. Counts per mg tumor of relevant immune populations shown.

Interestingly, neither IL-7-CBD nor CBD-IL-12 monotherapies altered NK or NK T cell infiltration, but combination therapy decreased both NK and NKT cell infiltration compared to CBD-IL-12 monotherapy. (**Fig 4.3**). This highlights that the therapeutic efficacy of CBD-IL-12 and IL-7-CBD combination therapy is likely independent of NK and NKT cells, and thus would be reliant on T cells, which is consistent with rechallenge model experiments.

4.3.3 IL-7-CBD combination differentially regulates CD127 on NK Cells and CD8 T cells

IL-12 stimulation on NK cells promotes IFN-γ secretion, which can also potentiate their anti-tumor properties [153]; however, IL-7R is expressed by NK cells as well, and thus leads to an interested question: does IL-7-CBD alter IL-7R differentialy between NK cells and CD8 T cells, and could this partially explain the alteration in NK cell numbers upon combination therapy. Interestingly, we observed that IL-7 monotherapy slighly increased CD127+ NK cells, but that this increase is abrogated with the addition of CBD-IL-12, which strongly decreases CD127+ NK cells (**Fig 4.4A**); however, on these CD127+ NK cells, the expression level of CD127 (as quantified by MFI) is substantially lower in the combination group compared to CBD-IL-12 (**Fig 4.4B**). In NKT cells we see that CBD-IL-12 reduces CD127+ expression, and that IL-7-CBD in combination reduces it even further (**Fig 4.4A**), and that the expression level of CD127 decreases compared to PBS and IL-7-CBD monotherapy, but not CBD-IL-12 monotherapy groups (**Fig 4.4B**). Contrastingly, we see the opposite phenomena with CD127 expression on CD8 T cells, that CBD-IL-12 increases CD127 expression on CD8 T cells by both MFI and percentage, but that IL-7-CBD does not substantially later this further (**Fig 4.4A-B**). This data seems to explain the differences in infiltration seen since the addition of IL-7-CBD to CBD-IL-12 lowers NK and NKT cell CD127 expression and thus we observe a decrease in NK and NKT cell infiltration (**Fig 4.3**). Thus even though we introduce a large pool of IL-7 as a therapy, the cells are less primed to respond to it due to downregulation of the receptor and thus their is less effective in vivo responsiveness to IL-7, which could explain their lack of expansion of NK and NKT cells even in the context of added IL-7 [154].

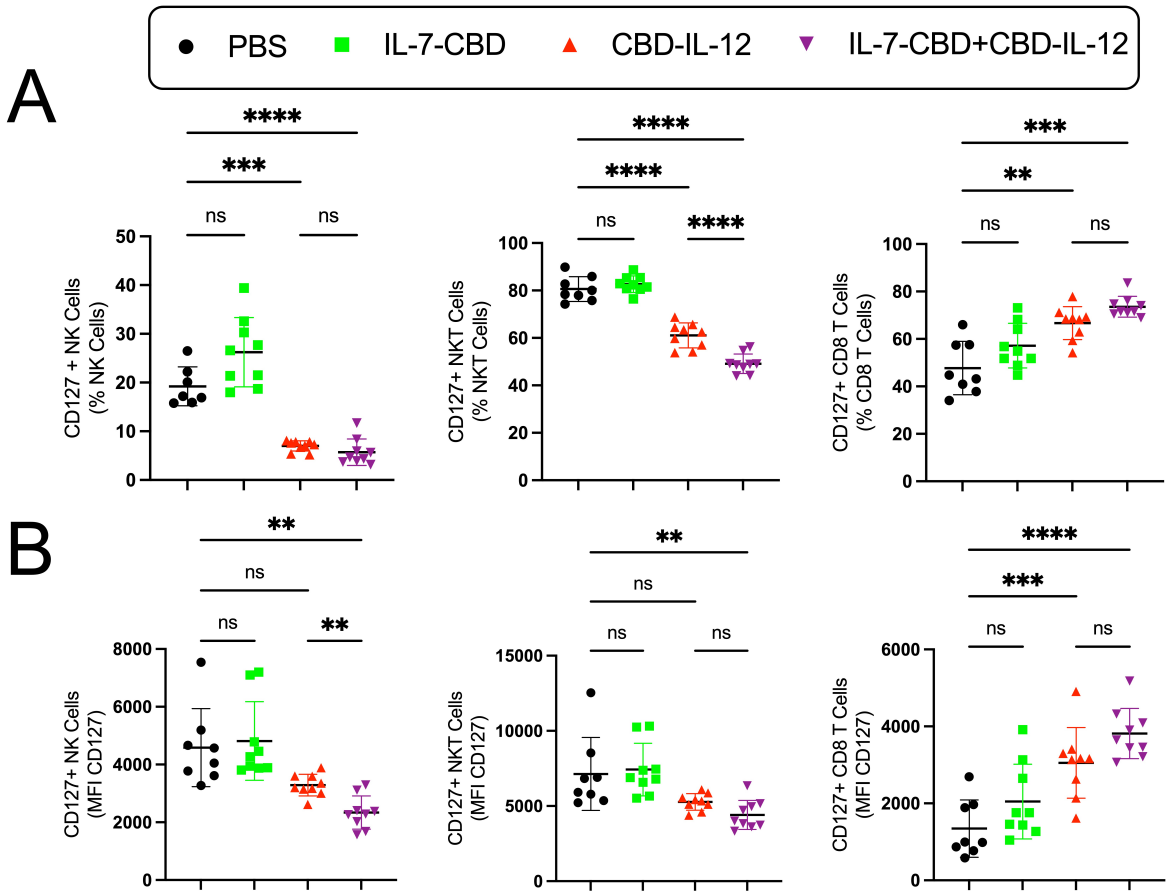

Figure 4.4: **IL-7-CBD combination therapy differentially alters CD127 on NK, NKT cells, compared to CD8 T cells** | B16F10 bearing mice were treated i.t. with either PBS, 33.3 pmol CBD-IL-12, 333 pmol IL-7-CBD, or 33.3 pmol CBD-IL-12 + 333 pmol IL-7-CBD, on day 7 and tumors were harvested day 13. Cells were digested into a single cell suspension, stained, and run by flow cytometry (A) Percentage of NK, NKT, and CD8 T cells that are CD127+. (B) MFI of CD127 of each of the CD127+ populations.

4.3.4 IL-7-CBD and CBD-IL-12 differentially alter the CD8 T cell phenotype

Because it is known that the quality of the T cell, and not just the total infiltration, is critical to immunotherapy responsiveness [39], we next assessed if the specific phenotype of the CD8 infiltrates was altered using unsupervised clustering via FlowSom, an algorithm specifically developed to analyze flow cytometry data, on CD8 T cells. We observed 7 distinct clusters as

determined by the algorithm, and they segregated distinctly when displayed on the UMAP (a way of visualizing high dimensional data in 2 dimensions) of the same CD8 T cells (**Fig. 4.5A**). The UMAP demonstrated that, while IL-7-CBD monotherapy does not seem to alter the CD8 T cell phenotype significantly compared to PBS treatment, IL-12 monotherapy does substantially modify the T cell landscape as we see a massive shift away from the clusters on the top of the UMAP (Cluster 6) and an enrichment of T cells in the clusters on the bottom of the UMAP (clusters 2-4) (**Fig. 4.5B-C**). The addition of IL-7-CBD further shifts the T cell landscape away from Cluster 6 and even more towards Cluster 2 and 4 (**Fig. 4.5B-C**). CBD-IL-12 monotherapy and combination therapy substantially increase Cluster 2, 3, 4, and 5 and substantially decrease Cluster 6 compared to PBS or IL-7 monotherapy treated groups while Clusters 0 and 1 are not substantially altered by CBD-IL-12 monotherapy (**Fig. 4.5C,F**).

We focused subsequent analysis on Clusters 2, 4, and 6 as they were significantly influenced by the IL-7-CBD combination when compared against CBD-IL-12 monotherapy (**Fig 4.5F**). Cluster 6 expressed high levels of canonical exhaustion markers such as Tim3 and PD-1 (30, 31), and it also uniquely expressed high levels of Tox, a marker known to be associated with terminal exhaustion (**Fig. 4.5E**) [42]. This indicates that supplementing CBD-IL-12 therapy with IL-7-CBD significantly reduces the frequency of exhausted CD8 T cells. Contrastingly, Cluster 2 and 4 both express high levels of KLRG1, a marker of effector function (**Fig. 4.5D-E**) [45]. Additionally, Cluster 4 has higher expression of IL-7Rα (CD127) as well as activation markers such as CD44, CD25 and ICOS and higher expression of PD-1, Lag3, and Tim3 compared to Cluster 2(**Fig. 4.5E**). Both Clusters 2 and 4 are distinctly enriched upon CBD-IL-12 treatment, but upon the addition of IL-7-CBD, these clusters are enriched even further and constitute about 70% of total CD8 T cells. (**Fig. 4.5F**). Thus, IL-7-CBD + CBD-IL-12 combination therapy alters the CD8 T cell landscape as evidenced by reduced abundance of the terminally exhausted Cluster 6 and increased

abundance of the “effector-like” Clusters 2 and 4.

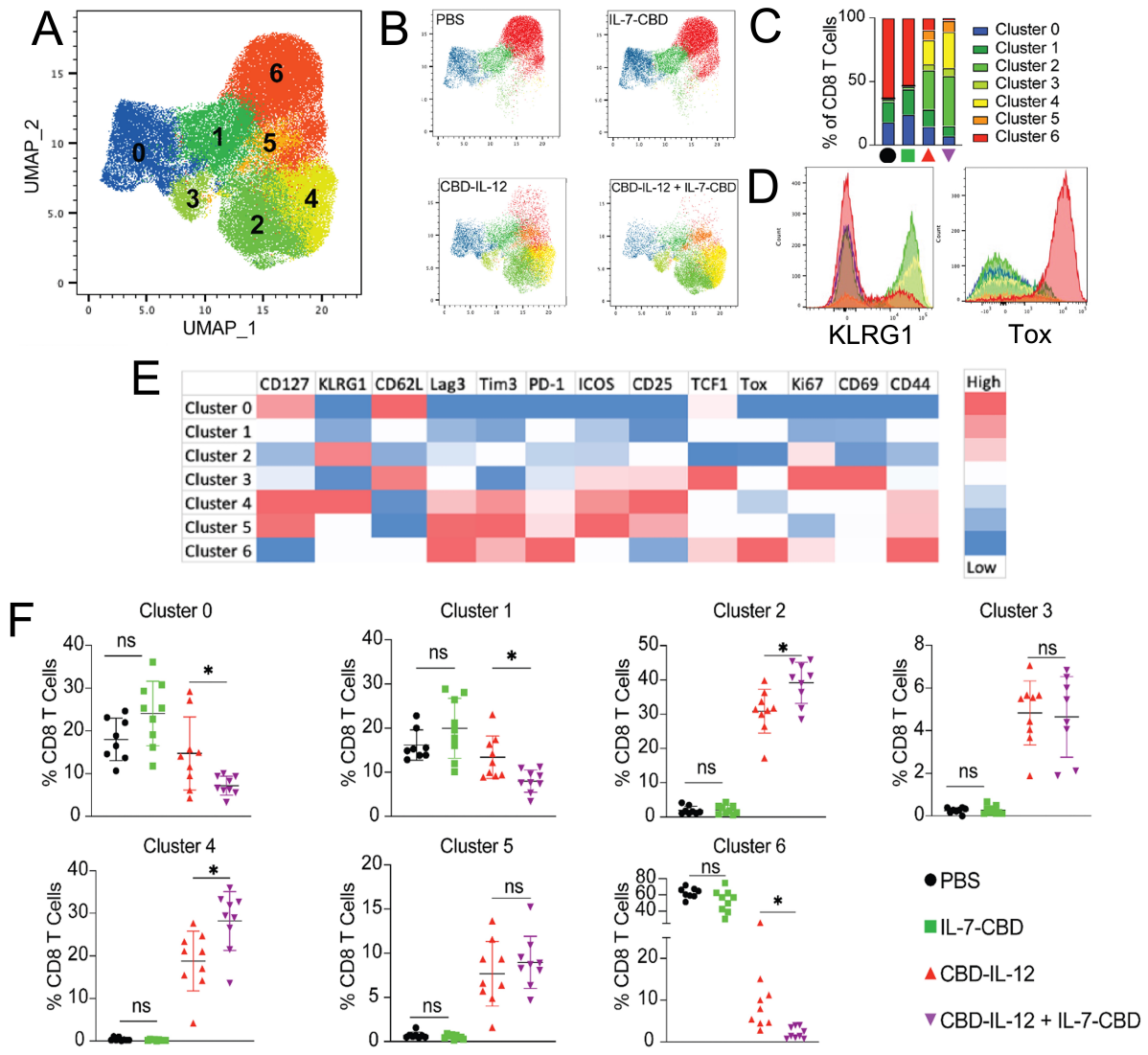

Figure 4.5: **IL-7-CBD synergizes with CBD-IL-12 to antagonize CD8 T cell exhaustion and promote CD8 effector T cells|** , B16F10 bearing mice were treated with either PBS (i.t., n=7), 33.3 pmol CBD-IL-12, 333 pmol IL-7-CBD (i.t., n=7), or 33.3 pmol CBD-IL-12 + 333 pmol IL-7-CBD (i.t., n=7) on day 7 and tumors were harvested day 13. Cells were digested into a single cell suspension, stained, and run by flow cytometry. (A) UMAP of concatenated CD8 T cells with FlowSom clustering displayed as an overlay. (B) UMAP displaying individual groups as labelled with clusters overlaid. (C) Stacked bar graph displaying the percentage of each group per cluster. (D) Expression of KLRG1 and Tox for each FlowSom cluster. (E) Heatmap of FlowSom clusters. (F) Percent population of each cluster for each sample.

4.3.5 CBD-GM-CSF and CBD-IL-12 combination therapy is a potent therapeutic that induces CD8 T cell memory

GM-CSF was explored in a very similar manner to IL-7-CBD as another potential combination therapeutic with CBD-IL-12. Using the same low dose of CBD-IL-12, the potential of CBD-GM-CSF was evaluated. When CBD-GM-CSF is combined with CBD-IL-12 we see an extension of survival compared to both the low-dose CBD-IL-12 (**Fig 4.6A**). We subsequently observed that this effect is dependent on the ability of CBD-IL-12 and CBD-GM-CSF to accumulate in the tumor as the unmodified versions of the cytokines did not substantially alter survival compared to CBD-IL-12 monotherapy (**Fig 4.6A**). We next assessed a high-dose (10 μg) single dose regimen as a monotherapy to determine if the low dose of IL-12 used in the combination therapy still allowed for similar efficacy of the high dose, without the associated toxicity of the higher dose of IL-12. With just this single dose, the low dose of CBD-IL-12 does not demonstrate much therapeutic benefit (**Fig 4.6B**). However, the combination therapy using the same dose has a very similar therapeutic benefit to that of the high dose of CBD-IL-12. Thus the addition of GM-CSF allows for a dramatic reduction in the required dose of IL-12, without compromising on efficacy.

Next, it was assessed if combination therapy could induce immunology memory, which we know from previous work that the high dose CBD-IL-12 monotherapy does not induce immunological memory, even though it can cure the tumors. Using the same approach as with the IL-7-CBD memory experiments, we observed that combination therapy mice that rejected the primary tumor, also could reject the secondary tumor in all cases, while high-dose CBD-IL-12 monotherapy mice that could reject the primary tumor succumbed to the rechallenge (**Fig 4.7B**). Thus the additional of CBD-GM-CSF with the lower dose of CBD-IL-12 allows for the formation of immunological memory. To determine which was the critical factor that determined this protection, mice from the combination therapy treatment that had cleared their primary tumor were the depleted of either CD4 or CD8 T cells, or

treated with an INFγ neutralizing antibody both before and during the early phase of tumor implantation. It was only the mice treated with the α-CD8 depleting antibody that lost almost all benefit of the combination therapy treatment, and all mice succumbed to the tumor while CD4 depletion and IFN-γ neutralization only had modest effects and behave very similar to the isotype control treated groups (**Fig4.7C**). Thus, combination therapy with CBD-GM-CSF also leads to an induction in CD8 T cell memory.

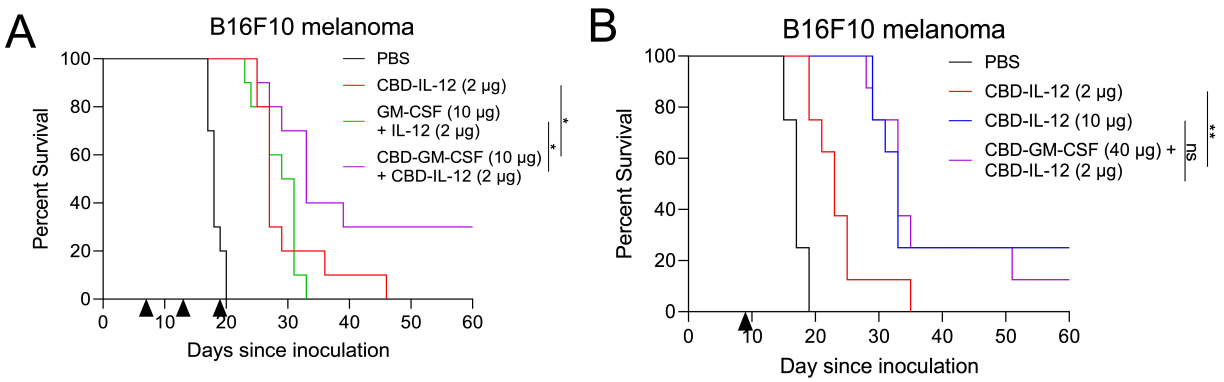

Figure 4.6: **CBD-GM-CSF and CBD-IL-12 combination therapy exhibit synergistic antitumor effect and reduce toxicity compared to high dose of CBD-IL-12|** C57BL/6 mice were inoculated with 5 x 10^5 B16F10 cells intradermally on day 0 and treated with either i.v. with PBS, IL-12 + GM-CSF, CBD-IL-12 or with CBD-IL-12 + CBD-GM-CSF on day 7, 13, 19, and 25. (A) Overall survival shown. C57BL/6 mice were inoculated with 5 x 10^5 B16F10 melanoma cells intradermally on day 0 and treated with either i.v. with PBS, 2 μg CBD-IL-12, 10 μg CBD-IL-12, or with 2 μg CBD-IL-12 + CBD-GM-CSF on day 9. (B) Overall survival shown. **Data Provided by Dr. Seounghun Kang**

4.3.6 Characterization of changes in immune populations in the tumor and tdLN due to CBD-IL-12 and CBD-GM-CSF

GM-CSF acts on a distinct immune population as IL-12, and thus to better assess the immunomodulatory effects of combination therapy, we assessed both the myeloid and the T cell aspects of the immune infiltrates after a single dose therapeutic regiment. CBD-GM-CSF and combination therapy have increased total CD45+ infiltrates and total macrophage

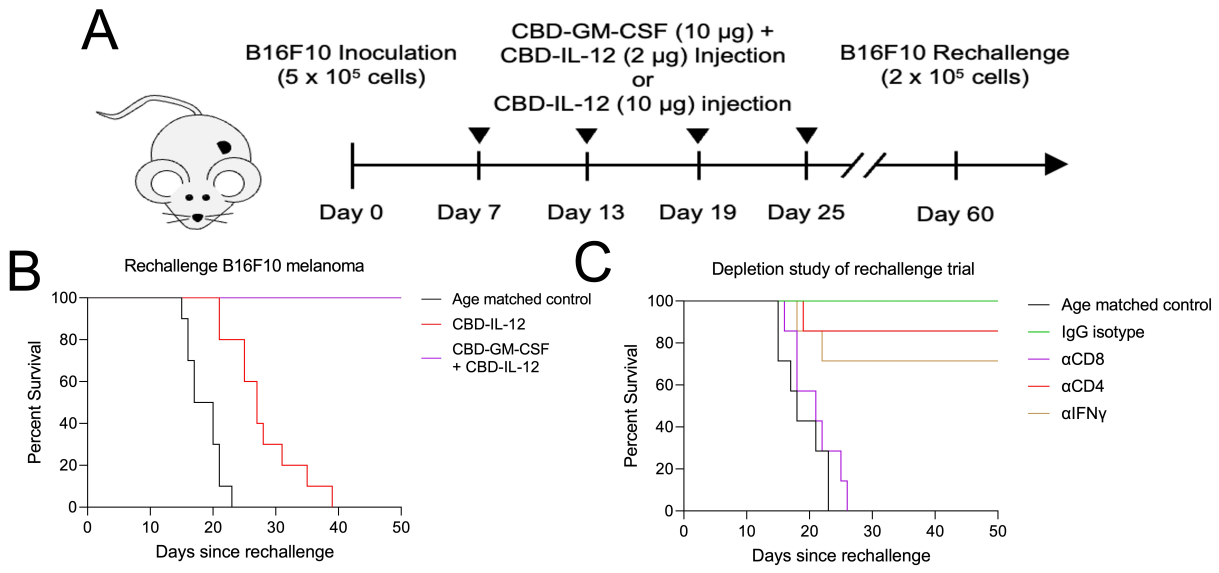

Figure 4.7: **CBD-GM-CSF and CBD-IL-12 combination promotes CD8 T cell memory** | C57BL/6 mice were inoculated with 5 x 10^5 B16F10 melanoma cells intradermally on day 0 and treated with either CBD-IL-12, or with CBD-IL-12 + CBD-GM-CSF as shown. After 60 days of the melanoma inoculation, tumor-free mice were rechallenged with 2 x 10^5 B16F10 melanoma (A) Experimental timeline (B) Overall survival shown of the rechallenged mice with no subsequent therapeutic intervention The tumor-free mice due to combination therapy, were rechallenged with 2 x 10^5 B16F10 melanoma and injected i.p with either 300 μg IgG isotype,α-CD8 depleting antibody, 300 μg α-CD4 depleting, or 300 μg α-IFN-γ blocking on day -1, 2, 5, and 8. The overall survival rate (C) is shown. **Data Provided by Dr. Seounghun Kang**

infiltration (**Fig 4.8A**). When analyzing the ratio of M1 (pro-inflammatory) to M2 (anti-inflammatory/tumor promoting), we observe that CBD-GM-CSF and combination induce massive increases in the proportion of M1 macrophages compared to CBD-IL-12 monotherapy (**Fig 4.8B**). We next assessed cDC1 infiltration of both CD8α+ and CD103+ DCs as these subsets are critical in the initiation of an anti-tumor immune response [152], and found no difference in cDC infiltration in any of the groups (**Fig 4.8C**). However, we observed a striking increase in cDC1 activation as assessed by CD86 expression in both CD103+ and CD8α+ DCs by the CBD-GM-CSF and combination, but not CBD-IL-12 ((**Fig 4.8D-E**). For all of this myeloid analysis, the CBD-GM-CSF affect dominates and there is no differ-

ence between CBD-GM-CSF monotherapy and combination. Thus CBD-GM-CSF promotes macrophage infiltration, M1 polarization, and DC activation and that this effect is dominant even in the presence of CBD-IL-12.

We next assessed if the T cell infiltration was altered. As shown previously, CBD-IL-12 monotherapy leads to dramatic increase in CD8 T cell infiltration and a decrease in Treg infiltration (**Fig 4.8F**). CBD-GM-CSF monotherapy does not increase CD8 T cell infiltration, and may slightly increase Treg infiltration (**Fig 4.8F**). With combination therapy, we observe a stark increase in CD8 T cell infiltration compared to either monotherapy, but no alteration in Treg infiltration compared to CBD-IL-12 (**Fig 4.8F**). Furthermore, when quantifying the ratio of CD8 T cells to Tregs in the tumor, we see that while CBD-IL-12 increases the CD8/Treg ratio dramatically from baseline, that the addition of CBD-GM-CSF in the combination therapy increases this ratio even further (**Fig 4.8G**). Thus, the addition of CBD-GM-CSF to CBD-IL-12 increases CD8 T cell infiltration, but does not alter Treg infiltration compared to CBD-IL-12 monotherapy, thus leading to a start increase in CD8 T cells compared to Treg (**Fig 4.8G)**).

We next wanted to assess if the CD8 T cell infiltrate quality changes substantially, so we performed clustering as described for IL-7-CBD. We observed 8 distinct clusters (**Fig 4.9A**), and that as shown previously, CBD-IL-12 substantially alters the T cell landscape ((**Fig 4.9B**). CBD-GM-CSF monotherapy does not alter the CD8 T cell landscape substantially (**Fig 4.9B**); however, with the addition as a combination therapy, we see only a clear shift in Cluster 7, which decreases in combination therapy compared to CBD-IL-12 monotherapy (**Fig 4.9B**). We observe that these clusters segregate nicely on the UMAP, which indicates that they do represent distinct populations of cells, and that when analyzing the expression profile of each cluster, they do have distinct patters of expression ((**Fig 4.9B-C**). We observe that Cluster 0 appears to be terminally exhausted to due the expression of all the canonical exhaustion markers such as Tim3, PD-1, and Tox (**Fig 4.9C**). Cluster 4 and 5 express

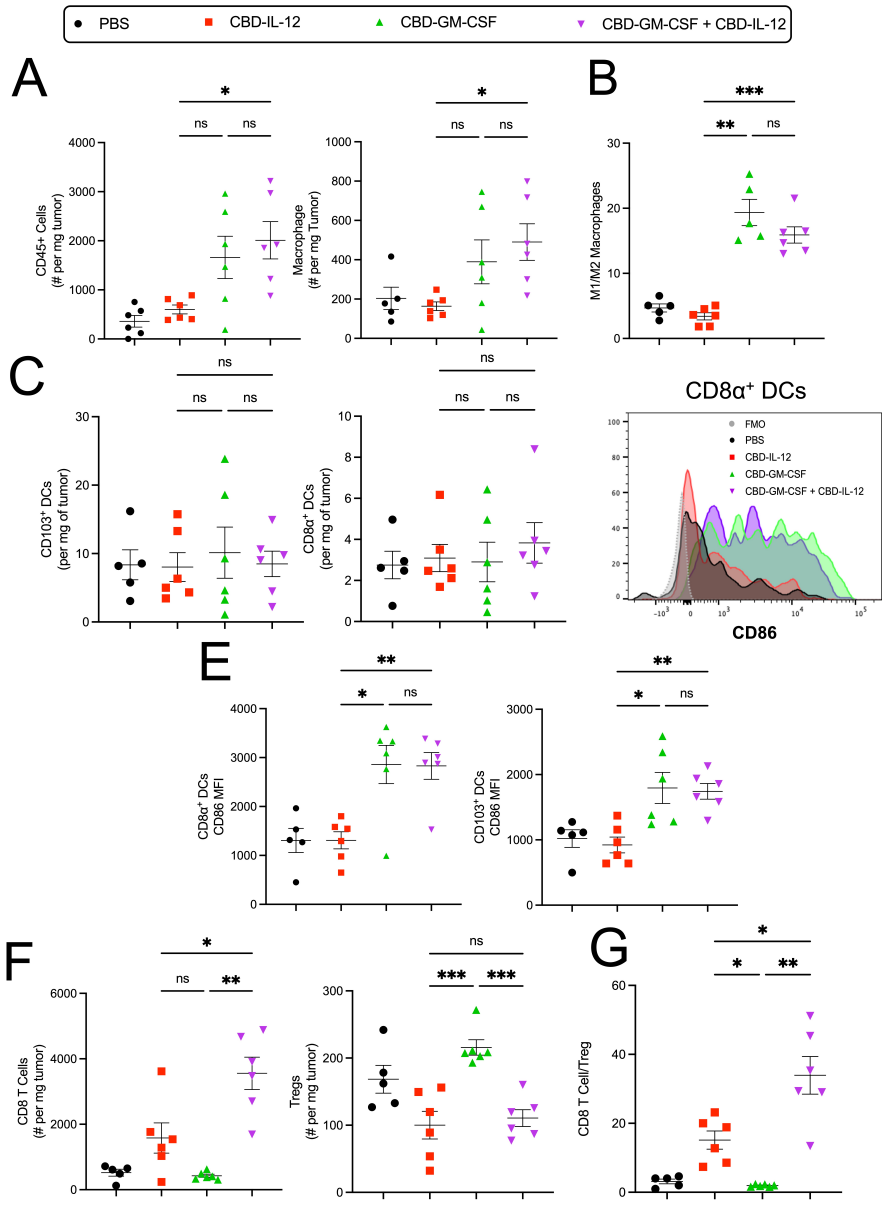

Figure 4.8: **CBD-GM-CSF increases intratumoral immune infiltration, antagonizes M2-macrophages, and increased cDC1 activation, which synergizes with CBD-IL-12 to enhance CD8 T cell infiltration**| B16F10 bearing mice were treated intratumorally with either PBS, CBD-IL-12, CBD-GM-CSF, or CBD-IL-12 + CBD-GM-CSF on day 7 and tumors were harvested day 13. Cells were digested into a single cell suspension, stained, and run by flow cytometry. (A) CD45+ and macrophage counts per mg of tumor (B) M1 /M2 macrophage ratio (C) CD103+ and CD8α+ DCs per mg of tumor (D) CD86 median fluorescence intensity (MFI) quantified forCD103 and CD8α+DCs (F) CD8 T cells and Tregs per mg of tumor (G) CD8 T cells to Treg ratio.

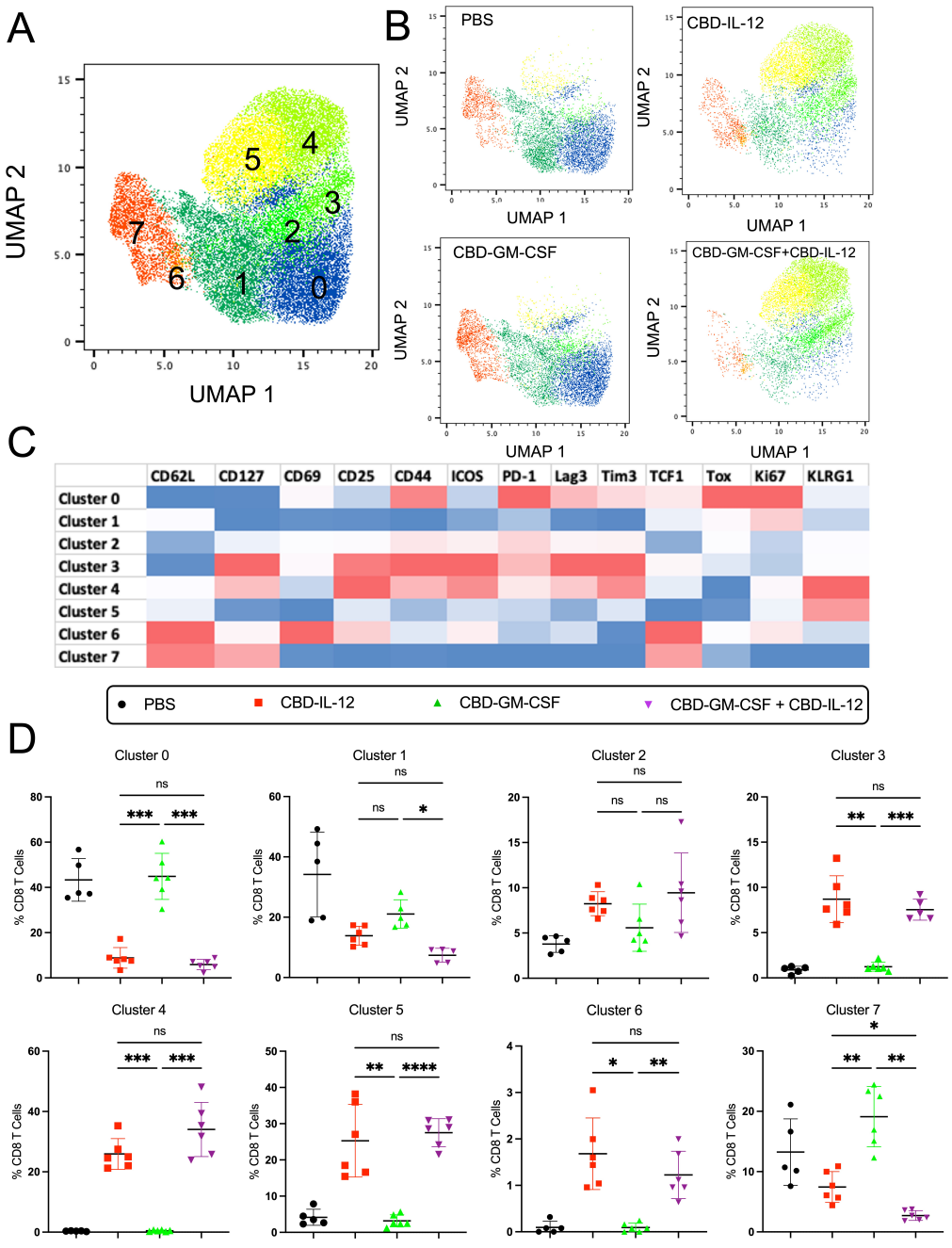

Figure 4.9: **CBD-GM-CSF does not substantially alter CD8 TIL populations**| B16F10 bearing mice were treated intratumorally with either PBS, CBD-IL-12, CBD-GM-CSF, or CBD-IL-12 + CBD-GM-CSF on day 7 and tumors were harvested day 13. Cells were digested into a single cell suspension, stained, and run by flow cytometry. (A) UMAP of concatenated CD8 T cells with FlowSom clustering displayed as an overlay. (B) UMAP displaying individual groups as labelled with clusters overlaid. (C) Heatmap of FlowSom clusters. (D) Percent population of each cluster for each sample.

high levels of KLRG1, and may be a more "effector-like" functional cell population (**Fig 4.9C**). The other clusters recommend various other activation and exhaustion states due to the varied expression of PD-1, CD44 and CD62L to name a few (**Fig 4.9B**). Thus this clustering does represent the diversity of the cell populations. When quantified individually, Cluster 7 is the only cluster that significantly changes compared to CBD-IL-12 monotherapy (**Fig 4.9D**). When looking at the holistic expression profile of this Cluster, they appear to be naive CD8 T cells as they express CD127 and CD62L, but do not express CD44 or any other activation markers (**Fig 4.9C**). Thus CBD-GM-CSF reduces the proportion of naive T cells in the tumor, but it is a modest effect (**Fig 4.9D**). Thus CBD-GM-CSF in combination increase CD8 T cell infiltration overall compared to either monotherapy, but does not substantially alter the phenotype of the CD8 T cell.

4.3.7 GM-CSF induces changes in immune cell populations in the tdLN

Lastly, since we see difference in DC activation in the T cell infiltrates, we wanted to assess the tumor draining lymph node (tdLN) to ascertain if there are differences in the lymph node APCs that could also help explain the difference in immune infiltrates in the tumor. We analyzed both the myeloid and T cell infiltrates in the tdLN by flow cytometry using the same experimental schedule as previosly described. Similar to the tumor, we observe an increase in macrophages (**Fig 4.10A**) and in M1 polarization (**Fig 4.10B**) with CBD-GM-CSF and combination compared to PBS and CBD-IL-12. Furthermore, while we did not observe alterations in DC infiltration in the tumor previously, we did observe an increase in DCs in the tdLN, and while there was no clear increase in migratory CD103+ DCs, there is a clear increase in lymph node resident CD8α+ DCs with combination therapy compared to CBD-IL-12 alone, though there is no further increase between CBD-GM-CSF monotherapy and combination (**Fig 4.10C**). When analyzing the activation state of these cDC1s through CD86 expression we observe that CD8α+ DCs strongly upregulate CD86

with CBD-GM-CSF and combination compared to PBS or CBD-IL-12 (**Fig 4.10D**). With CD103+ migratory cDC1s we see a similar, but not as striking trend where CBD-GM-CSF upregulates CD86 slightly compared to CBD-IL-12 and there is no difference between monotherapy and combination, but due to an increase in variance in the population, there is no statistical difference between combination therapy and CBD-IL-12 monotherapy either (**Fig 4.10D**). Thus CBD-GM-CSF therapy increases in macrophage infiltration in the tdLN and M1 polarization, and increased DCs and their activation. While we see slight difference in the CD103+ DCs, the more striking difference is LN-resident CD8α+ DCs, which implies that potentially T cells in the lymph node may be better activated in the CBD-GM-CSF and combination therapy groups.

When we analyze the T cell infiltrates in the lymph node, we see an increase in Tregs with CBD-GM-CSF monotherapy, but that this increase is lost with either CBD-IL-12 or combination therapy (**Fig 4.10E**). Furthermore, we observe that CBD-IL-12 enriches effector CD8 T cells and that this enrichment is preserved in the combination therapy as well while CBD-GM-CSF does not have any visible difference from PBS (**Fig 4.10E**). Lastly, we observe that CBD-IL-12 slightly increases the proportion of central memory CD8 T cells as well compared to PBS or CBD-GM-CSF, but uniquely combination therapy increases central memory formation in the lymph node compared to either monotherapy (**Fig 4.10F**). Thus combination therapy has overall more CD8 T cell activation, but no increase in Tregs that is seen by CBD-GM-CSF monotherapy. In the tdLN, combination therapy gets all the benefits of CBD-GM-CSF in the myeloid component and the benefits of the T cell activation of the CBD-IL-12 which synergize together for increases in central memory CD8 T cells in the tdLN. Furthermore, the CBD-IL-12 addition also counteracts the pitfalls of CBD-GM-CSF such as increases in Tregs, as CBD-IL-12 strongly antagonizes Tregs.

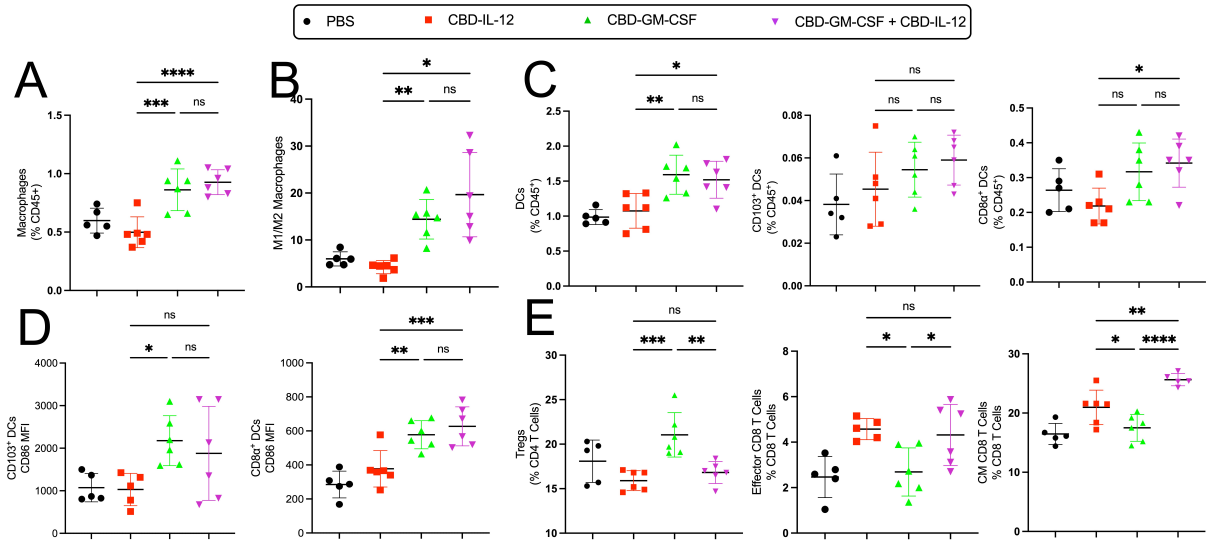

Figure 4.10: **In the tdLN, CBD-GM-CSF increases macrophage and DC infiltration, CBD-IL-12 increases CD8 T Cell activation while both these effects are observed upon combination therapy** | B16F10 bearing mice were treated intratumorally with either PBS, CBD-IL-12, CBD-GM-CSF, or CBD-IL-12 + CBD-GM-CSF on day 7 and tumors and tdLNs were harvested on day 13. Cells were digested into a single cell suspension, stained, and run by flow cytometry. (A) Macrophages as a percentage of CD45+ cells(B) M1/M2 Macrophage ratio (C) DC and DC subsets (CD8α+ and CD103+) as a percentage of CD45+ cells (D) CD86 median fluorescence intensity (MFI) quantified for both CD103 and CD8α+DCs (E) Tregs, effector CD8 and central memory CD8 quantified as a percentage of parental T cells

4.4 Discussion

IL-7-CBD and CBD-GM-CSF both potently synergize with CBD-IL-12 to lower the dose and thus reduce the toxicity of IL-12 without compromising efficacy. Furthermore, both are able to produce immunological memory in the B16F10 melanoma model that is CD8 dependent and that high dose CBD-IL-12 monotherapy is unable to induce. However, despite both of these achievements, it is interesting to observe that they clearly have distinct mechanisms of achieving this benefit.

IL-7-CBD acts in concert with CBD-IL-12 to alter the TILs directly. CBD-IL-12 and combination therapy reduced Treg infiltration but increased total CD45+ infiltration and

CD8 T cell infiltration (**Fig 4.3**). The addition of IL-7-CBD to the CBD-IL-12 also uniquely reduced NK and NKT cell infiltration and that their expression of CD127 is decreased as well (**Fig 4.3, 4.4A-B**). This is relevant since both NK and NKT cells can be producers of IFN-γ [155, 156], and its strong induction is one of the main reasons for the toxicity of IL-12 [139, 141]. Thus by reducing NK and NKT cell infiltration, there may be a decrease in offtarget IFN-γ induction. While NK cells may have some role in the anti-tumor response [157], it is likely not essential for the therapeutic efficacy of IL-7-CBD/CBD-IL-12 as even the blockade of INFγ did not substantially effect the protective effect of the immunological memory upon rechallenge (**Fig 4.2C**). Thus IL-7-CBD in combination seems to lower presence of cell types that could be making additional IFN-γ producing NK and NKT cells and thus could serve as sources of toxicity. Interestingly, even though IL-7 is a T cell survival cytokine, it did not alter CD8 T cell infiltration either as a monotherapy compared to PBS or a combination therapy compared to CBD-IL-12 (**Fig 4.3**); however, the addition of IL-7-CBD to CBD-IL-12 alters the T cell quality by reducing the presence of exhausted T cells and increasing the presence of "effector-like" KLRG1+ TILs compared to CBD-IL-12 monotherapy (**Fig 4.5F**). Thus IL-7-CBD and CBD-IL-12 act directly on the lymphocytes to reduce NK and NKT cells and enhance the quality of the CD8 TILs and this likely drives the therapeutic efficacy, reduced toxicity, and the CD8 T cell memory observed.

In contrast, GM-CSF works very differently. CBD-GM-CSF increases macrophage infiltration in the tumor and promotes the polarization of M1-macrophages (**Fig 4.8A**), which are classical pro-inflammatory macrophages and can have important anti-cancer effects while M2-macrophages generally promote tumor progression [149, 150]. Thus we posit this increase in M1-macrophage infiltration may contribute to the therapeutic efficacy of the combination therapy. Interestingly, while there was no increase in cDC1s, there was enhanced cDC1 activation due to CBD-GM-CSF and combination (**Fig 4.8C-E**). While we do not see substantial alterations in the CD8 T cell quality in the tumor in combination therapy compared

to CBD-IL-12 (**Fig 4.9**), we do see an increase in CD8 T cell infiltration and in the CD8/Treg ratio (**Fig 4.8F-G**). Thus CBD-GM-CSF enhanced DC activation and the accumulation of pro-inflammatory macrophages, and when combined with the T cell activating ability of CBD-IL-12 leads to a synergistic increase in CD8 T cell infiltration.

Interestingly, while CBD-GM-CSF alters all cDC1s in the tumor, it selectively targeting CD8α+ DCs in the tdLN as we see a clear increase and enhanced activation of CD8α+ DCs in the tdLN (**Fig 4.10C-D**). Thus, we hypothesize that with CBD-GM-CSF, T cells that traffic to the lymph node are able to get more strongly activated by cDC1s. Combined with the ability of CBD-IL-12 to activate the T cells directly, this leads to a synergistic effect of activation that leads to increased accumulation of these CD8 T cells in the tumor due to enhanced priming in the lymph node as well as the tumor. In short, GM-CSF induces activation of cDC1s in the tumor and the lymph node which synergize with CBD-IL-12 to lead to increases in CD8 T cell infiltration, without altering Tregs, compared to CBD-IL-12.

There are several limitations to these studies. First of all, though sophisticated methods were used to analyze the immune CD8 T cell infiltrates in both the therapeutic approaches, we cannot make any claims that these T cells are tumor-specific since we did not adoptive transfer in tumor-specific T cells that we could track nor did we use tetramers to look at the endogenous antigen specific component. We chose not to transfer in transgenic T cells since it is known that the affinity of the TCR can alter the ability of the T cell to get exhausted and we did not want to make broad claims about the ability of the therapeutic on one single affinity versus a pool of variable affinities that would be more like the endogenous repertoire [158]. While tetramers would avoid this complication, since they only represent one given peptide-MHC I epitope, the quantity of cells specific to that epitope would be quite small since the tumor has many associated antigens. Thus, we only make claims about how the infiltrates change, but deliberately have not made any claims of antigen-specificity from this data. For the CBD-GM-CSF characterization of the myeloid cells, a more rigorous

analysis of the DC's could have been performed including looking at antigen processing and presentation by using (for example) a tumor with a trackable fluorescent protein of these DCs and if CBD-GM-CSF can alter DC ability to process and present antigen. Furthermore, while we can say the DCs have a more activated phenotype with CBD-GM-CSF, without performing complex studies involving sorting out DCs from the tumor and determining if these DCs are better able to activate tumor specific T cells, we cannot make conclusive claims about if CBD-GM-CSF truly enhanced the activation of CD8 T cells, though based on the literature that does seem likely. Thus, while we are making these observations about the myeloid compartment and how that could explain the differences in the lymphocyte compartment, they would have to be tested more rigorously to truly show causation.

This chapter serves to highlight two different strategies for combination therapeutics with the aim of lowering the toxicity of IL-12 by lowering the required dose. Both IL-7-CBD and CBD-GM-CSF lower the required dose of CBD-IL-12 substantially, without altering efficacy, and promote bona fide CD8 T cell memory; however, these therapies have distinct immunomodulatory capabilities. IL-7-CBD acts on the side of the lymphocytes to directly promote T cell survival of these "effector-like" T cells and the reduction of terminally exhausted T cells while CBD-GM-CSF acts on the myeloid cells to increase M1-macrophage polarization and increase cDC1 activation in the tumor and the tdLN, which cause enhanced priming of CD8 T cells and thus overall increase CD8 T cell infiltrates. It would be interesting to probe if there could be any potential synergy by combining CBD-IL-12, IL-7-CBD, and CBD-GM-CSF into one therapeutic regimen. Potentially we could lower the dose of CBD-IL-12 even further.

4.5 Methods

4.5.1 Tumor size measurements and survival

For all experiments testing therapeutic efficacy, tumor size was calculated using the following formula: height x width x thickness x ($\pi/6$) for all experiments. The mice were euthanized when the tumor size reached 1,000 m^3 and/or based on humane end-point criteria.

4.5.2 Therapeutic evaluation of CBD-IL-12 + IL-7-CBD

To test for the synergystic effect of CBD-IL-12 with IL-7-CBD, C57BL/6 mice were inoculated with 5 x 10^5 B16F10 melanoma cells intradermally on day 0 and injected with intravenously (i.v.) with 100 μL PBS, 33.3 pmol CBD-IL-12, 33.3 pmol IL-12 + 1.3 nmol IL-7, or 33.3 pmol CBD-IL-12 + 1.3 nmol IL-7-CBD on day day 7, 13, 19, and 25. Tumors were measured until mice reached endpoint to generate survival curve.

To test the efficacy of combination therapy compared to high dose CBD-IL-12, C57BL/6 mice were inoculated with 5 x 10^5 B16F10 melanoma cells intradermally on day 0 and injected i.v. with 100 μL PBS, 33.3 pmol CBD-IL-12, 166.5 pmol CBD-IL-12, or 33.3 pmol CBD-IL-12 + 1.3 nmol IL-7-CBD on day 8. Tumors were measured until mice reached endpoint to generate survival curve.

4.5.3 Therapeutic evaluation of CBD-IL-12 + CBD-GM-CSF

C57BL/6 mice were inoculated with 5 x 10^5 B16F10 melanoma cells intradermally on day 0. To verify the synergistic effect of CBD-GM-CSF with CBD-IL-12, mice were treated i.v. with 100 μL PBS, 33.3 pmol CBD-IL-12, 657.9 pmol GM-CSF + 33.3 pmol IL-12, and 657.9 pmol CBD-GM-CSF + 33.3 pmol CBD-IL-12 on day 7, 13, 19, and 25. Tumors were measured until mice reached endpoint criteria to generate survival curve.

To test the efficacy of combination therapy compared to high dose CBD-IL-12, mice were

treated i.v. on day 9 with a single dose of 100 μL PBS, 33.3 pmol CBD-IL-12, 166.5 pmol CBD-IL-12, and 2.6 nmol CBD-GM-CSF + 33.3 pmol CBD-IL-12. Tumors were measured until mice reached endpoint criteria to generate survival curve.

4.5.4 Assaying for the development of immunological memory and identifying the key cell subsets involved in

To study the development of immunological memory formation, mice that were cured from either 10 μg CBD- IL-12 monotherapy or 2 μg CBD-IL-12 + IL-7-CBD combination therapy given intratumorally on days 7, 13, 19, and 25 were rechallenged with 2 x 10^5 B16F10 tumor cells on day 60 (60 days after the primary tumor inoculation) on the contralateral side of the back.

To understand which immune cell subsets were responsible for the rejection of B16F10 rechallenge, mice that were cured with intratumorally administered CBD-IL-12 + IL-7-CBD combination therapy were rechallenged with 2 x 10^5 B16F10 melanoma cells intradermally on day 60 (60 days after primary tumor inoculation) and injected intraperitoneally with IgG isotype antibody, 300 μg CD8 antibody, 300 μg CD4 antibody, and 300 μg IFN-γ antibody on days 59, 62, 65, and 68 (post primary tumor inoculation). The following anti- mouse antibodies were used for inhibition: IgG isotype antibody (clone: MOPC-21, BioXCell), αCD8 (clone: 2.43, BioXCell), αCD4 (clone: GK1.5, BioXCell), αIFN-γ (clone: XMG1.2, BioXCell).

For the CBD-GM-CSF experiments, the exact same experimental schedule is used, but the IL-7-CBD is replaced with a dose of 657.9 pmol of CBD-GM-CSF. Experiments to test the memory recall ability compared to the CBD-IL-12 high dose and to identify the subset involving using the depletion/blocking antibodies were both performed as described above.

4.5.5 Experimental model and sample preparation for analysis of immune infiltrates by flow cytometry in B16F10 melanoma

C57BL/6 mice were inoculated with 5 x 10^5 B16F10 melanoma cells intradermally on day 0 and injected with 30 μL PBS (n=8), 33.3 pmol CBD-IL-12 (n=8), 333 pmol IL-7-CBD, or 33.3 pmol CBD- IL-12 + 333 pmol IL-7-CBD on day 7. The exact dosing regimen was followed as well with CBD-GM-CSF, but just replace the presence of IL-7-CBD with 657.9 pmol of CBD-GM-CSF. The tumors were harvested and digested on day 13. In brief, the tumors were cut into small pieces and then digested in 1 mL digest solution (DMEM with 2 % FBS, 1 mg/mL collagenase IV (Worthington Biochemical), 3.3 mg/mL collagenase D (Sigma-Aldrich), 20 μg per mL DNase I (Worthington Biochemical), and 1.2 mM $CaCl_2$ for 60 min at 37°C on a shaker. Then, the tumor mixture was quenched by 5 mM EDTA, and single cell suspension was prepared using a cell strainer (70 μm). The single cells were resuspended in DMEM with 2 % FBS, and cell staining was performed. Lymph nodes were digested in 500 μL of the same digestion buffer, quenched with 5 mM EDTA and subsequently smashed through a 70 μm cell strainer.

4.5.6 Flow cytometry staining

20 mg of tumor is plated per sample per panel for both the IL-7-CBD and CBD-GM-CSF analysis. Analysis on the tdLN was performed as well for only the CBD-GM-CSF experiments. Cells were washed in PBS and then CD16/32 Fc block (Clone 93, Biolegend) at 1:100 dilution along with viability stain at 1:500 was performed for 15 min at 4°C in PBS. For the T cell panel, Live/Dead Blue (Thermo Fisher Scientific) was used. Cells were then washed in FACs Buffer (2 % FBS in PBS) and stained for all surface markers in 50 μL 15 min at 4°C in Brilliant Stain Buffer (BD). Single stains are stained in FACs Buffer during this step. Cells were washed again in PBS and fixed in 50 μL of Foxp3 Fixation/Permeabilization Kit (eBioscience) for 30 min at 4°C. Cells were then washed in 1x permeabilization buffer

(eBioscience) and cells were stained for intracellular markers overnight at 4°C. Cells were then washed one last time in FACs Buffer and resuspended in 100 μL FACs buffer before samples were run on the Cytek Aurora. Data analysis was performed using FlowJo (BD) and statistical analysis performed using Prism v9 (Graphpad). To see flow panel, refer to **Table 4.1** below for further information.

Fluorophore	Specificity	Clone	Purpose	Dilution
AF532	CD45	30-F11	Pan-Immune	400
CD3e	BUV395	145-2C11	T Cells	100
CD4	BUV496	GK1.5	CD4 T Cells	400
CD62L	BUV737	MEL-14	Naive/Memory T Cells	400
CD8a	BUV805	53-6.7	CD8 T cells	4400
Lag3	BV421	C9B7W	Exhaustion	200
TCF1	Pacific Blue	C63D9	Stemness	100
Tim3	BV480	5D12	Exhaustion	400
PD-1	BV605	29F.1A12	Activation/Exhaustion	200
ICOS	BV650	C398.4A	Activation	200
CD25	BV785	PC61	Activation/Treg	200
Foxp3	AF488	MF23	Tregs	200
CD44	PerCp-Cy5.5	IM7	Antigen experience	400
Tox	PE	TXRX10	Terminal Exhaustion	400
CD69	PE/Dazzle594	H1.2F3	Activation	400
Ki67	PE-Cy7	B56	Proliferation	400
CD127	AF647	A7R34	IL-7R	200
KLRG1	APC-Cy7	2F1/KLRG1	Effector-function	400
NK1.1	APC/Fire810	S17061D	NK Cells	400

Table 4.1: Flow cytometry panel for TIL Analysis

The myeloid panel was only utilized for the CBD-GM-CSF experiments in both the tumor and tdLN. All steps were as described above, with the following modifications. Viability was performed using Live/Dead Aqua (Thermo Fisher Scientific) at 1:500. Since there are no intracellular markers, cells were stained for surface markers, and then fixed in 2 % PFA for 15 min at 4°C. Cells were then washed in FACs buffer, resuspended in 100 μL, and samples were run on the BD Fortessa 4-15. Data analysis was performed using FlowJo (TreeStar Inc) and statistical analysis performed using Prism v9 (Graphpad). To see flow panel, refer

to **Table 4.2** below for further information.

Fluorophore	Specificity	Clone	Purpose	Concentration
ef450	CD103	2E7	DC Subsetting	1:400
BV605	Gr1	RB6-8C5	MDSC	1:400
BV650	CD11c	N418	DCs	1:400
FITC	CD11b	M1/70	Myeloid	1:400
PerCp-Cy5.5	MHC II	M5/114.15.2	DCs	1:400
PE	CD206	C068C2	M2-Macrophages	1:400
PE/Dazzle-594	CD86	GL-1	DC Activation	1:400
PE-Cy7	PD-L1	10F.9G2	Immunosuppression	1:400
CD8a	AF647	53-6.7	DC Subsetting	1:400
APC-R700	F4/80	T45-2342	Macrophages	1:400
APC-Cy7	CD45	30-F11	Pan-Immune	1:400

Table 4.2: Flow cytometry panel for Myeloid Analysis

4.5.7 Flow cytometry clustering

After spectral unmixing and conventional compensation was performed using a combination of single stained cells and compensation beads (Cat 01-3333-42, Thermo Fisher Scientific), CD8 T cells were manually gated as shown (**Fig 4.11**). Equal sampling of 1800 CD8 T cells per sample were then concatenated together into one file, and all subsequent analysis was performed. Individual samples could be identified from the concatenated file due to unique keyword identifiers added to the individual samples before concatenation. Dimensionality reduction was performed via Uniform Manifold Approximation and Projection (UMAP) while FlowSom was used for unsupervised clustering. Both UMAP and FlowSom are available as FlowJo plugins and can be freely downloaded from the FlowJo Exchange. Both dimensionality reduction and clustering were performed using the following markers: CD44, CD62L, Lag3, PD-1, Tim3, TCF1, Tox, CD69, CD127, CD25, ICOS, Ki67, KLRG1. UMAP was used to visualize the high-dimensional data into one 2-dimensional space. Unsupervised clustering was performed using FlowSom. The number of clusters was determined automatically by the algorithm, but the quality of the clustering was also visually confirmed

by overlaying the FlowSom clusters on the UMAP. Thus, no modifications to the FlowSom default program were necessary for this data.

4.5.8 Statistics

Unless otherwise stated, statistical significance was analyzed by unpaired, 2- tailed Student's t test or by ANOVA followed by Tukey's post- hoc test for group analysis using Prism (GraphPad). Differences in survival curves were assessed using the log- rank (Mantel-Cox) test. P-value < 0.05 was considered statistically significant.

4.6 Acknowledgments

Panel design (including selection of molecular targets), titrations of antibodies, and optimization were all performed by me. All flow analysis, both manual gating and clustering was performed by me. Staining for the T cell panel in the tumor and tdLN in both the IL-7-CBD and CBD-GM-CSF experiments was performed by me. Acquisition of the samples on the Cytek Aurora was performed by me. Special thanks to Dr. Seounghun Kang for help staining the myeloid panel for the GM-CSF experiments as well as help running those panels on the BD Fortessa 4-15.

Special thanks to Dr. Seounghun Kang for providing the data that demonstrated the therapeutic efficacy of IL-7-CBD and CBD-GM-CSF and for performing the in vivo experiments to generate the samples for flow cytometry analysis.

4.7 Supplemental Figures

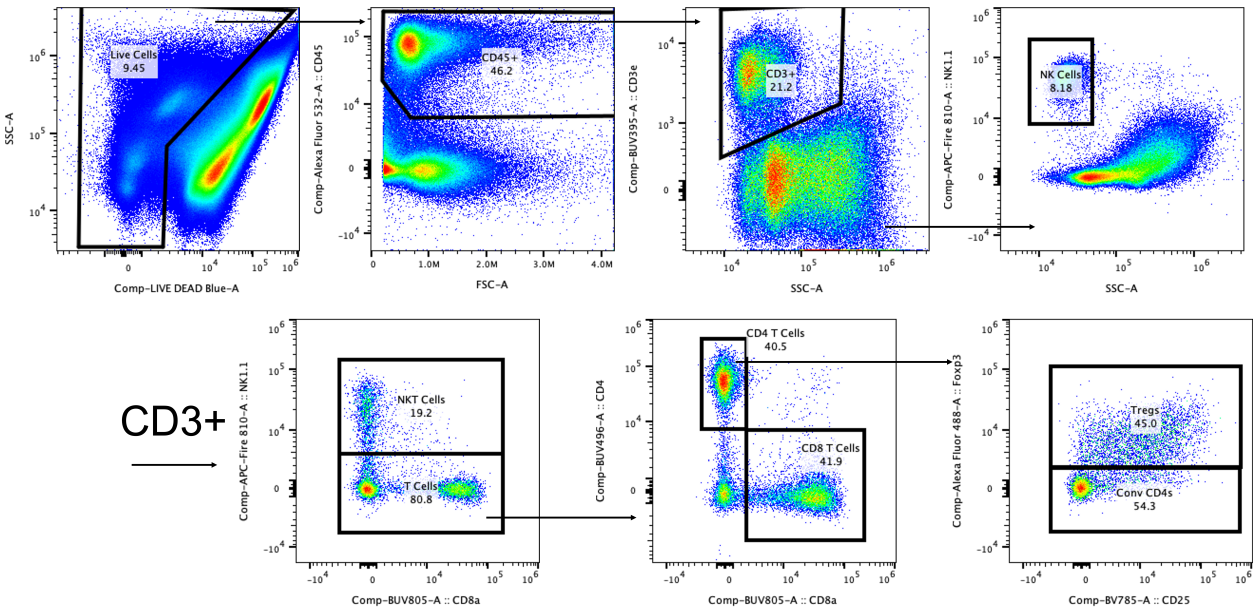

Figure 4.11: **Gating strategy for the identification of TILs**

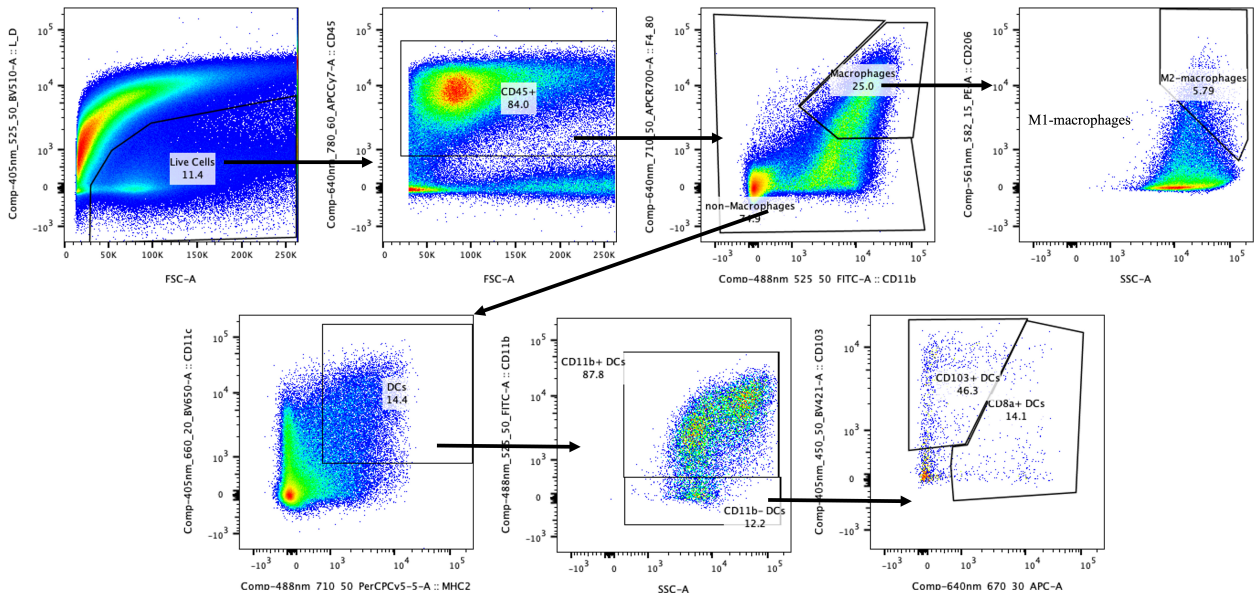

Figure 4.12: **Gating strategy for the identification of myeloid cells in the tumor**

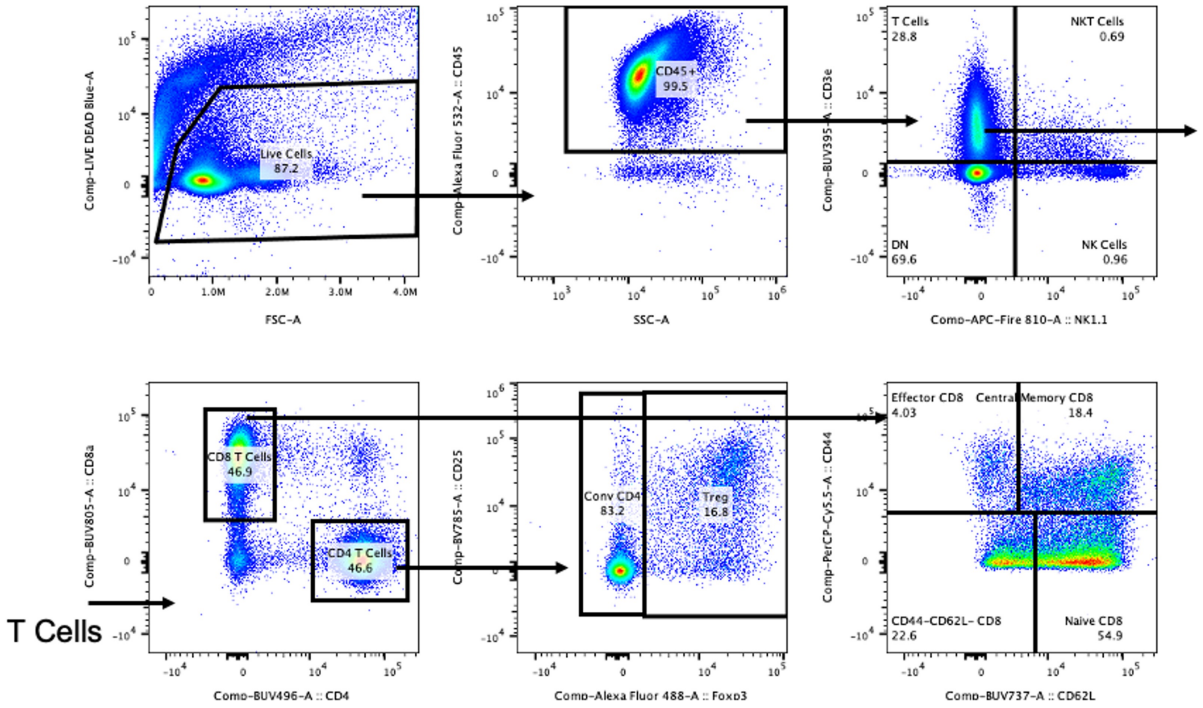

Figure 4.13: **Gating strategy for the identification of T Cells in the tdLN**

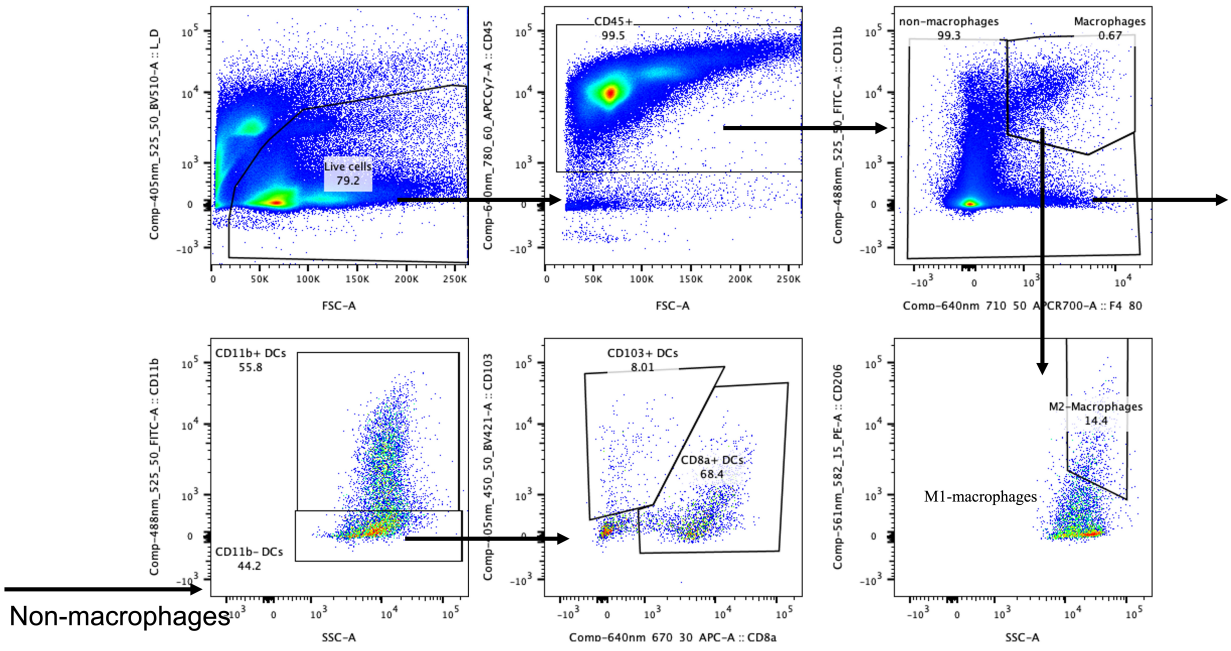

Figure 4.14: **Gating strategy for the identification of myeloid cells in the tdLN**

CHAPTER 5

FUTURE DIRECTIONS

5.1 Future exploration of mechanisms of LEC immunomodulation of immunization

In Chapter 2, I demonstrated that the VEGFR-3 axis modulates type 2 immunity in a CpG-based immunization mode. What remains to be established is if this phenomena is more generalizable to other types of adjuvants. We demonstrated using MPLA that VEGFR-3 stimulation led to a reduction of IgG2c, but no increase in IgG1 as we previously observed; however, we observed that the levels of IgG1 induced by MPLA were much higher than those induced by CpG. The immunological affect of LECs can be somewhat subtle and context dependent, thus it is possible that in this case the dose of MPLA was too high for LECs to be able to exert a measurable affect. Thus, to more definitively probe if this LEC immunomodulatory role is more generalizable, we could titrate the dose of MPLA down until levels of IgG1 are similar to those induced by CpG. Furthermore, we can test other adjuvants beyond MPLA and CpG. Another adjuvant that would be useful to explore as well would be alum, which has been FDA approved for decades. However alum is not a strong Type 1 adjuvant such as MPLA or CpG, and thus the ability of VEGFR-3 stimulation to increase Type 2 immunity may not hold with a non-Type 1 skewing adjuvant, but it would be relevant to explore either way.

We demonstrated that with CpG, MHC II on LECs was necessary for this VEGFR-3 dependent increase in Th2 cytokines that would promote elevated IgG1 levels. However, while we showed it was necessary, this does not mean that this is the only relevant factor expressed or produced by LECs that is critical for this phenotype. To further explore this phenomenon, we can use our inducible, conditional knockout system using our Prox1-CreER^{T2} mice. One promising LEC immunomodulatory candidate is PD-L1. LEC PD-L1 is particularly promising because there are two potential hypothesis that could explain our phenotype. One hypothesis is due to LEC expression of PD-L1 with the low levels of costimulation polarizes away from the Th1 response induced by CpG [35]. ILC2s that lack PD-L1

lead to defective Th2 priming [114]. Thus, potentially this MHC-II dependent interaction in the context of PD-L1 expression by LECs may be sufficient to alter this polarization. Other studies highlight the role of PD-L1 in promoting M2 macrophage infiltration and polarization [115, 116], and thus it is potentially some other mechanism indirectly involving this LEC specific PD-L1 interacting with macrophages that then would downstream produce a permissive environment for Th2 polarization near the LECs. Thus potentially PD-L1 could either directly promote Th2 cytokine secretion through cellular contact with T cells, or may indirectly promote a Th2 permissive environment.

5.2 Future directions for the study of lymphangiogenic potentiation of immunotherapy

While I demonstrated in Chapter 3 that T cells in lymphangiogenic tumors are phenotypically distinct, since exhaustion is epigenetically encoded [41], it would be useful to look at the chromatin accessibility using single cell assay for transposase-accessible chromatin (sc-ATAC-seq). Exhausted cells of various abilities to be reactivated by immunotherapy can look similar phenotypically, but would look very different epigenetically as they will have totally different chromatin accessibility [41]. Thus it would be informative to assess the epigenetic state of the intratumoral CD8 T cells to assess if the exhaustion profiles are truly distinct.

As demonstrated, the CXCR3 axis is critical for lymphangiogenic potentiation, and lymphangiogenic tumors are enriched in CXCL9. Furthermore LECs are able to make CXCL9 upon IFN-γ stimulation. However, we did not demonstrate that LECs were a substantial source of CXCL9 in the tumor. It would be relevant to quantify CXCL9 produced by LECs in the tumor, compared to other populations that are known to produce CXCL9 such as DCs [152]. This could be assessed by sorting out populations by flow cytometry, isolating RNA, and assess CXCL9 transcription using qRT-PCR. This would demonstrate more directly that LECs in the tumor make CXCL9, instead of only showing they have the potential. To show

definitely that LEC CXCL9 is the key source of CXCL9 in the tumor for this potentiation effect, the generation of a conditional LEC specific CXCL9 knockout is required. Currently the CXCL9 flox does not exist, to this author's knowledge, and thus it would have to be generated internally, which takes both considerable time and resources. However, this is the only way of showing definitely the importance of LEC CXCL9. Less specifically, but more achievable currently, is the use of the total CXCL9 knockout, which is currently available. We can utilized bone marrow chimeras upon which the CXCL9 KO mice are lethally irradiated, and bone marrow from WT mice is infused. This way the hematopoietic cells will express CXCL9, but the radio-resistant stromal and non-hematopoietic cells will be unable to make CXCL9. This at least would demonstrate the role of non-hematopoietic CXCL9 in lymphangiogenic potentiation.

The application of these findings towards a therapeutic goal remains difficult. While lymphangiogenic tumors are more responsive to immunotherapy, they are also more prone to metastasize, which means that promoting intratumoral lymphangiogenesis a non-starter for clinical therapy. However, since we demonstrated the importance of the CXCR3 axis in this potentiation, it would be interesting to explore the effect of CXCL9 (or the other CXCR3 ligand, CXCL10) based therapeutics and if that would be sufficient on it's own to potentiate immunotherapy efficacy without the negative aspects of lymphangiogenesis.

5.3 Future directions for CBD-IL-12 combination therapies

We demonstrated that IL-7-CBD in combination with CBD-IL-12 promotes effector T cell formation, and reduces T cell exhaustion on intratumoral CD8 T cells; however, while these populations were identified in an unbiased manner, it would be a worthwhile effort to explore the functionality of these cell populations and how combination therapy alters their function, and not just phenotype. Critically looking at cytokine production such as TNF-α and IFN-γ among these CD8 T cells in vivo as well as their ability to degranulate and kill target cells

would more directly show how combination therapy improves T cell function and cytotoxicity.

For CBD-GM-CSF combination with CBD-IL-12, we demonstrated that cDC1s in the tumor and lymph node are more activated by CD86 expression. However, it would be relevant to look more holistically at the DCs to assess several characteristics, which could be relevant for the increased efficacy we observe. First, using fluorescent particles, we can assess if combination therapy or CBD-GM-CSF monotherapy alters DC migration to the lymph node by looking at fluorescent DCs in the lymph node. Also, we can look if these DCs are truly more capable of activating CD8 T cells. We can isolate CD8α+ and CD103+ DCs from the lymph node or tumor, incubate them with OVA, and then add isolated naive OT-Is that would be specific to the antigen. Then we can assess the ability of the DCs to activate naive antigen-specific CD8 T cells and to determine if functionally GM-CSF combination therapy functionally alters cDC1s.

Also, since IL-7-CBD and the CBD-GM-CSF were both highly effective in combination with CBD-IL-12, but had distinct mechanisms of action, it would be interesting to assess whether therapy combining IL-7-CBD, CBD-IL-12, and CBD-GM-CSF together could lower the required dose of IL-12 even further. While the dose of CBD-IL-12 in combination therapy is much lower than with monotherapy for CBD-IL-12, it is still in the μg range, and thus would be more desirable to lower the dose even further due to how toxicity of IL-12.

REFERENCES

[1] James E Moore Jr and Christopher D Bertram. Lymphatic system flows. *Annual review of fluid mechanics*, 50:459–482, 2018.

[2] Tatiana V Petrova and Gou Young Koh. Biological functions of lymphatic vessels. *Science*, 369(6500):eaax4063, 2020.

[3] Jeffrey T Wigle and Guillermo Oliver. Prox1 function is required for the development of the murine lymphatic system. *Cell*, 98(6):769–778, 1999.

[4] Nicole C Johnson, Miriam E Dillard, Peter Baluk, Donald M McDonald, Natasha L Harvey, Sharon L Frase, and Guillermo Oliver. Lymphatic endothelial cell identity is reversible and its maintenance requires prox1 activity. *Genes & development*, 22(23):3282–3291, 2008.

[5] Susan N Thomas, Joseph M Rutkowski, Miriella Pasquier, Emma L Kuan, Kari Alitalo, Gwendalyn J Randolph, and Melody A Swartz. Impaired humoral immunity and tolerance in k14-vegfr-3-ig mice that lack dermal lymphatic drainage. *The Journal of Immunology*, 189(5):2181–2190, 2012.

[6] Erica Russo, Maximilian Nitschké, and Cornelia Halin. Dendritic cell interactions with lymphatic endothelium. *Lymphatic research and biology*, 11(3):172–182, 2013.

[7] Henry R Hampton and Tatyana Chtanova. Lymphatic migration of immune cells. *Frontiers in immunology*, 10:1168, 2019.

[8] Louise A Johnson and David G Jackson. Inflammation-induced secretion of ccl21 in lymphatic endothelium is a key regulator of integrin-mediated dendritic cell transmigration. *International immunology*, 22(10):839–849, 2010.

[9] Dragos C Dasoveanu, Hyeung Ju Park, Catherine L Ly, William D Shipman, Susan Chyou, Varsha Kumar, David Tarlinton, Burkhard Ludewig, Babak J Mehrara, and Theresa T Lu. Lymph node stromal ccl2 limits antibody responses. *Science immunology*, 5(45):eaaw0693, 2020.

[10] Jie Yang, Siya Zhang, Lingyun Zhang, Xiaoping Xie, Hui Wang, Zuliang Jie, Meidi Gu, Jin-Young Yang, Xuhong Cheng, and Shao-Cong Sun. Lymphatic endothelial cells regulate b-cell homing to lymph nodes via a nik-dependent mechanism. *Cellular & molecular immunology*, 16(2):165–177, 2019.

[11] Hannah Den Braanker, Astrid C van Stigt, Marc R Kok, Erik Lubberts, and Radjesh J Bisoendial. Single-cell rna sequencing reveals heterogeneity and functional diversity of lymphatic endothelial cells. *International Journal of Molecular Sciences*, 22(21):11976, 2021.

[12] Akira Takeda, Maija Hollmén, Denis Dermadi, Junliang Pan, Kevin Francis Brulois, Riina Kaukonen, Tapio Lönnberg, Pia Boström, Ilkka Koskivuo, Heikki Irjala, et al. Single-cell survey of human lymphatics unveils marked endothelial cell heterogeneity and mechanisms of homing for neutrophils. *Immunity*, 51(3):561–572, 2019.

[13] Akira Takeda, Marko Salmi, and Sirpa Jalkanen. Lymph node lymphatic endothelial cells as multifaceted gatekeepers in the immune system. *Trends in Immunology*, 2023.

[14] Maria H Ulvmar and Taija Mäkinen. Heterogeneity in the lymphatic vascular system and its origin. *Cardiovascular research*, 111(4):310–321, 2016.

[15] Jarish N Cohen, Eric F Tewalt, Sherin J Rouhani, Erica L Buonomo, Amber N Bruce, Xiaojiang Xu, Stefan Bekiranov, Yang-Xin Fu, and Victor H Engelhard. Tolerogenic properties of lymphatic endothelial cells are controlled by the lymph node microenvironment. *PloS one*, 9(2):e87740, 2014.

[16] Kari Alitalo, Tuomas Tammela, and Tatiana V Petrova. Lymphangiogenesis in development and human disease. *Nature*, 438(7070):946–953, 2005.

[17] Michael J Flister, Andrew Wilber, Kelly L Hall, Caname Iwata, Kohei Miyazono, Riccardo E Nisato, Michael S Pepper, David C Zawieja, and Sophia Ran. Inflammation induces lymphangiogenesis through up-regulation of vegfr-3 mediated by nf-κb and prox1. *Blood, The Journal of the American Society of Hematology*, 115(2):418–429, 2010.

[18] Harri Nurmi, Pipsa Saharinen, Georgia Zarkada, Wei Zheng, Marius R Robciuc, and Kari Alitalo. Vegf-c is required for intestinal lymphatic vessel maintenance and lipid absorption. *EMBO molecular medicine*, 7(11):1418–1425, 2015.

[19] RC Ji. Lymph node lymphangiogenesis, a new concept for modulating tumor metastasis and inflammatory process. *Histology and histopathology*, 2009.

[20] Yutaka Yonemura, Yoshio Endo, Kayoko Tabata, Taiichi Kawamura, Hyo-Yung Yun, Etsurou Bandou, Takuma Sasaki, and Masahiro Miura. Role of vegf-c and vegf-d in lymphangiogenesis in gastric cancer. *International journal of clinical oncology*, 10:318–327, 2005.

[21] Xujian Shao and Chao Liu. Influence of ifn-α and ifn-γ on lymphangiogenesis. *Journal of interferon & cytokine research*, 26(8):568–574, 2006.

[22] Ira L Savetsky, Swapna Ghanta, Jason C Gardenier, Jeremy S Torrisi, Gabriela D García Nores, Geoffrey E Hespe, Matthew D Nitti, Raghu P Kataru, and Babak J Mehrara. Th2 cytokines inhibit lymphangiogenesis. *PloS one*, 10(6):e0126908, 2015.

[23] Li Yuan, Delphine Moyon, Luc Pardanaud, Christiane Breant, Marika J Karkkainen, Kari Alitalo, and Anne Eichmann. Abnormal lymphatic vessel development in neuropilin 2 mutant mice. *Development*, 129:4797–4806, 2002.

[24] Takahiro Hara, Soichiro Shitara, Kumiko Imai, Hitoshi Miyachi, Satsuki Kitano, Hisayuki Yao, Shizue Tani-ichi, and Koichi Ikuta. Identification of il-7–producing cells in primary and secondary lymphoid organs using il-7–gfp knock-in mice. *The Journal of Immunology*, 189(4):1577–1584, 2012.

[25] Guangwei Cui, Takahiro Hara, Szandor Simmons, Keisuke Wagatsuma, Akifumi Abe, Hitoshi Miyachi, Satsuki Kitano, Masaru Ishii, Shizue Tani-Ichi, and Koichi Ikuta. Characterization of the il-15 niche in primary and secondary lymphoid organs in vivo. *Proceedings of the National Academy of Sciences*, 111(5):1915–1920, 2014.

[26] Erik L Brincks and David L Woodland. Novel roles for il-15 in t cell survival. *F1000 biology reports*, 2, 2010.

[27] Isabelle Mondor, Myriam Baratin, Marine Lagueyrie, Lisa Saro, Sandrine Henri, Rebecca Gentek, Delphine Suerinck, Wolfgang Kastenmuller, Jean X Jiang, and Marc Bajénoff. Lymphatic endothelial cells are essential components of the subcapsular sinus macrophage niche. *Immunity*, 50(6):1453–1466, 2019.

[28] Lucas Onder, Urs Mörbe, Natalia Pikor, Mario Novkovic, Hung-Wei Cheng, Thomas Hehlgans, Klaus Pfeffer, Burkhard Becher, Ari Waisman, Thomas Rülicke, et al. Lymphatic endothelial cells control initiation of lymph node organogenesis. *Immunity*, 47(1):80–92, 2017.

[29] Sachiko Hirosue and Juan Dubrot. Modes of antigen presentation by lymph node stromal cells and their immunological implications. *Frontiers in immunology*, 6:446, 2015.

[30] Sachiko Hirosue, Efthymia Vokali, Vidya R Raghavan, Marcela Rincon-Restrepo, Amanda W Lund, Patricia Corthésy-Henrioud, Francesca Capotosti, Cornelia Halin Winter, Stéphanie Hugues, and Melody A Swartz. Steady-state antigen scavenging, cross-presentation, and cd8+ t cell priming: a new role for lymphatic endothelial cells. *The Journal of Immunology*, 192(11):5002–5011, 2014.

[31] Efthymia Vokali, Shann S Yu, Sachiko Hirosue, Marcela Rinçon-Restrepo, Fernanda V. Duraes, Stefanie Scherer, Patricia Corthésy-Henrioud, Witold W Kilarski, Anna Mondino, Dietmar Zehn, et al. Lymphatic endothelial cells prime naïve cd8+ t cells into memory cells under steady-state conditions. *Nature communications*, 11(1):538, 2020.

[32] Laura Santambrogio, Stella J Berendam, and Victor H Engelhard. The antigen processing and presentation machinery in lymphatic endothelial cells. *Frontiers in immunology*, 10:1033, 2019.

[33] Juan Dubrot, Fernanda V Duraes, Guillaume Harlé, Anjalie Schlaeppi, Dale Brighouse, Natacha Madelon, Christine Göpfert, Nadine Stokar-Regenscheit, Hans Acha-Orbea, Walter Reith, et al. Absence of mhc-ii expression by lymph node stromal cells results in autoimmunity. *Life science alliance*, 1(6), 2018.

[34] Anastasia O. Gkountidi, Laure Garnier, Juan Dubrot, Julien Angelillo, Guillaume Harlé, Dale Brighouse, Ludovic J. Wrobel, Robert Pick, Christoph Scheiermann, Melody A. Swartz, and Stéphanie Hugues. MHC Class II Antigen Presentation by Lymphatic Endothelial Cells in Tumors Promotes Intratumoral Regulatory T cell–Suppressive Functions. *Cancer Immunology Research*, 9(7):748–764, 07 2021.

[35] Eric F Tewalt, Jarish N Cohen, Sherin J Rouhani, Cynthia J Guidi, Hui Qiao, Shawn P Fahl, Mark R Conaway, Timothy P Bender, Kenneth S Tung, Anthony T Vella, et al. Lymphatic endothelial cells induce tolerance via pd-l1 and lack of costimulation leading to high-level pd-1 expression on cd8 t cells. *Blood, The Journal of the American Society of Hematology*, 120(24):4772–4782, 2012.

[36] Alan J Korman, Karl S Peggs, and James P Allison. Checkpoint blockade in cancer immunotherapy. *Advances in immunology*, 90:297–339, 2006.

[37] Michael A Postow, Robert Sidlow, and Matthew D Hellmann. Immune-related adverse events associated with immune checkpoint blockade. *New England Journal of Medicine*, 378(2):158–168, 2018.

[38] Jonathan A Trujillo, Randy F Sweis, Riyue Bao, and Jason J Luke. T cell–inflamed versus non-t cell–inflamed tumors: a conceptual framework for cancer immunotherapy drug development and combination therapy selection. *Cancer immunology research*, 6(9):990–1000, 2018.

[39] Anne M Van der Leun, Daniela S Thommen, and Ton N Schumacher. Cd8+ t cell states in human cancer: insights from single-cell analysis. *Nature Reviews Cancer*, 20(4):218–232, 2020.

[40] Y Jiang, Y Li, and B Zhu. T-cell exhaustion in the tumor microenvironment. *Cell death & disease*, 6(6):e1792–e1792, 2015.

[41] Mary Philip, Lauren Fairchild, Liping Sun, Ellen L Horste, Steven Camara, Mojdeh Shakiba, Andrew C Scott, Agnes Viale, Peter Lauer, Taha Merghoub, et al. Chromatin states define tumour-specific t cell dysfunction and reprogramming. *Nature*, 545(7655):452–456, 2017.

[42] Omar Khan, Josephine R Giles, Sierra McDonald, Sasikanth Manne, Shin Foong Ngiow, Kunal P Patel, Michael T Werner, Alexander C Huang, Katherine A Alexander, Jennifer E Wu, et al. Tox transcriptionally and epigenetically programs cd8+ t cell exhaustion. *Nature*, 571(7764):211–218, 2019.

[43] Fotini Gounari and Khashayarsha Khazaie. Tcf-1: a maverick in t cell development and function. *Nature immunology*, 23(5):671–678, 2022.

[44] John L Johnson, Georgios Georgakilas, Jelena Petrovic, Makoto Kurachi, Stanley Cai, Christelle Harly, Warren S Pear, Avinash Bhandoola, E John Wherry, and Golnaz Vahedi. Lineage-determining transcription factor tcf-1 initiates the epigenetic identity of t cells. *Immunity*, 48(2):243–257, 2018.

[45] Dietmar Herndler-Brandstetter, Harumichi Ishigame, Ryo Shinnakasu, Valerie Plajer, Carmen Stecher, Jun Zhao, Melanie Lietzenmayer, Lina Kroehling, Akiko Takumi, Kohei Kometani, et al. Klrg1+ effector cd8+ t cells lose klrg1, differentiate into all memory t cell lineages, and convey enhanced protective immunity. *Immunity*, 48(4):716–729, 2018.

[46] Antoni Ribas and Jedd D Wolchok. Cancer immunotherapy using checkpoint blockade. *Science*, 359(6382):1350–1355, 2018.

[47] K Esfahani, L Roudaia, NA Buhlaiga, SV Del Rincon, N Papneja, and WH Miller. A review of cancer immunotherapy: from the past, to the present, to the future. *Current Oncology*, 27(s2):87–97, 2020.

[48] Maartje W Rohaan, Sofie Wilgenhof, and John BAG Haanen. Adoptive cellular therapies: the current landscape. *Virchows Archiv*, 474:449–461, 2019.

[49] Xiaonan Wang, Carlotta Peticone, Ekaterini Kotsopoulou, Berthold Göttgens, and Fernando J Calero-Nieto. Single-cell transcriptome analysis of car t-cell products reveals subpopulations, stimulation, and exhaustion signatures. *Oncoimmunology*, 10(1):1866287, 2021.

[50] Pedro Berraondo, Miguel F Sanmamed, María C Ochoa, Iñaki Etxeberria, Maria A Aznar, José Luis Pérez-Gracia, María E Rodríguez-Ruiz, Mariano Ponz-Sarvise, Eduardo Castañón, and Ignacio Melero. Cytokines in clinical cancer immunotherapy. *British journal of cancer*, 120(1):6–15, 2019.

[51] Tao Jiang, Caicun Zhou, and Shengxiang Ren. Role of il-2 in cancer immunotherapy. *Oncoimmunology*, 5(6):e1163462, 2016.

[52] John P Leonard, Matthew L Sherman, Gerald L Fisher, Lynn J Buchanan, Glenn Larsen, Michael B Atkins, Jeffrey A Sosman, Janice P Dutcher, Nicholas J Vogelzang, and John L Ryan. Effects of single-dose interleukin-12 exposure on interleukin-12–associated toxicity and interferon-γ production. *Blood, The Journal of the American Society of Hematology*, 90(7):2541–2548, 1997.

[53] Alvin S Stern, Frank J Podlaski, Jeffrey D Hulmes, YC Pan, Phyllis M Quinn, AG Wolitzky, Philip C Familletti, Donna L Stremlo, Terri Truitt, and Richard Chizzonite. Purification to homogeneity and partial characterization of cytotoxic lymphocyte maturation factor from human b-lymphoblastoid cells. *Proceedings of the National Academy of Sciences*, 87(17):6808–6812, 1990.

[54] Sid P Kerkar, Romina S Goldszmid, Pawel Muranski, Dhanalakshmi Chinnasamy, Zhiya Yu, Robert N Reger, Anthony J Leonardi, Richard A Morgan, Ena Wang, Francesco M Marincola, et al. Il-12 triggers a programmatic change in dysfunctional myeloid-derived cells within mouse tumors. *The Journal of clinical investigation*, 121(12):4746–4757, 2011.

[55] Sid P Kerkar, Anthony J Leonardi, Nicolas Van Panhuys, Ling Zhang, Zhiya Yu, Joseph G Crompton, Jenny H Pan, Douglas C Palmer, Richard A Morgan, Steven A Rosenberg, et al. Collapse of the tumor stroma is triggered by il-12 induction of fas. *Molecular Therapy*, 21(7):1369–1377, 2013.

[56] Mansi Saxena, Sjoerd H van der Burg, Cornelis JM Melief, and Nina Bhardwaj. Therapeutic cancer vaccines. *Nature Reviews Cancer*, 21(6):360–378, 2021.

[57] Bridget P Keenan and Elizabeth M Jaffee. Whole cell vaccines—past progress and future strategies. In *Seminars in oncology*, volume 39, pages 276–286. Elsevier, 2012.

[58] John Nemunaitis. Vaccines in cancer: Gvax®, a gm-csf gene vaccine. *Expert review of vaccines*, 4(3):259–274, 2005.

[59] Robert E Hollingsworth and Kathrin Jansen. Turning the corner on therapeutic cancer vaccines. *npj Vaccines*, 4(1):7, 2019.

[60] Masataka Matsumoto, Sally Roufail, Rachael Inder, Carol Caesar, Tara Karnezis, Ramin Shayan, Rae H Farnsworth, Teruhiko Sato, Marc G Achen, G Bruce Mann, et al. Signaling for lymphangiogenesis via vegfr-3 is required for the early events of metastasis. *Clinical & experimental metastasis*, 30:819–832, 2013.

[61] JD Shields, M Borsetti, H Rigby, SJ Harper, PS Mortimer, JR Levick, A Orlando, and DO Bates. Lymphatic density and metastatic spread in human malignant melanoma. *British journal of cancer*, 90(3):693–700, 2004.

[62] Jacqueline D Shields, Iraklis C Kourtis, Alice A Tomei, Joanna M Roberts, and Melody A Swartz. Induction of lymphoidlike stroma and immune escape by tumors that express the chemokine ccl21. *Science*, 328(5979):749–752, 2010.

[63] Ailsa Christiansen and Michael Detmar. Lymphangiogenesis and cancer. *Genes & cancer*, 2(12):1146–1158, 2011.

[64] Raghu P Kataru, Catherine L Ly, Jinyeon Shin, Hyeung Ju Park, Jung Eun Baik, Sonia Rehal, Sagrario Ortega, David Lyden, and Babak J Mehrara. Tumor lymphatic function regulates tumor inflammatory and immunosuppressive microenvironments. *Cancer immunology research*, 7(8):1345–1358, 2019.

[65] Miriam Nörder, Maximiliano G Gutierrez, Sonia Zicari, Edoardo Cervi, Arnaldo Caruso, and Carlos A Guzmán. Lymph node-derived lymphatic endothelial cells express functional costimulatory molecules and impair dendritic cell-induced allogenic t-cell proliferation. *The FASEB Journal*, 26(7):2835–2846, 2012.

[66] Veronika Lukacs-Kornek, Deepali Malhotra, Anne L Fletcher, Sophie E Acton, Kutlu G Elpek, Prakriti Tayalia, Ai-ris Collier, and Shannon J Turley. Regulated release of nitric oxide by nonhematopoietic stroma controls expansion of the activated t cell pool in lymph nodes. *Nature immunology*, 12(11):1096–1104, 2011.

[67] Simona Podgrabinska, Okebugwu Kamalu, Lloyd Mayer, Motomu Shimaoka, Hans Snoeck, Gwendalyn J Randolph, and Mihaela Skobe. Inflamed lymphatic endothelium suppresses dendritic cell maturation and function via mac-1/icam-1-dependent mechanism. *The Journal of Immunology*, 183(3):1767–1779, 2009.

[68] Kim Pin Yeo and Veronique Angeli. Bidirectional crosstalk between lymphatic endothelial cell and t cell and its implications in tumor immunity. *Frontiers in immunology*, 8:83, 2017.

[69] Manuel Fankhauser, Maria A. S. Broggi, Lambert Potin, Natacha Bordry, Laura Jeanbart, Amanda W. Lund, Elodie Da Costa, Sylvie Hauert, Marcela Rincon-Restrepo, Christopher Tremblay, Elena Cabello, Krisztian Homicsko, Olivier Michielin, Douglas Hanahan, Daniel E. Speiser, and Melody A. Swartz. Tumor lymphangiogenesis promotes t cell infiltration and potentiates immunotherapy in melanoma. *Science Translational Medicine*, 9(407):eaal4712, 2017.

[70] Eric Song, Tianyang Mao, Huiping Dong, Ligia Simoes Braga Boisserand, Salli Antila, Marcus Bosenberg, Kari Alitalo, Jean-Leon Thomas, and Akiko Iwasaki. Vegf-c-driven lymphatic drainage enables immunosurveillance of brain tumours. *Nature*, 577(7792):689–694, 2020.

[71] Tresa McGranahan, Kate Elizabeth Therkelsen, Sarah Ahmad, and Seema Nagpal. Current state of immunotherapy for treatment of glioblastoma. *Current treatment options in oncology*, 20:1–15, 2019.

[72] Janie Parrino and Barney S Graham. Smallpox vaccines: Past, present, and future. *Journal of allergy and clinical immunology*, 118(6):1320–1326, 2006.

[73] Wayne M Sullender, Karen B Fowler, Vivek Gupta, Anand Krishnan, Debjani Ram Purakayastha, Raghuram Srungaram Vln, Kathryn E Lafond, Siddhartha Saha, Francisco S Palomeque, Paul Gargiullo, et al. Efficacy of inactivated trivalent influenza vaccine in rural india: a 3-year cluster-randomised controlled trial. *The Lancet Global Health*, 7(7):e940–e950, 2019.

[74] CDC. Past seasons' vaccine effectiveness estimates, 2023.

[75] Namit Chaudhary, Drew Weissman, and Kathryn A Whitehead. mrna vaccines for infectious diseases: principles, delivery and clinical translation. *Nature reviews Drug discovery*, 20(11):817–838, 2021.

[76] Akiko Iwasaki and Saad B Omer. Why and how vaccines work. *Cell*, 183(2):290–295, 2020.

[77] CDC. Explaining how vaccines work, 2023.

[78] Charles A Janeway Jr, Paul Travers, Mark Walport, and Mark J Shlomchik. The distribution and functions of immunoglobulin isotypes. In *Immunobiology: The Immune System in Health and Disease. 5th edition*. Garland Science, 2001.

[79] José Javier Morales-Núñez, José Francisco Muñoz-Valle, Paola Carolina Torres-Hernández, and Jorge Hernández-Bello. Overview of neutralizing antibodies and their potential in covid-19. *Vaccines*, 9(12):1376, 2021.

[80] Lenette L Lu, Todd J Suscovich, Sarah M Fortune, and Galit Alter. Beyond binding: antibody effector functions in infectious diseases. *Nature Reviews Immunology*, 18(1):46–61, 2018.

[81] Invivogen. Antibody effector activities and affinities, 2011.

[82] John J O'Shea, Massimo Gadina, and Richard M Siegel. Cytokines and cytokine receptors. In *Clinical immunology*, pages 127–155. Elsevier, 2019.

[83] Tina M McIntyre, Dennis R Klinman, Petal Rothman, Michelle Lugo, James R Dasch, James J Mond, and Clifford M Snapper. Transforming growth factor beta 1 selectivity stimulates immunoglobulin g2b secretion by lipopolysaccharide-activated murine b cells. *The Journal of experimental medicine*, 177(4):1031–1037, 1993.

[84] Rishi Vishal Luckheeram, Rui Zhou, Asha Devi Verma, and Bing Xia. Cd4+ t cells: differentiation and functions. *Clinical and developmental immunology*, 2012, 2012.

[85] Paul Haase and David Voehringer. Regulation of the humoral type 2 immune response against allergens and helminths. *European Journal of Immunology*, 51(2):273–279, 2021.

[86] Brad Spellberg and John E Edwards Jr. Type 1/type 2 immunity in infectious diseases. *Clinical Infectious Diseases*, 32(1):76–102, 2001.

[87] Sirpa Jalkanen and Marko Salmi. Lymphatic endothelial cells of the lymph node. *Nature Reviews Immunology*, 20(9):566–578, 2020.

[88] Gwendalyn J Randolph, Veronique Angeli, and Melody A Swartz. Dendritic-cell trafficking to lymph nodes through lymphatic vessels. *Nature Reviews Immunology*, 5(8):617–628, 2005.

[89] Waldemar L Olszewski. The innate reaction of the human skin lymphatic system to foreign and self-antigens. *Lymphatic Research and Biology*, 3(2):50–57, 2005.

[90] Véronique Angeli, Florent Ginhoux, Jaime Llodrà, Laurence Quemeneur, Paul S Frenette, Mihaela Skobe, Rolf Jessberger, Miriam Merad, and Gwendalyn J Randolph. B cell-driven lymphangiogenesis in inflamed lymph nodes enhances dendritic cell mobilization. *Immunity*, 24(2):203–215, 2006.

[91] Luqing Zhang, Fei Zhou, Wencan Han, Bin Shen, Jincai Luo, Masabumi Shibuya, and Yulong He. Vegfr-3 ligand-binding and kinase activity are required for lymphangiogenesis but not for angiogenesis. *Cell research*, 20(12):1319–1331, 2010.

[92] Shan Liao and Pierre-Yves von der Weid. Inflammation-induced lymphangiogenesis and lymphatic dysfunction. *Angiogenesis*, 17:325–334, 2014.

[93] Jeremy Goldman, Joseph M Rutkowski, Jacqueline D Shields, Miriella C Pasquier, Yingjie Cui, Hugo G Schmökel, Stephen Willey, Daniel J Hicklin, Bronislaw Pytowski, and Melody A Swartz. Cooperative and redundant roles of vegfr-2 and vegfr-3 signaling in adult lymphangiogenesis. *The FASEB Journal*, 21(4):1003–1012, 2007.

[94] Masabumi Shibuya. Vascular endothelial growth factor (vegf) and its receptor (vegfr) signaling in angiogenesis: a crucial target for anti-and pro-angiogenic therapies. *Genes & cancer*, 2(12):1097–1105, 2011.

[95] Mikko T Visuri, Krista M Honkonen, Pauliina Hartiala, Tomi V Tervala, Paavo J Halonen, Heikki Junkkari, Nina Knuutinen, Seppo Ylä-Herttuala, Kari K Alitalo, and Anne M Saarikko. Vegf-c and vegf-c156s in the pro-lymphangiogenic growth factor therapy of lymphedema: a large animal study. *Angiogenesis*, 18:313–326, 2015.

[96] Vladimir Joukov, Vijay Kumar, Tarja Sorsa, Elena Arighi, Herbert Weich, Olli Saksela, and Kari Alitalo. A recombinant mutant vascular endothelial growth factor-c that has lost vascular endothelial growth factor receptor-2 binding, activation, and vascular permeability activities. *Journal of Biological Chemistry*, 273(12):6599–6602, 1998.

[97] Hajime Kubo, Renhai Cao, Ebba Bräkenhielm, Taija Mäkinen, Yihai Cao, and Kari Alitalo. Blockade of vascular endothelial growth factor receptor-3 signaling inhibits fibroblast growth factor-2-induced lymphangiogenesis in mouse cornea. *Proceedings of the National Academy of Sciences*, 99(13):8868–8873, 2002.

[98] Louise A Johnson and David G Jackson. Inflammation-induced secretion of ccl21 in lymphatic endothelium is a key regulator of integrin-mediated dendritic cell transmigration. *International immunology*, 22(10):839–849, 2010.

[99] Kit M Lee, Renzo Danuser, Jens V Stein, Delyth Graham, Robert JB Nibbs, and Gerard J Graham. The chemokine receptors ackr 2 and ccr 2 reciprocally regulate lymphatic vessel density. *The EMBO journal*, 33(21):2564–2580, 2014.

[100] Juan Dubrot, Fernanda V Duraes, Lambert Potin, Francesca Capotosti, Dale Brighouse, Tobias Suter, Salomé LeibundGut-Landmann, Natalio Garbi, Walter Reith, Melody A Swartz, et al. Lymph node stromal cells acquire peptide–mhcii complexes from dendritic cells and induce antigen-specific cd4+ t cell tolerance. *Journal of Experimental Medicine*, 211(6):1153–1166, 2014.

[101] Efthymia Vokali, Shann S Yu, Sachiko Hirosue, Marcela Rinçon-Restrepo, Fernanda V. Duraes, Stefanie Scherer, Patricia Corthésy-Henrioud, Witold W Kilarski, Anna Mondino, Dietmar Zehn, et al. Lymphatic endothelial cells prime naïve cd8+ t cells into memory cells under steady-state conditions. *Nature communications*, 11(1):538, 2020.

[102] Anastasia O Gkountidi, Laure Garnier, Juan Dubrot, Julien Angelillo, Guillaume Harlé, Dale Brighouse, Ludovic J Wrobel, Robert Pick, Christoph Scheiermann, Melody A Swartz, et al. Mhc class ii antigen presentation by lymphatic endothelial cells in tumors promotes intratumoral regulatory t cell–suppressive functions. *Cancer immunology research*, 9(7):748–764, 2021.

[103] Clifford M Snapper and William E Paul. Interferon-γ and b cell stimulatory factor-1 reciprocally regulate ig isotype production. *Science*, 236(4804):944–947, 1987.

[104] Jeffrey M Purkerson and Peter C Isakson. Interleukin 5 (il-5) provides a signal that is required in addition to il-4 for isotype switching to immunoglobulin (ig) g1 and ige. *The Journal of experimental medicine*, 175(4):973–982, 1992.

[105] Chieko Mizoguchi, Shoji Uehara, Shizuo Akira, and Kiyoshi Takatsu. Il-5 induces igg1 isotype switch recombination in mouse cd38-activated sigd-positive b lymphocytes. *The Journal of Immunology*, 162(5):2812–2819, 1999.

[106] Yan Yan, Renfang Chen, Xu Wang, Kai Hu, Lihua Huang, Mengji Lu, and Qinxue Hu. Ccl19 and ccr7 expression, signaling pathways, and adjuvant functions in viral infection and prevention. *Frontiers in cell and developmental biology*, 7:212, 2019.

[107] Kevin Kuonqui, Hyeung Ju Park, Adana Campbell, Stav Brown, Ananta Sarker, Jinyeon Shin, Raghu P Kataru, and Babak J Mehrara. 145. prolonged exposure to vegf-c induces resistance to subsequent stimulation of vegfr3 in lymphatic endothelial cells. *Plastic and Reconstructive Surgery Global Open*, 11(5 Suppl), 2023.

[108] Amine Issa, Thomas X Le, Alexander N Shoushtari, Jacqueline D Shields, and Melody A Swartz. Vascular endothelial growth factor-c and cc chemokine receptor 7 in tumor cell–lymphatic cross-talk promote invasive phenotype. *Cancer research*, 69(1):349–357, 2009.

[109] Yanbo Zhang, Yao Lu, Li Ma, Xudong Cao, Jun Xiao, Jiexia Chen, Shaozhuo Jiao, Yunzhen Gao, Chang Liu, Zhaojun Duan, et al. Activation of vascular endothelial growth factor receptor-3 in macrophages restrains tlr4-nf-κb signaling and protects against endotoxin shock. *Immunity*, 40(4):501–514, 2014.

[110] Melissa A Brown. Il-4 production by t cells: you need a little to get a lot. *The journal of immunology*, 181(5):2941–2942, 2008.

[111] SUSAN L Swain, ANDREW D Weinberg, MICHELE English, and GAIL Huston. Il-4 directs the development of th2-like helper effectors. *Journal of immunology (Baltimore, Md.: 1950)*, 145(11):3796–3806, 1990.

[112] Markus Mohrs, Kanade Shinkai, Katja Mohrs, and Richard M Locksley. Analysis of type 2 immunity in vivo with a bicistronic il-4 reporter. *Immunity*, 15(2):303–311, 2001.

[113] Sherin J Rouhani, Jacob D Eccles, Priscila Riccardi, J David Peske, Eric F Tewalt, Jarish N Cohen, Roland Liblau, Taija Mäkinen, and Victor H Engelhard. Roles of lymphatic endothelial cells expressing peripheral tissue antigens in cd4 t-cell tolerance induction. *Nature communications*, 6(1):6771, 2015.

[114] Christian Schwartz, Adnan R Khan, Achilleas Floudas, Sean P Saunders, Emily Hams, Hans-Reimer Rodewald, Andrew NJ McKenzie, and Padraic G Fallon. Ilc2s regulate adaptive th2 cell functions via pd-l1 checkpoint control. *Journal of Experimental Medicine*, 214(9):2507–2521, 2017.

[115] Yi Wei, Mengjun Liang, Liping Xiong, Ning Su, Xiang Gao, and Zongpei Jiang. Pd-l1 induces macrophage polarization toward the m2 phenotype via erk/akt/mtor. *Experimental cell research*, 402(2):112575, 2021.

[116] Zhiyuan Zhu, Hongbo Zhang, Baodong Chen, Xing Liu, Shizhong Zhang, Zhitao Zong, and Mengqi Gao. Pd-l1-mediated immunosuppression in glioblastoma is associated with the infiltration and m2-polarization of tumor-associated macrophages. *Frontiers in Immunology*, 11:588552, 2020.

[117] Monika Zajkowska, Emilia Lubowicka, Wojciech Fiedorowicz, Maciej Szmitkowski, Jacek Jamiołkowski, and Sławomir Ławicki. Human plasma levels of vegf-a, vegf-c, vegf-d, their soluble receptor-vegfr-2 and applicability of these parameters as tumor markers in the diagnostics of breast cancer. *Pathology & Oncology Research*, 25:1477–1486, 2019.

[118] Daye Cheng, Bin Liang, and Yunhui Li. Serum vascular endothelial growth factor (vegf-c) as a diagnostic and prognostic marker in patients with ovarian cancer. *PLoS One*, 8(2):e55309, 2013.

[119] Ming-Huei Cheng, David W Chang, and Ketan M Patel. *Principles and practice of lymphedema surgery*. Elsevier Health Sciences, 2021.

[120] Emoke Almasy, Janos Szederjesi, Bianca Liana Grigorescu, Iudita Badea, Marius Petrisor, Cristina Manasturean, Valentina Negrea, Agota-Evelyn Timar, Oana Coman, Leonard Azamfirei, et al. The diagnostic and prognostic role of vascular endothelial growth factor c in sepsis and septic shock. *The Journal of Critical Care Medicine*, 6(3):152–158, 2020.

[121] R Sathish Srinivasan, Miriam E Dillard, Oleg V Lagutin, Fu-Jung Lin, Sophia Tsai, Ming-Jer Tsai, Igor M Samokhvalov, and Guillermo Oliver. Lineage tracing demonstrates the venous origin of the mammalian lymphatic vasculature. *Genes & development*, 21(19):2422–2432, 2007.

[122] Maria AS Broggi, Mathias Schmaler, Nadège Lagarde, and Simona W Rossi. Isolation of murine lymph node stromal cells. *JoVE (Journal of Visualized Experiments)*, (90):e51803, 2014.

[123] Anne L Fletcher, Deepali Malhotra, Sophie E Acton, Veronika Lukacs-Kornek, Angelique Bellemare-Pelletier, Mark Curry, Myriam Armant, and Shannon J Turley. Reproducible isolation of lymph node stromal cells reveals site-dependent differences in fibroblastic reticular cells. *Frontiers in immunology*, 2:35, 2011.

[124] Ryan S Lane, Julia Femel, Alec P Breazeale, Christopher P Loo, Guillaume Thibault, Andy Kaempf, Motomi Mori, Takahiro Tsujikawa, Young Hwan Chang, and Amanda W Lund. Ifnγ-activated dermal lymphatic vessels inhibit cytotoxic t cells in melanoma and inflamed skin. *Journal of Experimental Medicine*, 215(12):3057–3074, 2018.

[125] Nikola Cousin, Stefan Cap, Manuel Dihr, Carlotta Tacconi, Michael Detmar, and Lothar C Dieterich. Lymphatic pd-l1 expression restricts tumor-specific cd8+ t-cell responses. *Cancer Research*, 81(15):4133–4144, 2021.

[126] Changping Zhou, Lu Ma, Han Xu, Yingqing Huo, and Jincai Luo. Meningeal lymphatics regulate radiotherapy efficacy through modulating anti-tumor immunity. *Cell Research*, 32(6):543–554, 2022.

[127] Amanda W Lund, Marek Wagner, Manuel Fankhauser, Eli S Steinskog, Maria A Broggi, Stefani Spranger, Thomas F Gajewski, Kari Alitalo, Hans P Eikesdal, Helge Wiig, et al. Lymphatic vessels regulate immune microenvironments in human and murine melanoma. *The Journal of clinical investigation*, 126(9):3389–3402, 2016.

[128] Joanna R Groom and Andrew D Luster. Cxcr3 in t cell function. *Experimental cell research*, 317(5):620–631, 2011.

[129] Jacob E Kohlmeier, Tres Cookenham, Shannon C Miller, Alan D Roberts, Jan P Christensen, Allan R Thomsen, and David L Woodland. Cxcr3 directs antigen-specific effector cd4+ t cell migration to the lung during parainfluenza virus infection. *The Journal of Immunology*, 183(7):4378–4384, 2009.

[130] Marco Wendel, Ioanna E Galani, Elisabeth Suri-Payer, and Adelheid Cerwenka. Natural killer cell accumulation in tumors is dependent on ifn-γ and cxcr3 ligands. *Cancer research*, 68(20):8437–8445, 2008.

[131] Kori L Wallace, Melissa A Marshall, Susan I Ramos, Joanne A Lannigan, Joshua J Field, Robert M Strieter, and Joel Linden. Nkt cells mediate pulmonary inflammation and dysfunction in murine sickle cell disease through production of ifn-γ and cxcr3 chemokines. *Blood, The Journal of the American Society of Hematology*, 114(3):667–676, 2009.

[132] Volker Brinkmann, Andreas Billich, Thomas Baumruker, Peter Heining, Robert Schmouder, Gordon Francis, Shreeram Aradhye, and Pascale Burtin. Fingolimod (fty720): discovery and development of an oral drug to treat multiple sclerosis. *Nature reviews Drug discovery*, 9(11):883–897, 2010.

[133] Maria M Steele, Abhinav Jaiswal, Ines Delclaux, Ian D Dryg, Dhaarini Murugan, Julia Femel, Sunny Son, Haley du Bois, Cameron Hill, Sancy A Leachman, et al. T cell egress via lymphatic vessels is tuned by antigen encounter and limits tumor control. *Nature Immunology*, 24(4):664–675, 2023.

[134] Jake Wang, Curtis J Perry, Katrina Meeth, Durga Thakral, William Damsky, Goran Micevic, Susan Kaech, Kim Blenman, and Marcus Bosenberg. Uv-induced somatic mutations elicit a functional t cell response in the yummer 1.7 mouse melanoma model. *Pigment cell & melanoma research*, 30(4):428–435, 2017.

[135] Amanda W Lund, Fernanda V Duraes, Sachiko Hirosue, Vidya R Raghavan, Chiara Nembrini, Susan N Thomas, Amine Issa, Stephanie Hugues, and Melody A Swartz. Vegf-c promotes immune tolerance in b16 melanomas and cross-presentation of tumor antigen by lymph node lymphatics. *Cell reports*, 1(3):191–199, 2012.

[136] Julie R Brahmer, Scott S Tykodi, Laura QM Chow, Wen-Jen Hwu, Suzanne L Topalian, Patrick Hwu, Charles G Drake, Luis H Camacho, John Kauh, Kunle Odunsi, et al. Safety and activity of anti–pd-l1 antibody in patients with advanced cancer. *New England Journal of Medicine*, 366(26):2455–2465, 2012.

[137] Stefani Spranger, Riyue Bao, and Thomas F Gajewski. Melanoma-intrinsic β-catenin signalling prevents anti-tumour immunity. *Nature*, 523(7559):231–235, 2015.

[138] Yuan-Tong Liu and Zhi-Jun Sun. Turning cold tumors into hot tumors by improving t-cell infiltration. *Theranostics*, 11(11):5365, 2021.

[139] Bruce D Car, Vicki M Eng, Jack M Lipman, and Timothy D Anderson. The toxicology of interleukin-12: a review. *Toxicologic pathology*, 27(1):58–63, 1999.

[140] Dragica Jorgovanovic, Mengjia Song, Liping Wang, and Yi Zhang. Roles of ifn-γ in tumor progression and regression: a review. *Biomarker research*, 8:1–16, 2020.

[141] Bruce D Car, Vicki M Eng, Bruno Schnyder, Michel LeHir, Alexander N Shakhov, Gaetane Woerly, Sui Huang, Michel Aguet, Timothy D Anderson, and Bernhard Ryffel. Role of interferon-gamma in interleukin 12-induced pathology in mice. *The American journal of pathology*, 147(6):1693, 1995.

[142] Jun Ishihara, Ako Ishihara, Koichi Sasaki, Steve Seung-Young Lee, John-Michael Williford, Mariko Yasui, Hiroyuki Abe, Lambert Potin, Peyman Hosseinchi, Kazuto Fukunaga, et al. Targeted antibody and cytokine cancer immunotherapies through collagen affinity. *Science Translational Medicine*, 11(487):eaau3259, 2019.

[143] Aslan Mansurov, Jun Ishihara, Peyman Hosseinchi, Lambert Potin, Tiffany M Marchell, Ako Ishihara, John-Michael Williford, Aaron T Alpar, Michal M Raczy, Laura T Gray, et al. Collagen-binding il-12 enhances tumour inflammation and drives the complete remission of established immunologically cold mouse tumours. *Nature biomedical engineering*, 4(5):531–543, 2020.

[144] Deng Chen, Ting-Xuan Tang, Hai Deng, Xiang-Ping Yang, and Zhao-Hui Tang. Interleukin-7 biology and its effects on immune cells: mediator of generation, differentiation, survival, and homeostasis. *Frontiers in Immunology*, page 5156, 2021.

[145] Linda M Bradley, Laura Haynes, and Susan L Swain. Il-7: maintaining t-cell memory and achieving homeostasis. *Trends in immunology*, 26(3):172–176, 2005.

[146] Claude Sportès, Rebecca R Babb, Michael C Krumlauf, Frances T Hakim, Seth M Steinberg, Catherine K Chow, Margaret R Brown, Thomas A Fleisher, Pierre Noel, Irina Maric, et al. Phase i study of recombinant human interleukin-7 administration in subjects with refractory malignancyphase i study of rhil-7 in refractory malignancy. *Clinical Cancer Research*, 16(2):727–735, 2010.

[147] Irina Ushach and Albert Zlotnik. Biological role of granulocyte macrophage colony-stimulating factor (gm-csf) and macrophage colony-stimulating factor (m-csf) on cells of the myeloid lineage. *Journal of Leucocyte Biology*, 100(3):481–489, 2016.

[148] Marcela Rosas, Siamon Gordon, and Philip R Taylor. Characterisation of the expression and function of the gm-csf receptor α-chain in mice. *European journal of immunology*, 37(9):2518–2528, 2007.

[149] Zhaojun Duan and Yunping Luo. Targeting macrophages in cancer immunotherapy. *Signal transduction and targeted therapy*, 6(1):127, 2021.

[150] Yueyun Pan, Yinda Yu, Xiaojian Wang, and Ting Zhang. Tumor-associated macrophages in tumor immunity. *Frontiers in immunology*, 11:583084, 2020.

[151] In-Sun Hong. Stimulatory versus suppressive effects of gm-csf on tumor progression in multiple cancer types. *Experimental & molecular medicine*, 48(7):e242–e242, 2016.

[152] Stefani Spranger, Daisy Dai, Brendan Horton, and Thomas F Gajewski. Tumor-residing batf3 dendritic cells are required for effector t cell trafficking and adoptive t cell therapy. *Cancer cell*, 31(5):711–723, 2017.

[153] Robin Parihar, Julie Dierksheide, Yan Hu, William E Carson, et al. Il-12 enhances the natural killer cell cytokine response to ab-coated tumor cells. *The Journal of clinical investigation*, 110(7):983–992, 2002.

[154] Joo-Young Park, Hee Yeun Won, Devon T DiPalma, Hye Kyung Kim, Tae-Hyoun Kim, Can Li, Noriko Sato, Changwan Hong, Ninan Abraham, Ronald E Gress, et al. In vivo availability of the cytokine il-7 constrains the survival and homeostasis of peripheral inkt cells. *Cell Reports*, 38(2):110219, 2022.

[155] Hisashi Arase, Noriko Arase, and Takashi Saito. Interferon gamma production by natural killer (nk) cells and nk1. 1+ t cells upon nkr-p1 cross-linking. *The Journal of experimental medicine*, 183(5):2391–2396, 1996.

[156] Jessica C Kling, Margaret A Jordan, Lauren A Pitt, Jana Meiners, Thao Thanh-Tran, Le Son Tran, Tam TK Nguyen, Deepak Mittal, Rehan Villani, Raymond J Steptoe, et al. Temporal regulation of natural killer t cell interferon gamma responses by β-catenin-dependent and-independent wnt signaling. *Frontiers in immunology*, 9:483, 2018.

[157] Sizhe Liu, Vasiliy Galat, Yekaterina Galat4, Yoo Kyung Annie Lee, Derek Wainwright, and Jennifer Wu. Nk cell-based cancer immunotherapy: from basic biology to clinical development. *Journal of hematology & oncology*, 14:1–17, 2021.

[158] Mojdeh Shakiba, Paul Zumbo, Gabriel Espinosa-Carrasco, Laura Menocal, Friederike Dündar, Sandra E Carson, Emmanuel M Bruno, Francisco J Sanchez-Rivera, Scott W Lowe, Steven Camara, et al. Tcr signal strength defines distinct mechanisms of t cell dysfunction and cancer evasion. *Journal of Experimental Medicine*, 219(2):e20201966, 2021.

[159] Witold Lasek, Radosław Zagożdżon, and Marek Jakobisiak. Interleukin 12: still a promising candidate for tumor immunotherapy? *Cancer Immunology, Immunotherapy*, 63:419–435, 2014.

[160] Paula Haiko, Taija Makinen, Salla Keskitalo, Jussi Taipale, Marika J Karkkainen, Megan E Baldwin, Steven A Stacker, Marc G Achen, and Kari Alitalo. Deletion of vascular endothelial growth factor c (vegf-c) and vegf-d is not equivalent to vegf receptor 3 deletion in mouse embryos. *Molecular and cellular biology*, 28(15):4843–4850, 2008.

[161] Manfred B Lutz, Nicole Kukutsch, Alexandra LJ Ogilvie, Susanne Rößner, Franz Koch, Nikolaus Romani, and Gerold Schuler. An advanced culture method for generating large quantities of highly pure dendritic cells from mouse bone marrow. *Journal of immunological methods*, 223(1):77–92, 1999.

[162] Cara N Skon, June-Yong Lee, Kristin G Anderson, David Masopust, Kristin A Hogquist, and Stephen C Jameson. Transcriptional downregulation of s1pr1 is required for the establishment of resident memory cd8+ t cells. *Nature immunology*, 14(12):1285–1293, 2013.

[163] Michael D Gunn, Kirsten Tangemann, Carmen Tam, Jason G Cyster, Steven D Rosen, and Lewis T Williams. A chemokine expressed in lymphoid high endothelial venules promotes the adhesion and chemotaxis of naive t lymphocytes. *Proceedings of the National Academy of Sciences*, 95(1):258–263, 1998.

[164] Jie Yang, Siya Zhang, Lingyun Zhang, Xiaoping Xie, Hui Wang, Zuliang Jie, Meidi Gu, Jin-Young Yang, Xuhong Cheng, and Shao-Cong Sun. Lymphatic endothelial cells regulate b-cell homing to lymph nodes via a nik-dependent mechanism. *Cellular & molecular immunology*, 16(2):165–177, 2019.